

JAERI-M

9 5 3 5

THROUGH ANALYSIS OF LOFT L2-2 BY
THYDE-P CODE (I)
(SAMPLE CALCULATION RUN 30)

June 1981

Masashi HIRANO and Yoshiro ASAH

この報告書は、日本原子力研究所が JAERI-M レポートとして、不定期に刊行している研究報告書です。入手、複製などのお問合わせは、日本原子力研究所技術情報部（茨城県那珂郡東海村）あて、お申しこしください。

JAERI-M reports, issued irregularly, describe the results of research works carried out in JAERI. Inquiries about the availability of reports and their reproduction should be addressed to Division of Technical Information, Japan Atomic Energy Research Institute, Tokai-mura, Naka-gun, Ibaraki-ken, Japan.

Through Analysis of LOFT L2-2 by THYDE-P Code (I)

(Sample Calculation Run 30)

Masashi HIRANO and Yoshiro ASAH

Division of Reactor Safety Evaluation,
Tokai Research Establishment, JAERI

(Received May 27, 1981)

A Through analysis of the Test L2-2 loss-of-coolant experiment (LOCE) in the Loss-of-Fluid Test (LOFT) program was made by the THYDE-P code. LOFT Test L2-2 was the first test in the Power Ascension Test Series (Test Series L2) of nuclear full double-ended cold leg break tests. THYDE-P is a computer code to analyze both blowdown and refill-reflood phases of loss-of-coolant accidents (LOCAs) of pressurized water reactors (PWRs) and is now under verification study and modifications. Therefore, the LOFT experimental data play an important role at the present stage of the THYDE-P code. The present analysis was performed by best estimate (BE) options as sample calculation Run 30, which is a portion of a series of THYDE-P sample calculations. In this report, the calculated results are compared with the experimental data and discussed. In the present calculation, the core nodes were completely submerged with subcooled water at 55 sec. after the test initiation. It showed a good agreement with the experimental result.

Keywords: LOFT, LOCA, PWR, THYDE-P Code, Verification Study, Sample Calculation, Blowdown, Reflood

THYDE - Pコードによる LOFT L2-2の一貫解析(I)
(サンプル計算 Run 30)

日本原子力研究所東海研究所安全解析部
平野雅司・朝日義郎

(1981年5月27日受理)

LOFT計画の冷却材喪失実験L2-2の一貫解析をTHYDE-Pコードを用いて行った。L2-2実験は、核炉心、コールドレグ両端破断の出力上昇実験シリーズ(シリーズL2)の最初のものである。THYDE-Pは、加圧水型軽水炉の冷却材喪失事故のブローダウン、および再冠水過程を解析する計算コードであり、現在、検証計算、および修正を行っている。それゆえ、LOFT実験の結果は、現段階のTHYDE-Pコードにとって有用である。本解析は、最適評価オプションを用い、サンプル計算Run 30として行ったものであり、一連のTHYDE-Pサンプル計算の一部を成すものである。本報告では、解析結果を実験結果と比較し、検討した。本計算では実験開始後55秒で炉心ノードは、完全に未飽和水中に没した。それは、実験結果との良い一致を示している。

CONTENTS

1.	Introduction	1
2.	Description of LOFT LOCE L2-2	2
2.1	Primary Objectives	2
2.2	LOFT System Description	3
3.	Description of THYDE-P	7
3.1	Characteristic Features of THYDE-P	7
3.2	Nodes and Junctions in THYDE-P	7
3.3	Heat Transfer Model	9
3.3.1	CHF Correlations	9
3.3.2	Heat Transfer Correlations	10
3.4	Critical Flow Model	13
3.5	Two-Phase Pump Model	14
3.6	Loss Coefficient k	14
3.7	Needs for Further Code Modifications	18
4.	Models Specifically Used in Analysis of LOFT L2-2 ..	18
4.1	Steady State Adjustment	18
4.2	Break Flow and Discharge Tank Simulation	19
4.3	Mass Conservation Equation	20
4.4	Non-Equilibrium Model	21
5.	Input Data and Results of Steady State Adjustment ..	25
6.	Calculated Results and Discussion	35
6.1	Cladding Surface Temperature and Thermal-Hydraulic Behavior in Core	35
6.2	ECC Water Penetration through Core	38
6.3	Broken Loop Hot Leg	39
6.4	Broken Loop Cold Leg	39
6.5	Intact Loop Hot Leg and Pressurizer	41

6.6	Intact Loop Cold Leg and Primary Coolant Pump	41
6.7	ECC Water Penetration through Downcomer Node	43
6.8	Steam Generator	44
6.9	Accumulator	44
6.10	Temporal Behavior of Pressure	45
6.11	Time Step Width and CPU Time	45
7.	Conclusion	64
	Acknowledgement	64
	References	65
Appendix A	Input Data List	67
Appendix B	Function Codes of Experimental Data in Figures	75
Appendix C	Nomenclature	76
C.1	Alphabetic Symbols	76
C.2	Greek Symbols	77
C.3	Subscripts and Superscripts	78

目 次

1. 序	1
2. LOFT LOCE L2-2 の記述	2
2.1 主目的	2
2.2 LOFT 実験の記述	3
3. THYDE-P の記述	7
3.1 THYDE-P の特徴	7
3.2 THYDE-P のノードとジャンクション	7
3.3 熱伝達モデル	9
3.3.1 臨界熱流束実験式	9
3.3.2 熱伝達実験式	10
3.4 臨界流モデル	13
3.5 二相ポンプモデル	14
3.6 損失係数 K	14
3.7 コードの修正すべき点	18
4. LOFT L2-2 の解析に用いたモデル	18
4.1 定常状態の調整	18
4.2 破断流および放出タンクの模擬	19
4.3 質量保存方程式	20
4.4 非平衡モデル	21
5. 入力データ及び定常状態調整の結果	25
6. 解析結果および議論	35
6.1 燃料棒表面温度と炉心の熱流動	35
6.2 ECC 水の炉心への流入	38
6.3 破断ループホットレグ	39
6.4 破断ループコールドレグ	39
6.5 健全ループホットレグと加圧器	41
6.6 健全ループコールドレグと主冷却材ポンプ	41
6.7 ダウンカマノードを経ての ECC 水の流入	43
6.8 蒸気発生器	44
6.9 蓄圧器	44
6.10 圧力の時間挙動	45
6.11 時間巾および CPU 時間	45
7. 結 論	64
8. 参考文献	65

9. 謝 辞	64
付録 A インプットデータリスト	67
B 図中の実験データのファンクションコード	75
C 記号表	76
C. 1 アルファベット記号	76
C. 2 ギリシャ文字記号	77
C. 3 添 字	78

LIST OF FIGURES

<u>No.</u>	<u>Title</u>	<u>Page</u>
1	LOFT major components	4
2	LOFT Core 1 configuration showing rod designations .	5
3	Nodes and junctions in THYDE-P	
	(a) Normal node	8
	(b) Normal junction	8
	(c) Mixing junction	8
4	Single-phase homologous head and torque curves	15
5	Head difference homologous curves	15
6	Head and torque multiplier curves	16
7	Delay parameter τ_{α} in present analysis	21
8	Schematic explanation for non-equilibrium model	
	(a) Extreme cases	24
	(b) Typical cases	24
9	Nodalization for LOFT LOCE L2-2	
	(a) Major components	29
	(b) Within fuel rod	30
10	Initial pressure distribution along intact loop ...	31
11	Initial linear heat generation rate	31
12	Loss coefficients	
	(a) Pressurizer surge line	32
	(b) Simulated SG and pump	32
13	Cladding surface temperatures	
	(a) Comparison of calculated cladding surface temper- ature at node 27 with experimental data	46

LIST OF FIGURES (continued)

<u>No.</u>	<u>Title</u>	<u>Page</u>
	(b) Comparison of calculated cladding surface temperature at node 28 with experimental data 46
14	Calculated heat transfer coefficient	
	(a) Core node 27 47
	(b) Core node 28 47
15	Calculated mass flux at core node 28 48
16	Calculated coolant quality at core node 28 48
17	Calculated cladding surface temperatures at core nodes at early stage of blowdown 49
18	Calculated heat transfer coefficients at core nodes at early stage of blowdown 49
19	Calculated mass fluxes at core nodes at early stage of blowdown 50
20	Calculated coolant qualities at core nodes at early stage of blowdown 50
21	Calculated mass fluxes at inlet and outlet points of core nodes 27 and 28 in refill-reflood phase 51
22	Calculated enthalpies at inlet and outlet points of core nodes 27 and 28 in refill-reflood phase 51
23	Mass flow rate at broken loop hot leg 52
24	Coolant density at broken loop hot leg 52
25	Mass flow rate at broken loop cold leg 53
26	Coolant density at broken loop cold leg 53

LIST OF FIGURES (continued)

<u>No.</u>	<u>Title</u>	<u>Page</u>
27	Nodalization for downcomer region	
	(a) Present analysis	54
	(b) Example for split downcomer	54
28	Mass flow rate at intact loop hot leg	55
29	Coolant density at intact loop hot leg	55
30	Calculated pressure and water level at pressurizer .	56
31	Mass flow rate at intact loop cold leg	56
32	Coolant density at intact loop cold leg	57
33	Calculated mass fluxes at intact loop cold leg (node 20) in refill-reflood phase	57
34	Calculated enthalpies at intact loop cold leg (node 20) in refill-reflood phase	58
35	Normalized pump speed	58
36	Calculated pump head at pump node 18	59
37	Calculated normalized pump volumetric flow rate and coolant quality at pump node 18	59
38	Calculated mass fluxes at downcomer node 22	60
39	Calculated enthalpies at downcomer node 22	60
40	Calculated coolant temperatures at inlet and outlet plenums of SG (nodes 13 and 16)	61
41	Calculated pressures at SG secondary and primary systems	61

LIST OF FIGURES (continued)

<u>No.</u>	<u>Title</u>	<u>Page</u>
42	Mass flow rate at accumulator	62
43	Accumulator pressure	62
44	Enthalpy at accumulator	63
45	Pressure above active core	63

LIST OF TABLES

	<u>Title</u>	<u>Page</u>
1	Initial Conditions for Test L2-2	6
2.1	Heat Transfer Correlations	13
2.2	Heat Transfer Mode 4	11
3	Function $F(p^*)$	13
4	Node Geometrical Data	33
5	Loss Coefficients	34
6	Chronology of Events	36

1. Introduction

A through calculation of LOFT loss-of-coolant experiment (LOCE) L2-2⁽¹⁾ was made by the THYDE-P code^{(2), (3)} not only to verify the system performance of the THYDE-P code but also to obtain better understandings of the experiment. The thermal-hydraulic calculation in THYDE-P at first is based on a homogeneous equilibrium model. In the course of the work, however, a time delay model for density change, which takes non-equilibrium effects into account, was used to analyze the refill-reflood phase of the experiment. One of the major purposes of the present analysis was to accumulate experiences on needs for upgrading of the simple non-equilibrium model as well as for code modifications. The present analysis was performed as sample calculation Run 30, which is a portion of a series of THYDE-P sample calculations.

Test L2-2 was the first test in the Power Ascension Test Series (test Series L2) of nuclear double-ended cold leg break tests and was conducted at 50% power (25 MW, 26.38 kW/m). In this test, emergency core cooling (ECC) water was injected into the intact loop cold leg to provide data on the effects of ECC on system thermal-hydraulic response. The core volume reflood time was reported to be 55 sec. after the test initiation⁽⁴⁾.

In the present analysis, the LOFT system was nodalized into 43 nodes and 37 junctions. The active core was nodalized into 6 nodes. A hot channel analysis was not performed but only an average channel analysis was done. The discharge coefficient for the Moody correlation⁽⁶⁾ was set to be 0.8. The two-phase pump model to treat the LOFT two-phase pump data⁽¹⁷⁾ was newly implemented and was used.

Sensitivity studies for the heat transfer model in the core are now being performed. Therefore, the heat transfer model in the present analysis should be regarded as tentative. For example, a pool boiling curve and transition boiling were taken into consideration in the present analysis.

The calculation proceeded until the core nodes were completely submerged with subcooled water, i.e. 55 sec. after the break, without any calculation mode change during the entire process. At the early stage of the blowdown phase, one or several peaks of the cladding surface temperature were also calculated as were observed in the experiment. The departure from nucleate boiling (DNB) was calculated under the pool flow condition. Prior to quenching, the rapid decrease of the cladding surface temperature from the

peak, however, was calculated due to transition boiling under the forced convection condition and quenching was calculated at all core nodes.

After the accumulator (ACC) injection was calculated to start, i.e. about 17 sec. after the rupture, the non-equilibrium model was introduced to avoid unrealistically large pressure decreases due to rapid condensation processes. The non-equilibrium model made the present through analysis possible although its physical basis should be scrutinized.

2. Description of LOFT L2-2

The LOFT program is conducted by EG & G Idaho, Inc., for the U.S. Nuclear Regulatory Commission and administered by the Department of Energy. Test L2-2 was conducted on December 9, 1978 as the first test of the Power Ascension Test Series (Test Series L2). This test was designed to provide data for a 200% double-ended offset shear in the pump discharge line in the cold leg of a four-loop, large PWR. The detailed information on Test L2-2 is presented in Ref. (1). It would be convenient to depict some parts of the reference in this section.

2.1 Primary Objectives

The primary objectives of Test L2-2 were to:

- (1) Provide a test in which the hottest fuel rods are predicted to encounter departure from nucleate boiling and not immediately reenter the nucleate boiling heat transfer regime to allow assessment of fuel rod-to-coolant heat transfer in the postcritical heat flux regime
- (2) Determine LOFT fuel rod temperature response during a 26.25 kW/m maximum linear heat generation rate double-ended cold leg break LOCE
- (3) Determine blowdown thermal-hydraulic response at a 67% nominal hot-leg-to-cold-leg temperature difference of 23.8 K
- (4) Determine if any cladding perforation occurs in a 26.25 kW/m maximum linear heat generation rate, double-ended cold leg break LOCE by

peak, however, was calculated due to transition boiling under the forced convection condition and quenching was calculated at all core nodes.

After the accumulator (ACC) injection was calculated to start, i.e. about 17 sec. after the rupture, the non-equilibrium model was introduced to avoid unrealistically large pressure decreases due to rapid condensation processes. The non-equilibrium model made the present through analysis possible although its physical basis should be scrutinized.

2. Description of LOFT L2-2

The LOFT program is conducted by EG & G Idaho, Inc., for the U.S. Nuclear Regulatory Commission and administered by the Department of Energy. Test L2-2 was conducted on December 9, 1978 as the first test of the Power Ascension Test Series (Test Series L2). This test was designed to provide data for a 200% double-ended offset shear in the pump discharge line in the cold leg of a four-loop, large PWR. The detailed information on Test L2-2 is presented in Ref. (1). It would be convenient to depict some parts of the reference in this section.

2.1 Primary Objectives

The primary objectives of Test L2-2 were to:

- (1) Provide a test in which the hottest fuel rods are predicted to encounter departure from nucleate boiling and not immediately reenter the nucleate boiling heat transfer regime to allow assessment of fuel rod-to-coolant heat transfer in the postcritical heat flux regime
- (2) Determine LOFT fuel rod temperature response during a 26.25 kW/m maximum linear heat generation rate double-ended cold leg break LOCE
- (3) Determine blowdown thermal-hydraulic response at a 67% nominal hot-leg-to-cold-leg temperature difference of 23.8 K
- (4) Determine if any cladding perforation occurs in a 26.25 kW/m maximum linear heat generation rate, double-ended cold leg break LOCE by

monitoring fission product concentration in the coolant

- (5) Provide integral nuclear system code verification data on a low-to-intermediate power double-ended cold leg break
- (6) Provide continued data to evaluate LOFT ECCS scaling techniques
- (7) Determine LOFT reflood characteristics at 26.25 kW/m maximum linear heat generation rate initial conditions.

2.2 LOFT System Description

The LOFT system configuration for Test L2-2 are shown in Fig. 1. The LOFT reactor vessel has an annular downcomer, a lower plenum, lower core support plates, a nuclear core and an upper plenum. The core contains 1300 nuclear fuel rods arranged in five square and four triangular (corner) fuel modules, shown in Fig. 2. The fuel rods have an active length of 167.64 cm and an outside diameter of 1.07 cm. The intact loop simulates the three unbroken loops of a large PWR and contains a steam generator, two circulating coolant pumps connected in parallel, a pressurizer, a venturi flowmeter, and connecting piping. The broken loop consists of a hot leg and a cold leg that are connected to the reactor vessel and the blowdown suppression tank header. Each leg consists of a break plane orifice which determines the break size to be simulated, a quick-opening blowdown valve (QOBV) which simulates a pipe break, a recirculation line, an isolation valve, and connecting piping. The broken loop hot leg also contained a simulated steam generator and a simulated pump. These simulators have hydraulic orifice plate assemblies which have similar (passive) flow resistances as a real steam generator and a free-rotating pump. The break flow area (break plane orifice area) in this configuration is 0.0084 m^2 in each line which is 100% of the possible break flow area of each line. The LOFT ECCS simulates the ECCS of a large PWR. The accumulator (ACC), the high-pressure injection system (HPIS), and the low-pressure injection system (LPIS) were used during this experiment. Each system was arranged to inject scaled flow rates of ECC directly into the primary coolant system cold leg.

The initial conditions for Test L2-2 are listed in Table 1 along with those used in the present analysis by the THYDE-P code.

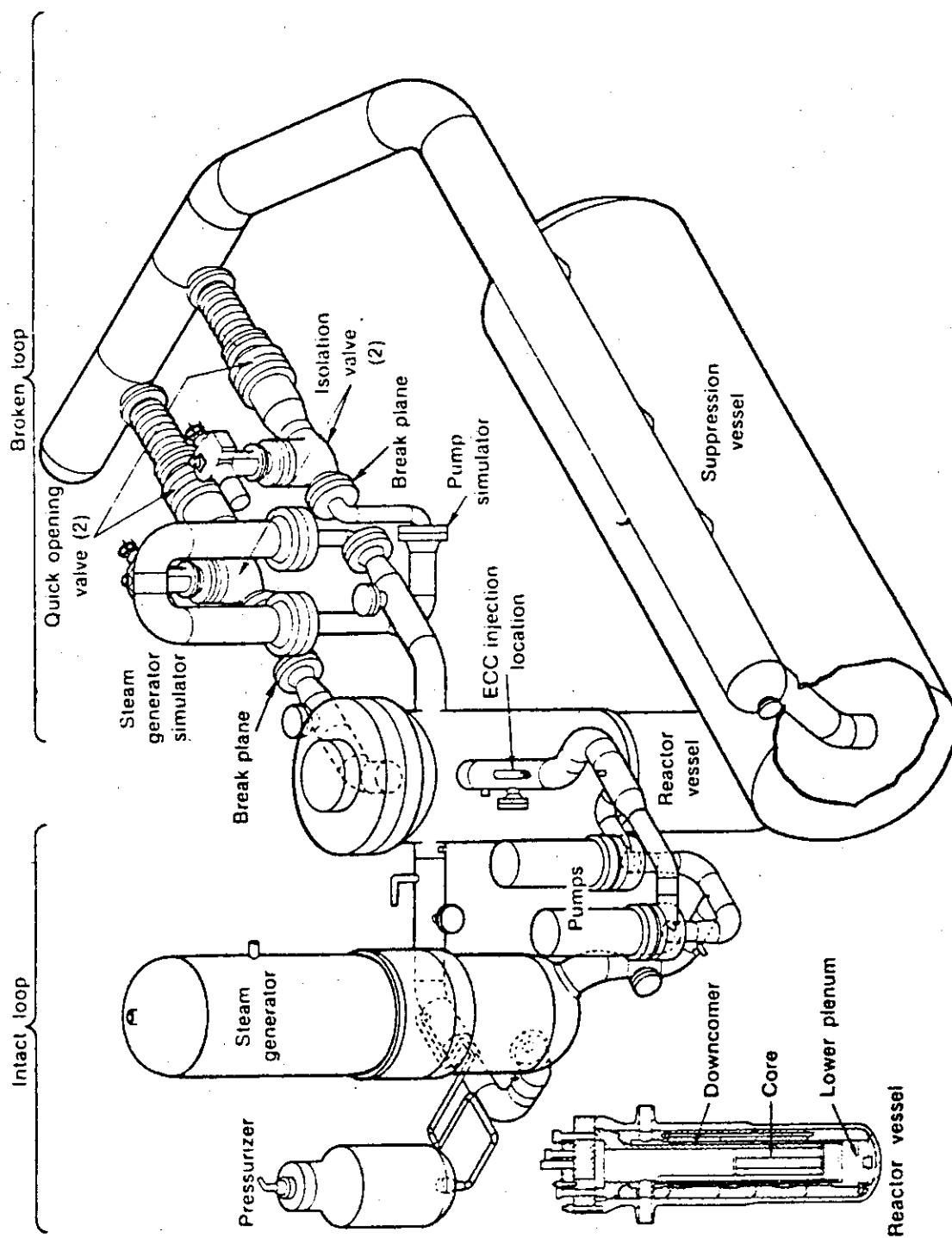


Fig. 1 LOFT major components

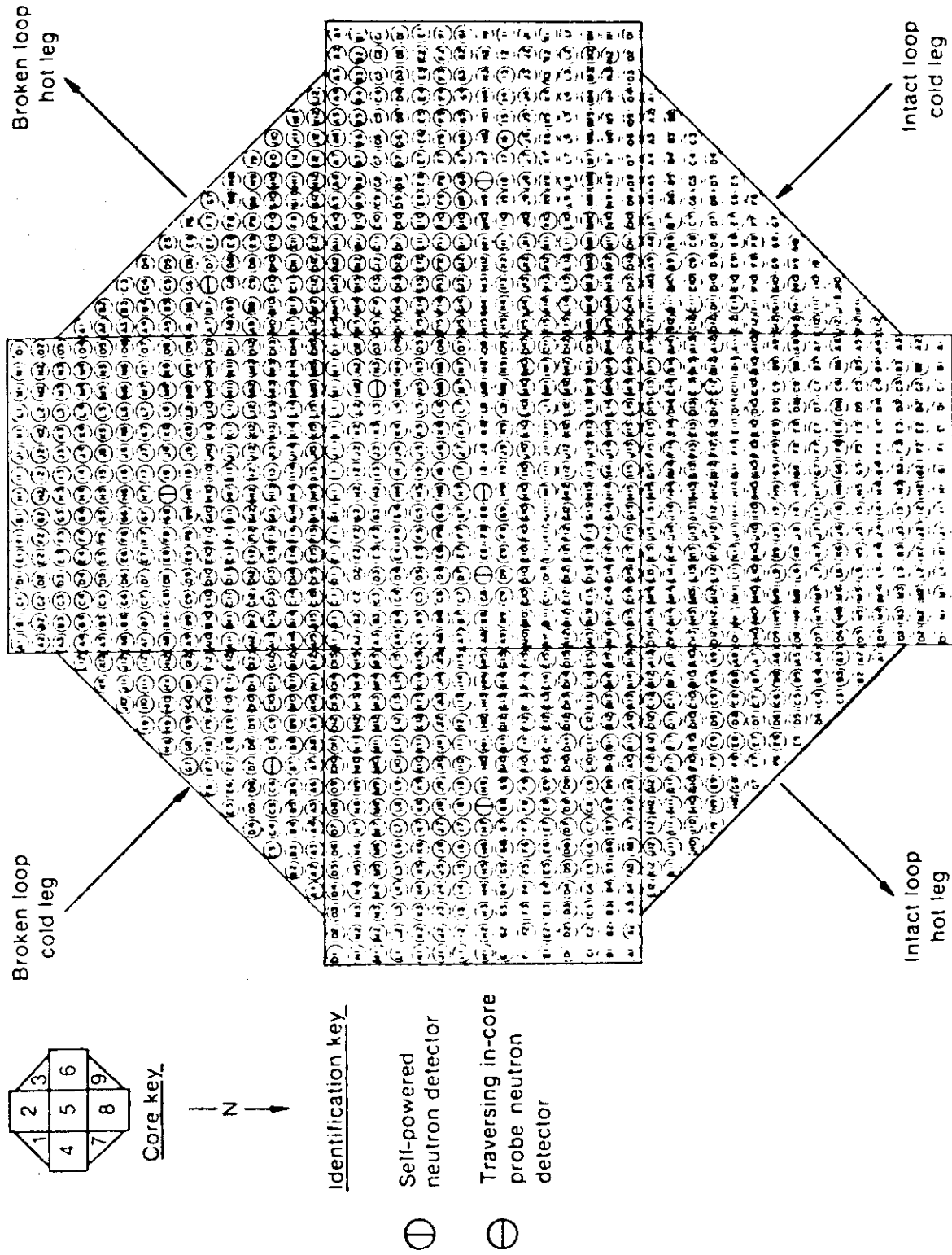


Fig. 2 LOFT Core 1 configuration showing rod designations

Table 1 Initial Conditions for Test L2-2

Items	Experiment	Input Data
Primary Coolant System		
Intact Loop		
Pressure	15.64 MPa	15.6 MPa
Mass Flow Rate	194.2 kgm/sec	194 kgm/sec
Cold Leg Temperature	284.7 °c	283 °c
Hot Leg Temperature	307.4 °c	307 °c
Broken Loop		
Cold Leg Temperature		
Near Vessel	282 °c	283 °c
Near Break	265.3 °c	283 °c
Hot Leg Temperature		
Near Vessel	288.2 °c	307 °c
Near Break	269.6 °c	307 °c
Power Level	24.88 MW	24.9 MW
Pressurizer		
Pressure	15.62 MPa	15.6 MPa
Steam Volume	0.353 m ³	0.355 m ³
Water Volume	0.607 m ³	0.605 m ³
Water Temperature	346 °c	343 °c
Water Level	1.089 m	1.00 m ^(a)
Steam Generator Secondary Side		
Pressure	6.35 MPa	6.35 MPa
Water Volume	3.74 m ³	1.01 m ³
Water Level	3.14 m	0.6 m ^(b)
Mass Flow Rate	12.67 kgm/sec	12.67 kgm/sec
Accumulator		
Pressure	4.11 MPa	4.11 MPa
Gas Volume	1.05 m ³	1.05 m ³
Water Temperature	27.8 °c	27.8 °c

(a), (b) : Initial water levels in THYDE-P are subcooled water level

3. Brief Description of THYDE-P

The models and the methods of the THYDE-P code are presented in detail in Ref. (2), some of which have been revised. In this section, some of them are briefly reviewed along with the newly implemented models.

3.1 Characteristic Features of THYDE-P

In the THYDE-P code, a PWR plant is regarded hydraulically as a network of various coolant components which may be classified into nodes and junctions. The one-dimensional mass, momentum and energy equations are suitably integrated in each node and junction. In integrating the resulting equations with respect to time, a non-linear implicit method is used on the basis of the Newton method. The Jacobian matrix of the basic equations can be reduced to a simple form by the network theory, which is one of the characteristics of THYDE-P. To solve the basic equations by the non-linear implicit method, various smoothing functions with respect to time are introduced for mode changes such as phase change and flow reversal.

New models for a steam generator and a pressurizer are implemented, about which reference should be made to Ref. (2).

A calculation by THYDE-P is started by steady state adjustment, where the basic equations are exactly solved without time derivatives. THYDE-P is able to calculate through both blowdown and refill-reflood phases without any change of models and physical conditions of the coolant. A model which takes non-equilibrium effects into account is newly implemented and is presented in Subsec. 4.4.

3.2 Nodes and Junctions in THYDE-P

Nodes are classified into normal nodes, linkage nodes and special nodes. The linkage node is a node which branches off a loop and does not form a loop. The coolant in the linkage node is assumed to be stagnant at the steady state. The special nodes include a steam generator secondary system, a pressurizer and an accumulator. The other nodes are called normal nodes which are components of loops in the hydraulic network. In the normal and linkage nodes, physical parameters such as mass flux G , pressure p and enthalpy h are assigned

at both the inlet and the outlet of each node, which we call point A and E, respectively, as shown in Fig. 3(a). In the present version of THYDE-P, G^A , p^A , G^E and p^E are included in the implicit scheme but h^A and h^E are integrated explicitly.

There are two types of junctions. One is called a normal junction which does not have volume and connects two adjacent nodes. The other type of junction is called a mixing junction which has volume and connects more than three normal or linkage nodes. These two types of junctions are schematically shown in Fig. 3(b) and (c).

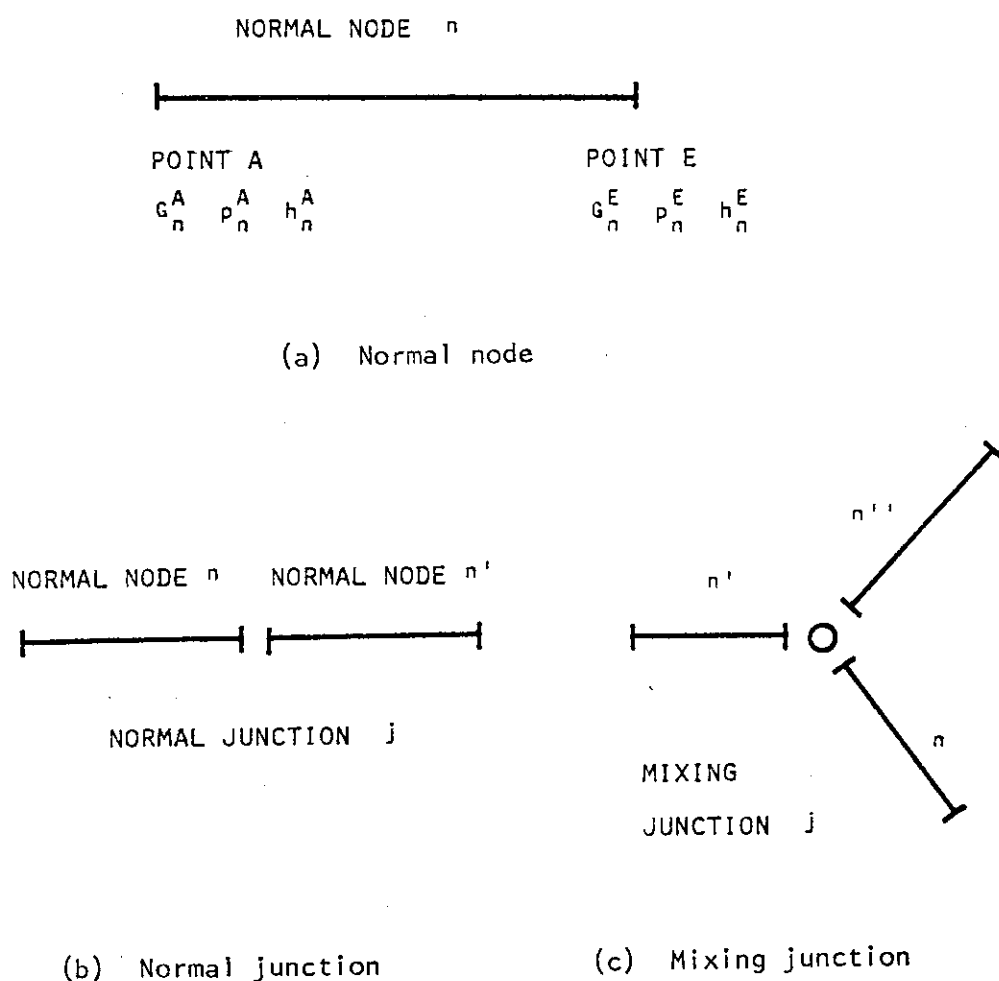


Fig. 3 Nodes and Junctions in THYDE-P

3.3 Heat Transfer Model

3.3.1 CHF Correlations

In the present analysis, the Biasi⁽¹⁴⁾ and modified Zuber^{(20), (21)} correlations were used to predict CHF values for $G > G_{min}$ and $G \leq G_{min}$, respectively.

(1) Biasi Correlation⁽¹⁴⁾

$$\phi_{CHF} = \frac{1.833 \times 10^3}{G_b^{1/6} D_b^m} \left\{ \frac{Y(p_b)}{G_b^{1/6}} - x_{out} \right\} / J_c \times 10^{-1}$$

for low quality (1)

$$\phi_{CHF} = \frac{3.78 \times 10^3}{G_b^{0.6} D_b^m} H(p_b) (1 - x_{out}) / J_c \times 10^{-1}$$

for high quality (2)

where

$$m = \begin{cases} 0.4 & \text{for } D_b > 1 \text{ cm} \\ 0.6 & \text{for } D_b < 1 \text{ cm} \end{cases}$$

$$Y(p_b) = 0.7249 + 0.099 p_b \exp(-0.032 p_b) \quad (3)$$

and

$$H(p_b) = -1.159 + 0.149 p_b \exp(-0.019 p_b) \quad (4)$$

The range of validity of the correlation is the following:

$$\begin{aligned} 0.3 \text{ cm} &< D_b < 3.75 \text{ cm} \\ 20 \text{ cm} &< L_b < 600 \text{ cm} \\ 2.7 \text{ ata} &< p_b < 140 \text{ ata} \\ 10 \text{ g/cm}^2\text{sec} &< G_b < 600 \text{ g/cm}^2\text{sec} \\ x_{in} &< 0.0 \\ 1/(1 + \rho_l/\rho_g) &< x_{out} < 1.0 \end{aligned}$$

(2) Modified Zuber Correlation^{(20), (21)}

The Zuber pool CHF correlation⁽²⁰⁾ is

$$\phi_{CHF} = (1 - \alpha) 0.131 \rho_g h_{fg} \left\{ \frac{\sigma g (\rho_l - \rho_g)}{\rho_g^2} \right\}^{1/4} \quad (5)$$

where the factor $(1 - \alpha)$ was recommended by Griffith⁽²¹⁾ for low flow and counter-current flow conditions.

3.3.2 Heat Transfer Correlations

The heat transfer correlations applied in the present analysis were summarized in Tables 2.1 and 2.2. Newly applied correlations in the present analysis are briefly described in this section.

(1) Thom Correlation⁽²²⁾ (mode 1)

$$\phi^* = \left\{ \frac{\Delta T_s^* \exp(p^*/1260)}{0.072} \right\}^2 \quad (6)$$

vertical up flow of water

Round tube : 0.5 inch diameter, 60 inch length

Annulus : 0.7 inch I.D., 0.9 inch O.D. and 12 inch length

Mass flux : 0.77×10^6 lbm/ft²hr to 2.80×10^6 lbm/ft²hr

Heat flux : to 0.5×10^6 Btu/ft²hr

(2) McDonough, Milich and King Correlation⁽¹⁸⁾ (mode 4-1)

$$\phi^* = \phi_{CHF}^* - h_t(p^*) (T_w^* - T_{w, CHF}^*) \quad (7)$$

where h_t is a function of p^* as follows:

p^*	$h_t(p^*)$
2000	1101.6
1200	1180.8
800	1501.2

Table 2.1 Heat Transfer Correlations

Mode		Conditions		Correlations
Core	SG	Coolant Condition	Other conditions	
1	1	Subcooled water	$T_{\text{wall}} < T_{\text{sat}}$	Dittus-Boelter ⁽¹⁰⁾
2	2	Subcooled water	$T_{\text{wall}} > T_{\text{sat}}$	Interpolation between D-B and Thom
3	3	Saturated state	$\phi < \phi_{\text{CHF}}$	Thom ⁽²²⁾
4	/	Saturated state	$\phi > \phi_{\text{CHF}}$	(see Table 2.2)
5	5	Superheated steam	$Re < 3000$	McEligot ⁽¹³⁾
6	6	Superheated steam	$3000 < Re < 5000$	McEligot ⁽¹³⁾
7	7	Superheated steam	$Re > 5000$	McEligot ⁽¹³⁾
/	8	Saturated state	$T_{\text{coolant}} > T_{\text{wall}}$	Condensation ⁽¹⁶⁾

Table 2.2 Heat Transfer Correlations in Mode 4

Mode	Conditions	Correlations
4-1	$G > G_{\text{min}}, \phi_{4-1} > \phi_{4-2}$	McDonough, Milich and King ⁽¹⁸⁾
4-2	$G > G_{\text{min}}, \phi_{4-1} < \phi_{4-2}$	Groenevelt ⁽¹²⁾
4-3	$G < G_{\text{min}}, \Delta T_s^* < \Delta T_{\text{min}}^*$	Pool transition boiling correlation ⁽¹⁹⁾
4-4	$G < G_{\text{min}}, \Delta T_s^* > \Delta T_{\text{min}}^*$	Berenson ⁽²³⁾
4-5	$G < G_{\text{min}}, x_{\text{coolant}} < x_c$	Pool transition boiling

Vertical up flow

Diameter : 0.152 inch

Mass flux : 0.2×10^6 to 1.4×10^6 lbm/ft²hr

Wall temperature : T_w^* 1030 °F

Pressure : 800, 1200 and 2000 psia

(3) Pool Transition Boiling Correlation⁽¹⁹⁾ (mode 4-3)

$$\phi^* = 20,000 \left(\frac{\Delta T_{\min}^*}{\Delta T_s^*} \right)^{\frac{1.504}{\ln(\Delta T_{\min}^*/20)}} \quad (8)$$

where

$$\Delta T_{\min}^* = \left\{ \frac{20,000}{F(p^*)} \right\}^{4/3} \quad (9)$$

and $F(p^*)$ is shown in Table 3. However, if $\Delta T_s^* < 20$, then ϕ^* is set to 90,000 Btu/ft²hr.

(4) Berenson Correlation⁽²³⁾ (mode 4-4)

$$h_{tr} = 0.425 \left\{ \frac{k_g^3 \rho_g (\rho_l - \rho_g) g h_{fg}}{\mu_g \Delta T_s \lambda_c / 2\pi} \right\}^{1/4} \quad (10)$$

where

$$\lambda_c / 2\pi = \left\{ \frac{g_c \sigma}{g(\rho_l - \rho_g)} \right\} \quad (11)$$

Carbon tetrachloride, n-pentane

Horizontal flat tube facing upwards

Pressure : atmospheric

The equation is approximated⁽¹⁹⁾ in the coding by

$$\phi^* = F(p^*) \Delta T_s^{3/4} \quad (12)$$

where $F(p^*)$ is dependent on pressure as shown in Table 3.

Table 3 Function $F(p^*)$

p^*	$F(p^*)$
15	128
100	236
500	412
1000	510
1500	615
2000	705

(5) Pool Transition Boiling (mode 4-5)

In the post CHF calculation, it is assumed that film boiling could not exist when the coolant quality is small enough, i.e. less than x_c . Then pool transition boiling may be assumed in this region. For simplicity in the present analysis, the heat flux value is set to be constant ϕ_c , which should exist between the upper limit and the lower limit of the pool transition boiling correlation (mode 4-3), which is shown in Eq. (8). In the present calculation, x_c and ϕ_c are assumed as follows:

$$\begin{aligned} x_c &= 0.05 \\ \phi_c &= 50 \text{ kcal/m}^2\text{sec} \text{ (64,000 Btu/ft}^2\text{hr)} \end{aligned} \quad (13)$$

3.4 Critical Flow Calculation

A slightly modified⁽²⁾ Zaloudek's equation⁽⁵⁾ and the Moody correlation⁽⁶⁾ are implemented for a subcooled condition and a saturated condition, respectively. To avoid the discontinuity of the break flow with mode change, the calculated critical flows by these correlations are connected continuously. Therefore, the discharge coefficients for these correlations are not independent and only one of the two is to be given as an input. In the present version of the THYDE-P code, the critical flow calculation in a duct is not implemented.

3.5 Two-Phase Pump Model

The two-phase pump model in THYDE-P was modified to treat the LOFT two-phase pump data⁽¹⁷⁾ as follows:

$$h_{\text{head}} = h_{\text{head}}^{1\phi} - m_h(\alpha) (h_{\text{head}}^{1\phi} - h_{\text{head}}^{2\phi}) \quad (14)$$

$$b = b^{1\phi} - m_b(\alpha) (b^{1\phi} - b^{2\phi}) \quad (15)$$

where

h_{head} : normalized pump head

b : normalized pump hydraulic torque

m_h : head multiplier as a function of void fraction

m_b : torque multiplier as a function of void fraction

The single-phase head and torque homologous curves are shown in Fig. 4. The head difference homologous curves (single-phase minus two-phase head) are shown in Fig. 5. The head and torque multipliers as functions of void fraction are shown in Fig. 6. These curves were given as inputs. The single-phase homologous torque data for the LOFT pumps are also used for the torque difference curve with the normalized torque "b" for the two-phase pump operation being calculated as

$$b = b^{1\phi} \{1 - m_b(\alpha)\} \quad (16)$$

3.6 Loss Coefficient k

There are two kinds of loss coefficients in THYDE-P. The loss coefficients of one kind are so called "residual k-factors", which are to be calculated for normal nodes as a result of steady state adjustment. For a linkage node, however, coolant is stagnant at the steady state so that the loss coefficient is to be given as an input. The loss coefficients of the other kind, which take into account irreversible pressure drops due to area change, bending of ducts etc., are assigned at both points A and E of the normal and linkage nodes. Since the loss coefficients of the latter kind is newly

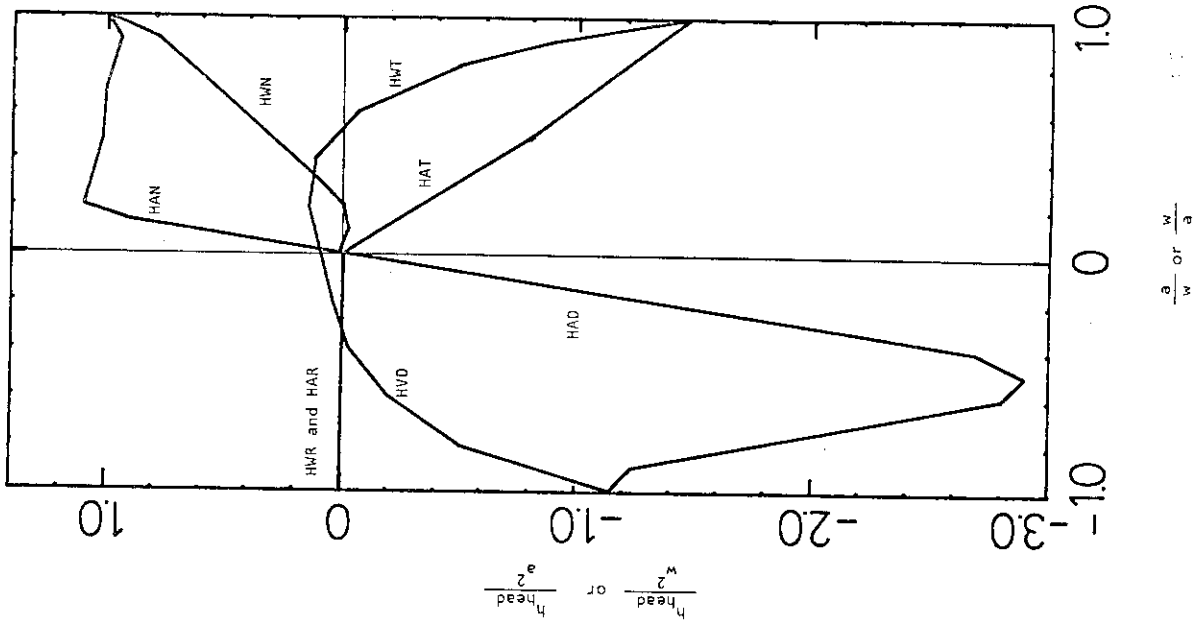


Fig. 5 Head difference homologous curves

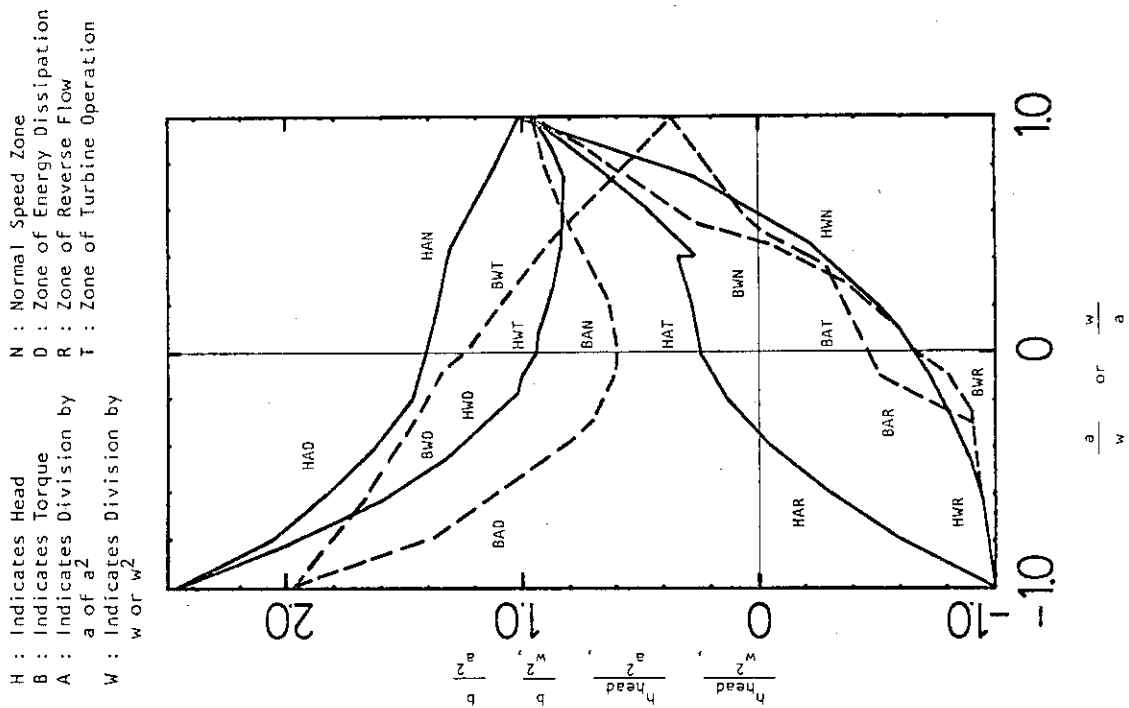


Fig. 4 Single-phase homologous head and torque curves

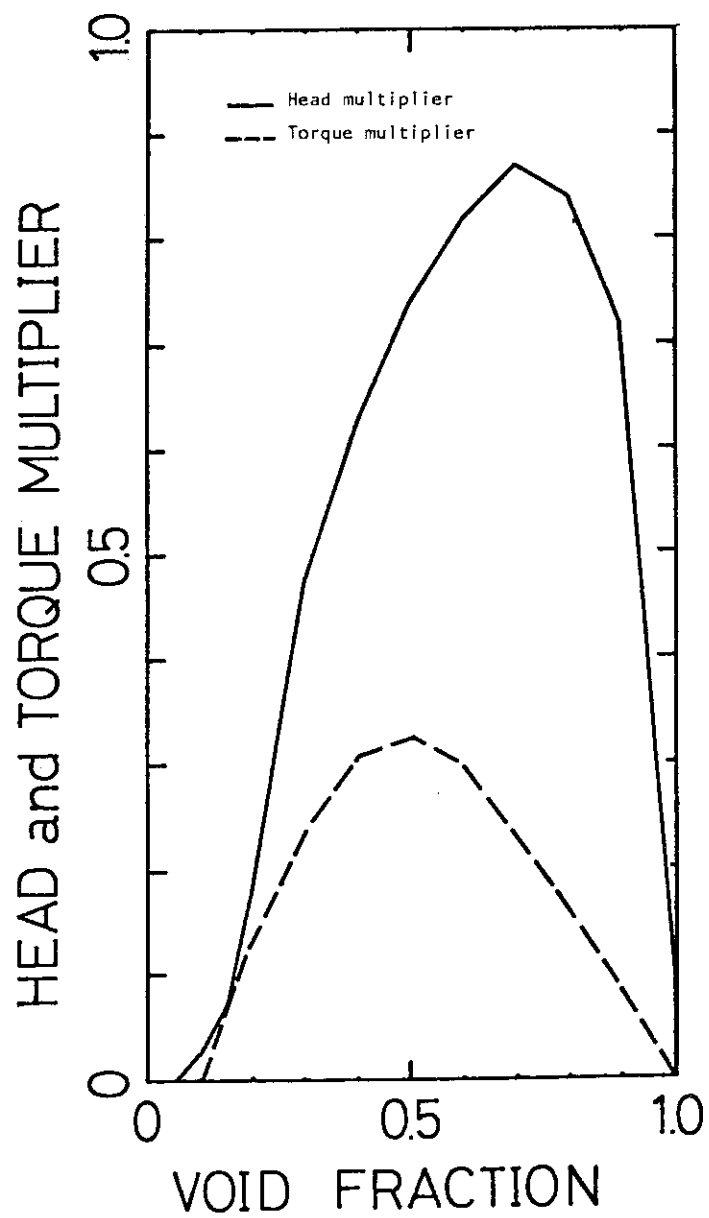


Fig. 6 Head and torque multiplier curves

implemented, they are described in some detail in this subsection.

The pressure drops at junction j , which is located between point A of node n and point E of node n' , for forward and reverse flows may be expressed as follows:

$$\Delta p_j = k_{n'}^{Ed} \frac{G_{n'}^E |G_{n'}^E|}{2\rho_{n'}} + k_n^{Ad} \frac{G_n^A |G_n^A|}{2\rho_n} \quad (17)$$

where

$$d = \begin{cases} f & \text{for forward flow} \\ r & \text{for reverse flow} \end{cases}$$

and

k_n^{Af} : loss coefficient at point A of node n for forward flow

k_n^{Ar} : loss coefficient at point A of node n for reverse flow

$k_{n'}^{Ef}$: loss coefficient at point E of node n' for forward flow

$k_{n'}^{Er}$: loss coefficient at point E of node n' for reverse flow

which are inputs.

In THYDE-P, there is another option. When at least one of these four loss coefficients concerning a normal junction j is given to be -1 , $k_{n'}^{Ef}$ and $k_{n'}^{Er}$ are set equal to zero and k_n^{Af} and k_n^{Ar} are calculated by the following empirical correlations⁽⁹⁾ for sudden area changes.

$$k_n^{Af \text{ or } r} = \begin{cases} 0.45 (1 - \beta) & \text{for sudden contraction} \\ (1/\beta - 1)^2 & \text{for sudden expansion} \end{cases} \quad (18)$$

where

$$\beta = (\text{smaller cross sectional area})/(\text{larger cross sectional area}).$$

The loss coefficients k_n^{Af} , k_n^{Ar} , k_n^{Ef} and k_n^{Er} are given in the last four items of each node data in the data block number BB06 as shown in the input data list in App. A.

3.7 Needs for Further Code Modifications

In Ref. (3), needs for modifications for the present version of THYDE-P are summarized. Some models have been modified or newly implemented till now but there still exist lots of needs for further modifications and upgradings. Two major deficiencies which were thought to be important as a result of the present analysis are reviewed.

- (1) A discharge tank model is not implemented.
- (2) Heat transfer between coolant and structures is not able to be taken into account.

In the present analysis, heat transfer between coolant and structures was neglected. The treatment of the discharge tank in the present analysis will be shown in Subsec. 4.2. As will be shown in Sec. 6, there exist several discrepancies between the calculated results and the experimental data which might be caused mainly by these deficiencies.

4. Models Specifically Used in Analysis of LOFT L2-2

4.1 Steady State Adjustment

The THYDE-P code is designed to analyze large scale commercial PWR LOCAs so that special treatments were needed to simulate the LOFT facility. In the LOFT program, two broken legs are separated and do not form a loop and the coolants in these legs were stagnant prior to the break. In the case of a postulated PWR LOCA, however, generally normal operational conditions are assumed prior to the break. Therefore, such a stagnant coolant condition in a primary loop need not be assumed for actual PWR plants.

In the present analysis of Test L2-2, the broken loop hot and cold legs were supposed to be connected and forming a loop with a very small amount of mass flow at the initial steady state. In order to obtain the desired initial conditions as a result of steady state adjustment⁽²⁾, a dummy pump with a dummy heat sink was placed at the break junction 6, prior to the break and it was made to vanish after the break. The pressure rise and the enthalpy drop at the dummy pump were assumed to be as follows:

3.7 Needs for Further Code Modifications

In Ref. (3), needs for modifications for the present version of THYDE-P are summarized. Some models have been modified or newly implemented till now but there still exist lots of needs for further modifications and upgradings. Two major deficiencies which were thought to be important as a result of the present analysis are reviewed.

- (1) A discharge tank model is not implemented.
- (2) Heat transfer between coolant and structures is not able to be taken into account.

In the present analysis, heat transfer between coolant and structures was neglected. The treatment of the discharge tank in the present analysis will be shown in Subsec. 4.2. As will be shown in Sec. 6, there exist several discrepancies between the calculated results and the experimental data which might be caused mainly by these deficiencies.

4. Models Specifically Used in Analysis of LOFT L2-2

4.1 Steady State Adjustment

The THYDE-P code is designed to analyze large scale commercial PWR LOCAs so that special treatments were needed to simulate the LOFT facility. In the LOFT program, two broken legs are separated and do not form a loop and the coolants in these legs were stagnant prior to the break. In the case of a postulated PWR LOCA, however, generally normal operational conditions are assumed prior to the break. Therefore, such a stagnant coolant condition in a primary loop need not be assumed for actual PWR plants.

In the present analysis of Test L2-2, the broken loop hot and cold legs were supposed to be connected and forming a loop with a very small amount of mass flow at the initial steady state. In order to obtain the desired initial conditions as a result of steady state adjustment⁽²⁾, a dummy pump with a dummy heat sink was placed at the break junction 6, prior to the break and it was made to vanish after the break. The pressure rise and the enthalpy drop at the dummy pump were assumed to be as follows:

$$\Delta p = 0.05 \text{ MPa}$$

$$\Delta h = -31 \text{ kcal/kgm}$$

where

$$\Delta p = p_8^A - p_7^E$$

$$\Delta h = h_8^A - h_7^E$$

In the present version of the THYDE-P code, heat transfer between coolant and structures is not taken into consideration, as was mentioned in Subsec. 3.7, so that the coolant temperatures near the vessel and near the break point were calculated to be nearly equal as a result of steady state adjustment without heat transfer between coolant structures. On the other hand, in the experiment a considerably large difference between these temperatures existed. This situation is clearly shown in Table 1. As will be discussed in the following sections, the differences in the initial temperature distributions in the broken legs may lead to considerably large differences in the hydraulic behaviors between the analysis and the experiment at the early stage of the blowdown.

4.2 Break Flow and Discharge Tank Simulation

Discharge coefficient was set to be 0.8 for the Moody correlation⁽⁶⁾ in the present analysis. The containment pressure was set to be:

$$p = 5 \text{ atm}$$

and the time constant to specify the decrease of the break pressure to the containment pressure just after the break was set to be 0.1 sec. When a reverse flow was calculated at the break point, the enthalpy of the coolant, which flowed into the system, could not be determined realistically because of a lack of the discharge tank model. In the present analysis, the coolant enthalpy for the reverse flow was set to be the value which had been calculated at the preceding time step. This approximation might be suitable for the case when the period of the reverse flow was short but might not be suitable when the reverse flow continued for a considerably long time. To avoid a

large amount of mass flow into the system through the break point, the loss coefficient for the reverse flow at the break node was assumed to be a large value:

$$k_8^{Er} = 50.0 \quad (19)$$

A reverse flow at a break point, in general, may be calculated in a reflooding phase as a result of depressurization due to low enthalpy ECC water. Therefore, a discharge tank model and the loss coefficient at the break point for the reverse flow play an important role at the latest stage of the reflooding phase.

4.3 Mass Conservation Equation

When this analysis was started out, the mass conservation equation for normal node n took the following form:

$$f_{nl} = G_n^A - G_n^E - \frac{L_n}{\Delta t} \{a_1(p_n^{\text{new}} - p_n^{\text{old}}) + a_2(h_n^{\text{new}} - h_n^{\text{old}})\} = 0 \quad (20)$$

where

$$a_1 = \left(\frac{\partial \rho}{\partial p} \right)_{h = h_n^{\text{new}}, p = p_n^{\text{new}}} \quad \text{and} \quad a_2 = \left(\frac{\partial \rho}{\partial h} \right)_{h = h_n^{\text{new}}, p = p_n^{\text{new}}} \quad (21)$$

But the applicability of this type of the mass conservation equation to the low pressure and low quality region was found to be questionable. Because the non-linearity of coolant density with respect to pressure and enthalpy becomes considerably high, the first order approximation to the density change in Eq. (20) gives a large truncation error at low pressure and low quality. Therefore, the mass conservation equation in the refill-reflood phase in the present analysis was revised as follows:

$$f_{nl} = G_n^A - G_n^E - \frac{L_n}{\Delta t} (\rho_n^{\text{new}} - \rho_n^{\text{old}}) = 0 \quad (22)$$

where

$$\rho_n^{\text{new}} = \rho(p_n^{\text{new}}, h_n^{\text{new}}) \quad \text{and} \quad \rho_n^{\text{old}} = \rho(p_n^{\text{old}}, h_n^{\text{old}}) \quad (23)$$

4.4 Non-Equilibrium Model

After ECC water was injected into the intact loop cold leg, thermal non-equilibrium effects due to low enthalpy ECC water became considerably large. Generally speaking, in the analyses by homogeneous equilibrium models, unrealistically large pressure decreases may be calculated due to very rapid condensation processes calculated in the nodes where high enthalpy primary coolant encounters with low enthalpy ECC water. Such a situation is prominent especially at low pressure. In the refill-reflood phase of Test L2-2, the enthalpy of ECC water was as low as 30 kcal/kgm whereas it was more than 700 kcal/kgm for the core nodes, so that such a situation was thought to be beyond the scope of the equilibrium models. In the present analysis, a simple non-equilibrium model was introduced, where the change of an average density had a time delay from that determined by the equilibrium model according to the following equations.

$$\frac{d\rho}{dt} = \frac{\rho - \rho^*}{\tau_\alpha} \quad (24)$$

$$\begin{aligned} \rho^* &= \alpha^* \rho_{gs} + (1 - \alpha^*) \rho_{fs} \\ \rho &= \alpha \rho_{gs} + (1 - \alpha) \rho_{fs} \end{aligned} \quad (25)$$

where

- ρ equilibrium density
- ρ^* non-equilibrium density
- α equilibrium void fraction
- α^* non-equilibrium void fraction

and τ_α was called a delay parameter which specifies the time delay of the average density of a node.

It should be noted that when τ_α asymptotically approached to be zero, the model reduces to the equilibrium model, i.e. $\rho = \rho^*$.

In this model, what

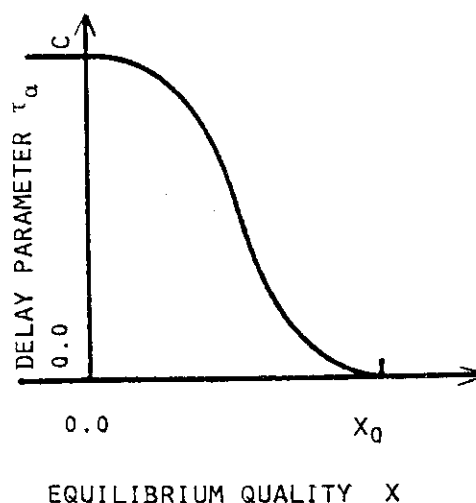


Fig. 7

Delay parameter τ_α in present analysis.

is the most difficult is to determine the delay parameter τ_α , which may depend on flow regimes, node geometries, pressure etc. In the present analysis, to evaluate the performance of this model, a simple formulation was assumed, where the parameter was assumed as a function of node volume and equilibrium quality x , which is related to the equilibrium void fraction α such that

$$x = \alpha \rho_{gs} / \{ \alpha \rho_{gs} + (1 - \alpha) \rho_{fs} \}.$$

When the quality is high in some node even at low pressure, rapid hydraulic transients are not calculated, so that τ_α can be assumed zero for a high quality region. The assumed function for τ_α in the present analysis, which is schematically shown in Fig. 4, is as follows:

$$\tau_\alpha^n = \begin{cases} 0 & x > x_0 \\ c_n/2 \{ \cos(\pi x/x_0) + 1 \} & 0 \leq x \leq x_0 \\ c_n & x < 0 \end{cases} \quad (26)$$

where the constant c_n is so given as to be proportional to the volume of each node with $c = 2$ sec. for the core nodes. Since there is no physical basis to determine τ_α until now, the value of the constant c was given, for the sake of convenience, by the following manner in the present analysis.

Equation (24) was differenced for node n as follows:

$$\rho_n^{*new} = \rho_n^{*old} + (\rho_n^{new} - \rho_n^{*old}) \Delta t / \tau_\alpha^n \quad (27)$$

where it should be noted that when $\tau_\alpha^n = \Delta t$, any time delay is not calculated, i.e. $\rho_n^{*new} = \rho_n^{new}$. On the other hand, the mass conservation equation for node n , i.e. Eq. (22), is expressed by using Eq. (27) as

$$W_n^E - W_n^A = (\rho_n^{new} - \rho_n^{*old}) / \tau_\alpha^n \quad (28)$$

which can be approximated as follows:

$$W_n^A - W_n^E \approx V_n (\rho_{fs}^n - \rho_{gs}^n) (\alpha_n^{new} - \alpha_n^{*old}) / \tau_\alpha^n \quad (29)$$

where the dependences of ρ_{fs}^n and ρ_{gs}^n on p_n are neglected. Equation (29) shows that $|W_n^A - W_n^E|$ is bounded by that in the extreme cases when $\alpha_n^{new} = 1$ and $\alpha_n^{*old} = 0$, or $\alpha_n^{new} = 0$ and $\alpha_n^{*old} = 1$, namely,

$$|W_n^E - W_n^A| < V_n (\rho_{fs}^n - \rho_{gs}^n) / \tau_\alpha^n \quad (30)$$

These idealized extreme cases are schematically shown in Fig. 8(a).

Now we assume

$$|w_n^A - w_n^E| < w_{ECC} \quad (31)$$

which means that the mass flow rate into the node where a condensation process is being calculated, for example, does not exceed that supplied by the ECCS. If Eq. (31) is not satisfied, unrealistic situation may be calculated due to a large amount of mass flowed into one node as is often experienced in the analyses by equilibrium models.

By comparing Eq. (30) with Eq. (31), τ_α^n has to satisfy the following equation.

$$\tau_\alpha^n > V_n (\rho_{fs}^n - \rho_{gs}^n) / w_{ECC} \quad (32)$$

in the extreme cases. Here we can approximately obtain at low pressure

$$\rho_{fs}^n - \rho_{gs}^n \approx 10 \quad (\text{kgm/m}^3)$$

$$w_{ECC} \approx 50 \quad (\text{kgm/sec}) .$$

Then, Eq. (32) gives

$$\tau_\alpha^n > 20 V_n \quad (\text{sec}) .$$

In the present analysis, since V_n 's for core nodes are 0.063, we assume c_n for core nodes as follows:

$$\begin{aligned} \tau_\alpha^n &\approx c_c && \text{at low pressure} \\ &= 2 \quad (\text{sec}). \end{aligned}$$

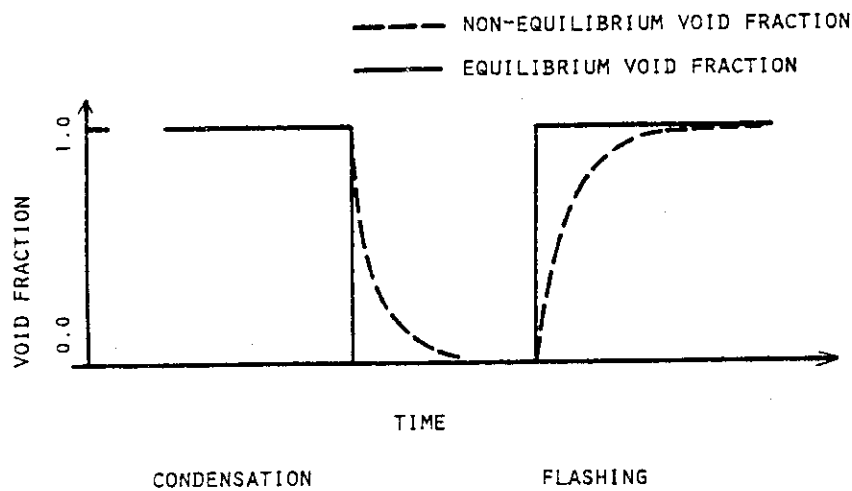
Because c_n is assumed to be proportional to node volume, it means

$$c_n = 2 V_n^* \quad (\text{sec})$$

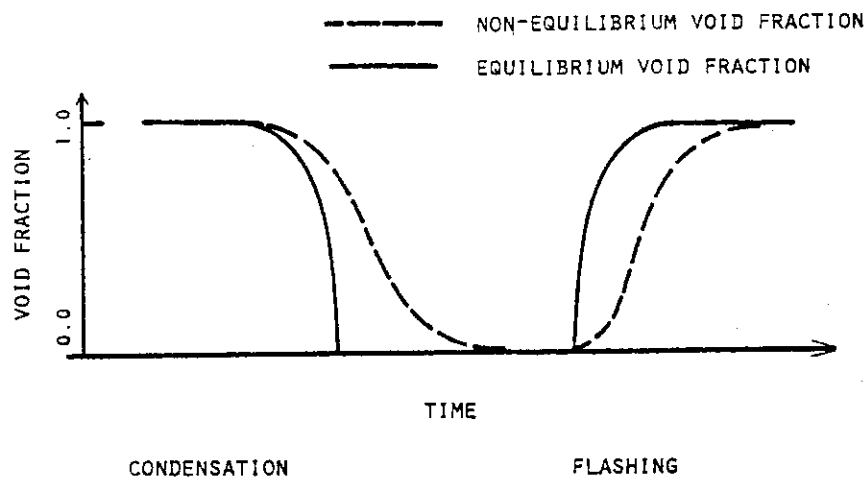
where

$$v_n^* = v_n / v_{\text{core}} \quad (33)$$

In Fig. 8, the typical changes of the equilibrium and non-equilibrium void fractions are shown for the condensation and flashing cases.



(a) Extreme cases



(b) Typical cases

Fig. 8 Schematic explanation for non-equilibrium model

5. Input Data and Results of Steady State Adjustment

The nodalization scheme in the present analysis is shown in Fig. 9(a), where numbering is made separately for nodes and junctions. Nodes from 1 to 7 and nodes from 8 to 10 form the broken loop hot and cold legs, respectively. Nodes from 11 to 21 are the components in the intact loop. The pressure vessel is expressed by an assembly of nodes from 22 to 33. The downcomer was simulated by a single node whose number was 22. The active core is nodalized into 6 nodes, i.e. nodes from 25 to 30, in which nodes 25 and 30 simulated the non-heated parts of the fuel rods. In these core nodes, the fuel and cladding are nodalized into 5 and 2 nodes radially, respectively, as shown in Fig. 9 (b). The upperhead was simulated by linkage node 33. Linkage nodes 34 and 35 are the reflood assist lines and 36 and 37 form the pressurizer surge line. Also linkage nodes 38, 39 and 40 are the ECCS pipings. The pressurizer, steam generator and accumulator are nodalized into special nodes 41, 42 and 43, respectively.

The input data used in the present analysis are listed in App. A. The major parts of them are summarized in this section with the results of steady state adjustment. The geometrical data and loss coefficients for each node are shown in Table 4 and 5, respectively.

(1) Break Data

The double-ended break was assumed to occur at junction 6 at 0.085 sec. after the test initiation. The flow areas of nodes 7 and 8, which are the same as the break flow areas after the break, were set to be 0.0084 m^2 .

(2) Initial Mass Flux, Enthalpy and Pressure Distribution

The initial mass flux and enthalpy at point A of node 1 were

$$G_1^A = 3.0644 \quad (\text{kgm/m}^2\text{sec})$$

$$h_1^A = 329.2 \quad (\text{kcal/kgm})$$

Some of the initial values as a result of steady state adjustment are shown in Table 1 with the experimental data and the initial pressure distribution along the intact loop is shown in Fig. 10.

(3) Core Data

The axial profile of the linear heat generation rate is shown in Fig. 8 with some of the experimental data. Input data for the core nodes were:

Initial power level 24.5 (MWt)
Initial heat flux

Node No	Heat flux (kcal/m ² s)
24	non-heated
25	73.6
26	124.2
27	94.7
28	31.4
29	non-heated

Numer of fuel rods 1300
Clad outer diameter 1.072×10^{-2} (m)
Clad thickness 6.172×10^{-4} (m)
Fuel pelet diameter 8.934×10^{-3} (m)
Rod pitch 1.430×10^{-2} (m)

(4) Steam Generator Data

The primary and secondary systems of the steam generator were simulated by nodes from 13 to 16 and node 42, respectively. Nodes 13 and 16 are the inlet and outlet plenums, respectively. Nodes 14 and 15 simulated the primary coolant in the U-tubes. The input data for these nodes were:

Plenums
Volume 0.353 (m³)
Hydraulic diameter 0.908 (m)
Height 0.518 (m)
U-tubes
Number of U-tubes 1845

Outer diameter	1.021	$\times 10^{-2}$	(m)
Height	2.483		(m)
Pitch	1.905	$\times 10^{-2}$	(m)
Secondary system			
Pressure	62.7		(atm)
Feed water enthalpy	196		(kcal/kgm)
Feed water mass flow rate	12.7		(kgm/sec)
Volume	6.66		(m ³)
Height	4.188		(m)
Hydraulic diameter	1.42		(m)
Water volume	1.01		(m ³)
Steam volume	5.65		(m ³)
Subcooled water level	0.6		(m)
Void fraction of saturated region	0.99		

Initial heat flux

Node No.	Heat flux (kcal/m ² sec)
14	29.3
15	9.78

The time for feed water shutdown was 0.002 sec. after the test initiation. In the present analysis, the effects by the electric heaters were neglected.

(5) Pressurizer Data

The initial pressure of the pressurizer was obtained as a result of steady state adjustment to be

$$p_{pzs} = 15.6 \text{ (MPa) .}$$

Input data for the pressurizer were:

Total volume	0.96	(m ³)
Water volume	0.605	(m ³)

Steam volume	0.355	(m ³)
Subcooled water level	1.0	(m)
Void fraction of saturated region	0.88	

The loss coefficients for the surge line are schematically shown in Fig.12(a).

(6) Pump Data

The pump data were:

Rated speed	3530	(rpm)
Rated flow	0.3155	(m ³ /sec)
Rated head	108.1	(m)
Rated torque	500.24	(J/rad)
Rated density	613.73	(kgm/m ³)
Moment of inertia	1.4382	(kgm m ² /rad ²)
Steady speed	1270	(rpm)

In Test L2-2, the pump power was on and the pump speed was almost constant throughout the experiment. Therefore, the constant pump speed option was used as follows:

$$a = a_0$$

where

a_0 : initial normalized pump speed.

(7) ECCS Data

ECC water was assumed to be injected into mixing junction 26. The input data for ECCS were:

Accumulator		
Liquid volume	2.63	(m ³)
Gas volume	1.05	(m ³)
Liquid enthalpy	27.8	(kcal/kgm)

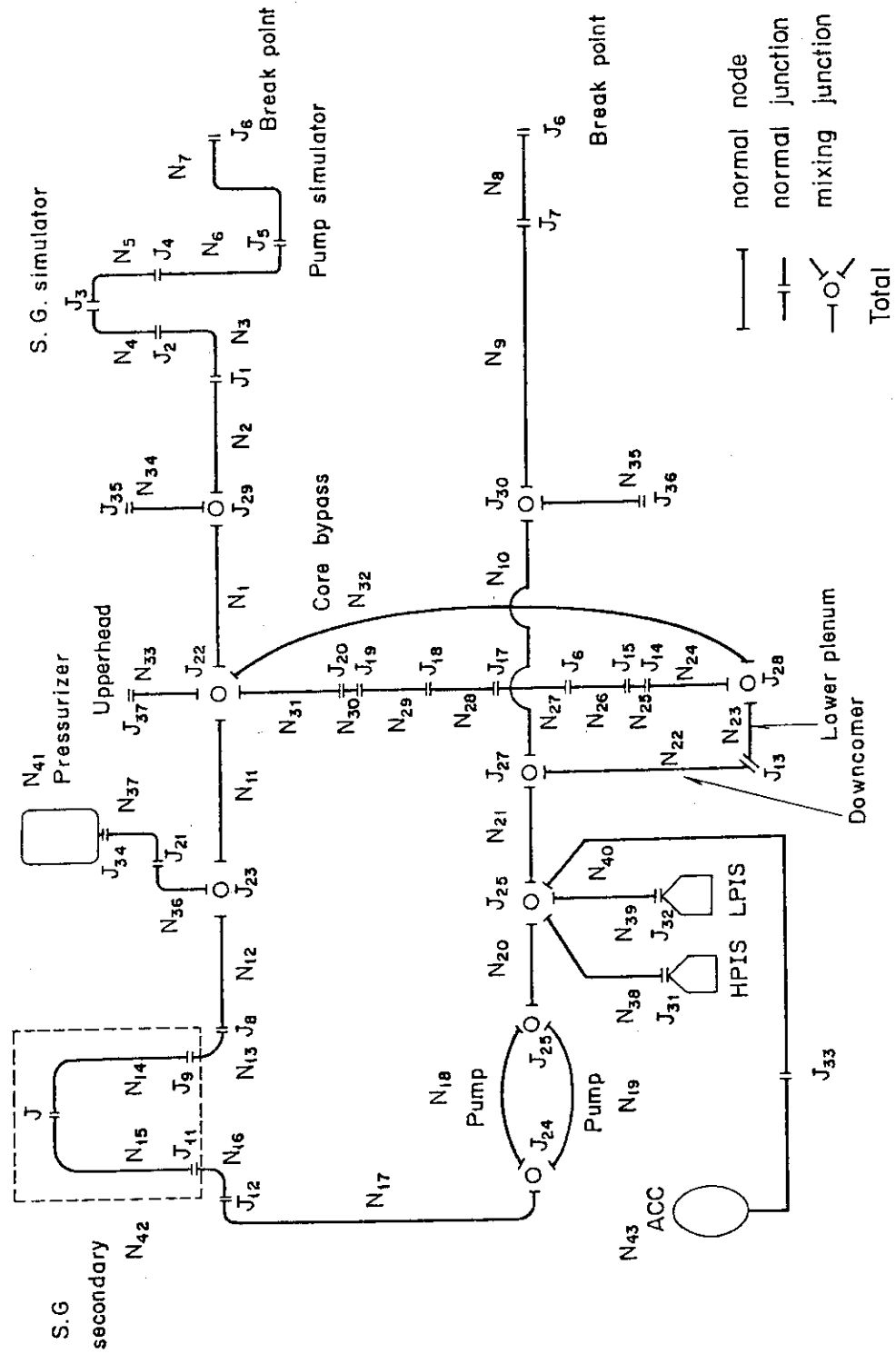


Fig. 9 Nodalization for LOFT LOCE L2-2

(a) Major components

Pressure

40.56 (atm)

HPIS and LPIS

Liquid enthalpy

24.0 (kcal/kgm)

HPI and LPI were assumed to start at 12 and 29 sec. after the test initiation, respectively, and the mass flow rates were given by inputs as time tables consistent to the experimental data.

(8) Steam Generator and Pump Simulators

The simulated SG and pump in the broken loop hot leg were nodalized into nodes from 3 to 7. The loss coefficients in these nodes are schematically shown in Fig. 12(b).

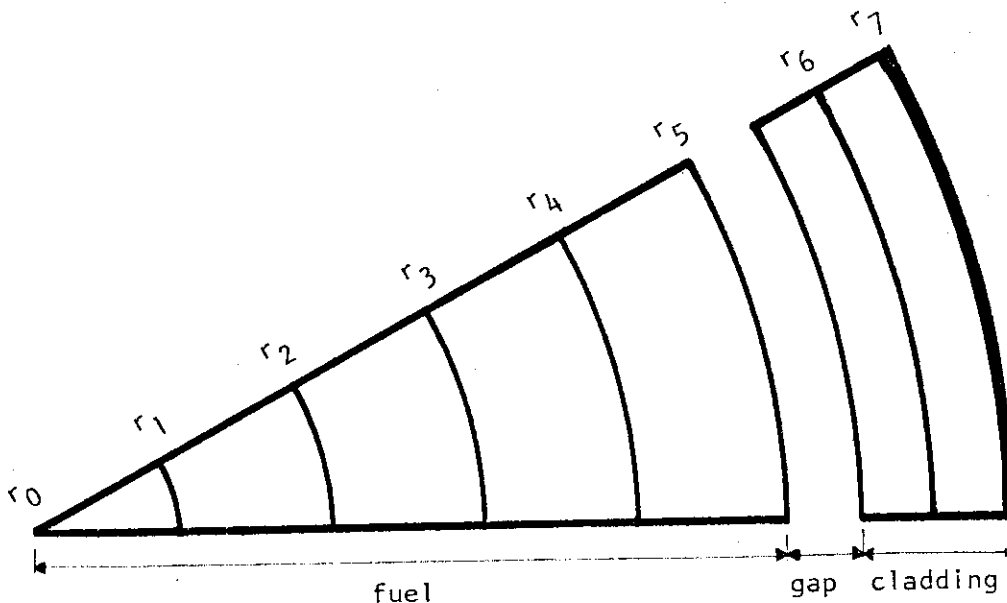


Fig. 9 Nodalization for LOFT LOCE L2-2

(b) Within fuel rod

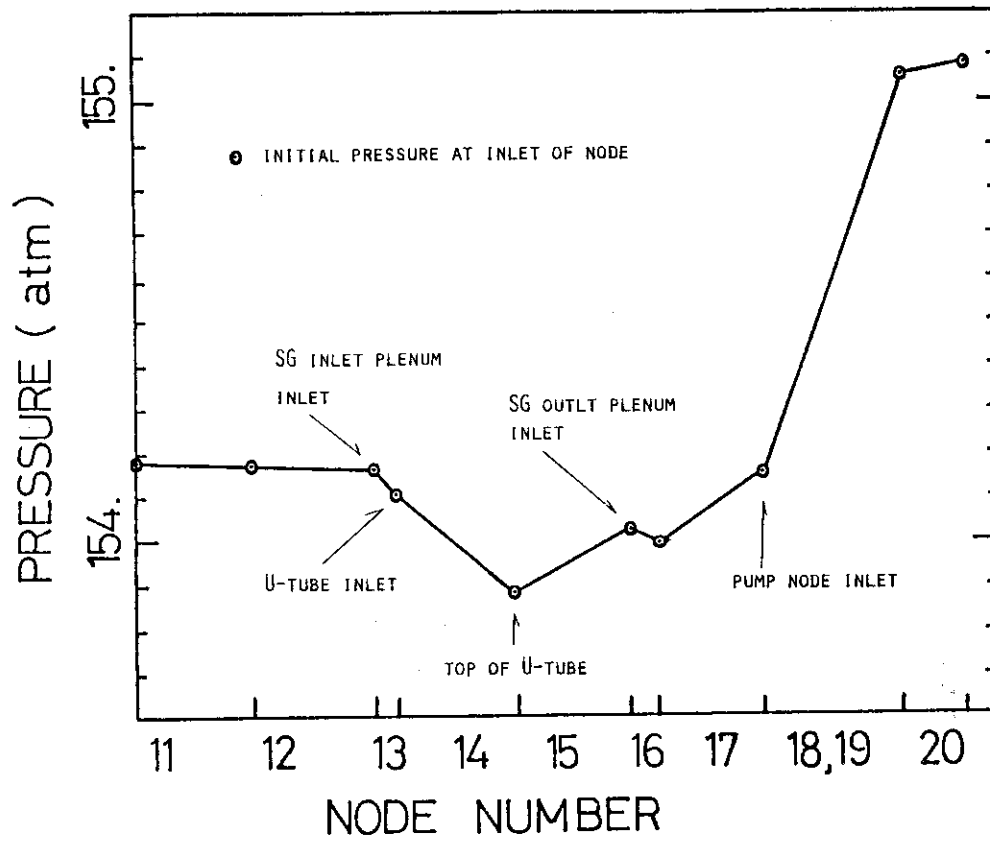


Fig. 10 Initial pressure distribution along intact loop

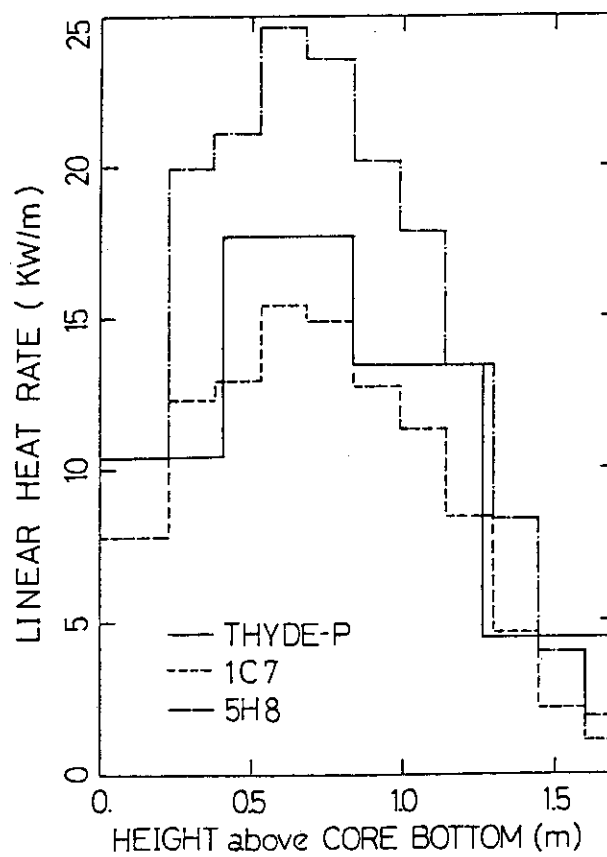
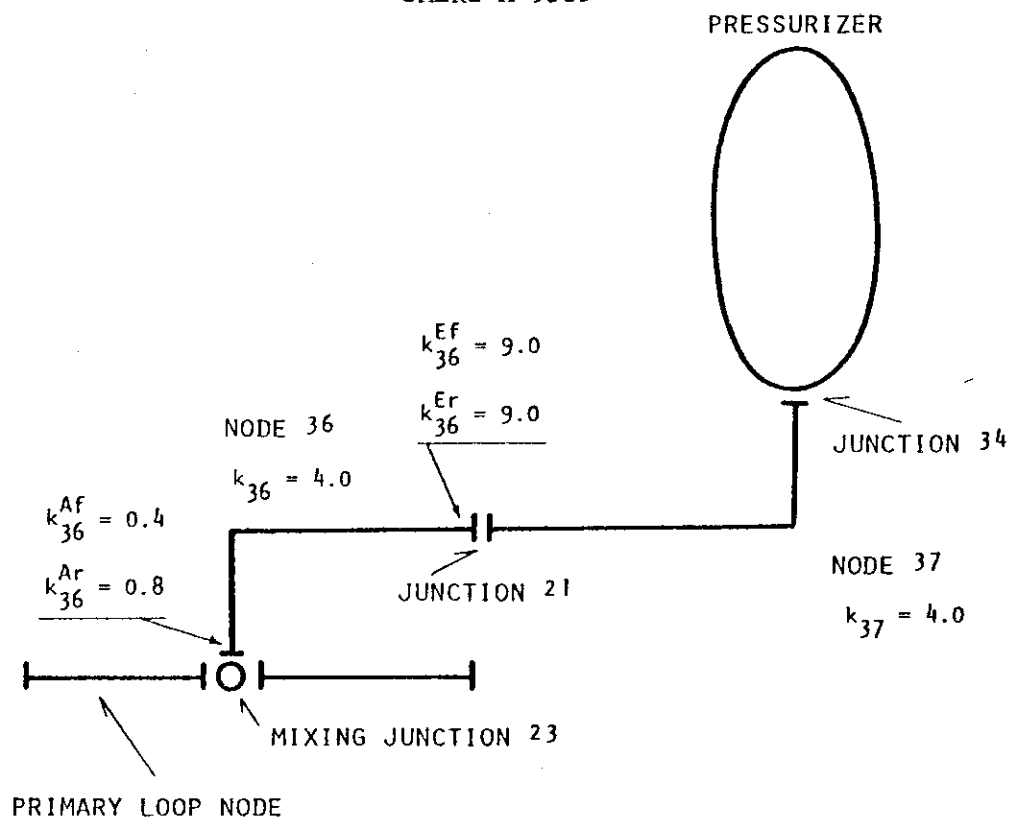
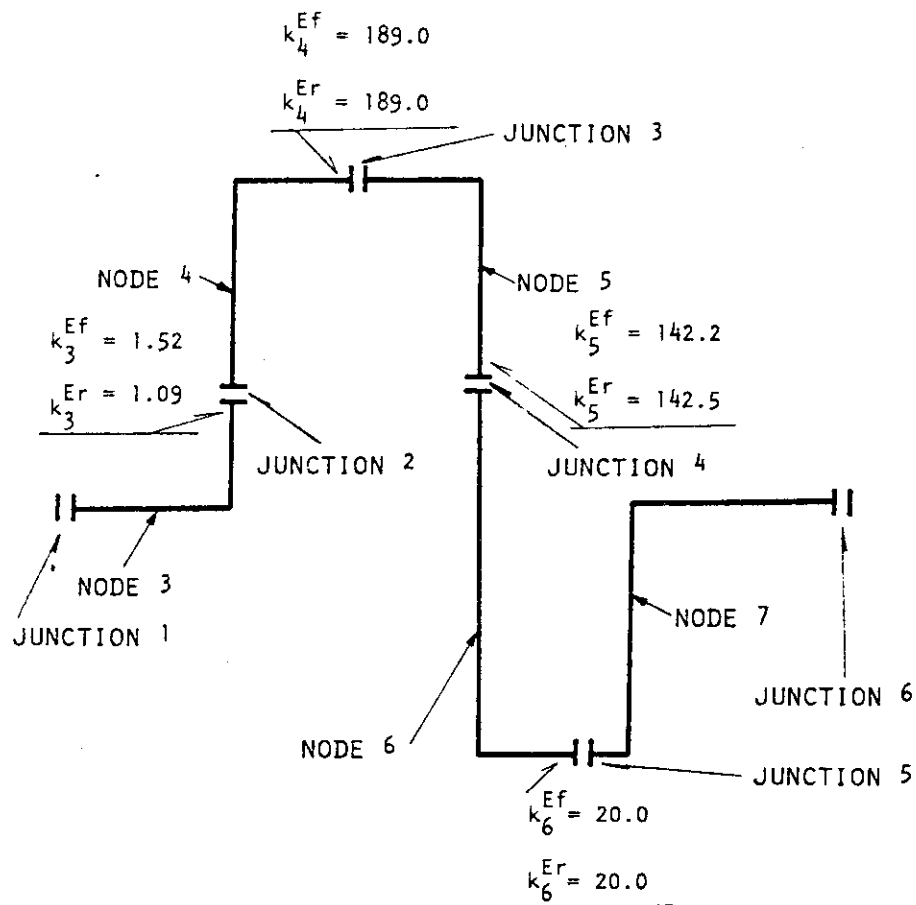


Fig. 11 Initial linear heat generation rate



(a) Pressurizer surge line



(b) Simulated SG and pump

Fig. 12 Loss coefficients

Table 4 Node Geometrical Data

Node No.	Description	Flow Area A (m ²)	Node Length L (m)	Node Height H _L (m)
1	Broken loop hot leg	0.06344	1.332	0.0
2	Broken loop hot leg	0.06344	0.6965	0.0
3	Broken loop hot leg	0.00836	1.517	0.7174
4	Broken loop hot leg	0.09539	3.228	2.705
5	Broken loop hot leg	0.09539	3.228	-2.705
6	Broken loop hot leg	0.01271	2.423	-2.039
7	Broken loop hot leg	0.008365	1.883	1.322
8	Broken loop cold leg	0.008365	0.4877	0.0
9	Broken loop cold leg	0.06344	0.6965	0.0
10	Broken loop cold leg	0.06344	0.9510	0.0
11	Intact loop hot leg	0.06344	2.6160	0.0
12	Intact loop hot leg	0.06299	2.643	0.2423
13	SG inlet plenum	0.6481	0.5175	0.5175
14	SG U-tube	8.187 E-5	2.568	2.483
15	SG U-tube	8.187 E-5	2.568	-2.483
16	SG outlet plenum	0.6481	0.5175	-0.5175
17	Crossover leg	0.06793	2.429	-1.523
18	Pump	0.09446	1.867	1.281
19	Pump	0.07273	3.111	1.281
20	Intact loop cold leg	0.0597	1.399	0.0
21	Intact loop cold leg	0.06343	0.5313	0.0
22	Downcomer	0.1604	4.256	-4.256
23	Lower plenum	0.7917	0.7318	0.0
24	Mixing box	0.1532	0.4285	0.4285
25	Active core	1.143 E-4	0.09423	0.09423
26	Active core	1.143 E-4	0.4191	0.4191
27	Active core	1.143 E-4	0.4191	0.4191
28	Active core	1.143 E-4	0.4191	0.4191
29	Active core	1.143 E-4	0.4191	0.4191
30	Active core	1.143 E-4	0.01753	0.01753
31	Upper core structures	0.2387	1.668	1.668
32	Core bypass	4.766 E-3	4.146	4.146
33	Upper head	0.2306	0.9144	0.9144
34	Reflood assist line	0.03871	4.048	0.8620
35	Reflood assist line	0.03871	4.840	0.6075
36	Pressurizer surge line	1.452 E-3	4.592	0.4255
37	Pressurizer surge line	1.452 E-3	4.767	0.7678
38	ECCS piping	6.221 E-3	5.5	0.0
39	ECCS piping	6.221 E-3	5.5	0.0
40	ECCS piping	6.221 E-3	58.0	0.0

Table 5 Loss Coefficients

Node No.	k	k ^{AF}	k ^{Ar}	k ^{Ef}	k ^{Er}
1	0.019	0.400	0.800	0.800	0.800
2	0.016	0.0	0.0	0.0	0.0
3	0.020	0.319	0.754	1.52	1.09
4	0.011	0.0	0.0	189.	189.
5	0.052	0.0	0.0	142.	198.
6	0.020	0.0	0.0	20.0	20.0
7	0.021	0.0	0.0	-1.18 E5	0.0
8	0.011	0.0	0.0	0.754	0.391
9	0.035	0.0	0.0	0.0	0.0
10	0.029	0.0	0.0	3.58	3.00
11	0.020	0.400	0.800	0.0	0.0
12	0.020	0.0	0.0	0.815	0.406
13	0.020	0.0	0.0	0.0	0.0
14	0.554	0.345	0.588	0.0	0.0
15	0.020	0.0	0.0	0.588	0.345
16	0.019	0.0	0.0	0.0	0.0
17	0.020	0.403	0.801	0.0	0.0
18	0.109	0.0	0.0	0.0	0.0
19	0.016	0.0	0.0	0.0	0.0
20	0.013	0.0	0.0	0.0	0.0
21	0.021	0.0	0.0	3.58	3.00
22	0.020	0.620	0.620	3.50	3.50
23	0.038	0.0	0.0	0.0	0.0
24	10.1	0.0	0.0	0.0	0.0
25	3.31	0.0138	9.34 E-4	0.0	0.0
26	3.33	0.0	0.0	0.0	0.0
27	3.49	0.0	0.0	0.0	0.0
28	3.15	0.0	0.0	0.0	0.0
29	3.33	0.0	0.0	0.0	0.0
30	3.33	0.0	0.0	0.143	0.170
31	20.9	0.0	0.0	0.0	0.0
32	40.6	0.0	0.0	0.0	0.0
33	0.10	0.0	0.0	0.0	0.0
34	0.10	0.400	0.800	0.0	0.0
35	0.10	0.400	0.800	0.0	0.0
36	4.0	0.400	0.800	9.00	9.00
37	4.0	0.0	0.0	0.0	0.0
38	10.0	0.400	0.800	0.0	0.0
39	10.0	0.400	0.800	0.0	0.0
40	10.0	0.400	0.800	0.0	0.0

6. Calculated Results and Discussion

In a postulated LOCA, it has been conventional to divide the whole process into three phases, i.e. blowdown, refill and reflood phases. In Test L2-2, however, it seems difficult to distinguish these phases. As for the end of blowdown, it may be said to occur at 36 sec. after the break in the present analysis, since it is often defined as the time when the system pressure has almost decreased to the containment pressure. Therefore, we call the period before 36 sec. the blowdown phase and the period after that refill-reflood phase for convenience's sake. As will be shown in this section, in the refill-reflood phase, the effects of ECC water on thermal-hydraulics became apparent and rapid condensation processes were calculated.

The chronology of events is shown in Table 6. Detailed discussions about the events will be made in the following subsections.

6.1 Cladding Surface Temperature and Thermal-Hydraulic Behavior in Core

The calculated cladding surface temperatures at nodes 27 and 28 are shown in Figs. 13(a) and (b), respectively, along with the experimental data. In those figures, the heights of the measurement points from the bottom of the core are nearly equal to those of the calculated results, but their horizontal locations in the core are arbitrarily chosen.

The calculated heat transfer coefficients at nodes 27 and 28 are shown in Figs. 14(a) and (b), respectively, with the heat transfer modes. The mass flux and coolant quality calculated at node 28 are shown in Figs. 15 and 16, respectively. The experimental core flow data are not available due to the failure of the instrumentation. When Fig. 13(b) is compared with Figs. 15 and 16, we can understand that the calculation clarified the fact that the cladding surface temperature was closely coupled with the thermal-hydraulic behavior of coolant.

As shown in Figs. 13(a) and (b), the trends of the calculated cladding surface temperatures at nodes 27 and 28 were very similar to those observed in the experiment in the sense that a peak was calculated at the very early stage of the blowdown and the final quenching was calculated at about 50 sec. after the rupture. The time when the quenching was calculated in the blowdown, however, was earlier than that observed. And the calculated results

Table 6 Chronology of Events

Events	Time after Test Initiation (sec)	
	Experiment	THYDE-P
Subcooled blowdown ended (a)	0.07	0.05
Reactor SCRAM	0.085	0.085*
Earliest departure of cladding temperature from liquid saturation temperature	1.0	1.0
Subcooled blowdown ended (b)	3.8	2.6
Maximum cladding temperature attained	5.8	3.2
Earliest return of cladding temperature to fluid saturation temperature	8.0	3.4
HPIS injection initiated	12	12*
ACC injection initiated	18	17
LPIS injection initiated	29	29*
Lower plenum filled with liquid	35	41
Saturated blowdown ended	44	36
ACC liquid flow ended	49	not ended
Core volume reflood	55	55

(a) End of subcooled blowdown is defined as the occurrence of the first phase transition in the system other than at the pipe break location.

(b) End of subcooled blowdown is defined as the completion of subcooled fluid discharge from the break (hot and cold legs) in the broken loop.

* indicates that the value was set by an input.

showed about 10 sec. delay for the final quenching as compared with the experimental data.

First of all, the calculated results of thermal-hydraulic behavior in the core region is discussed for the blowdown and refill-reflood phases, separately in the following.

(1) Blowdown Phase

The calculated cladding surface temperatures, heat transfer coefficients, mass fluxes and coolant qualities at the heated core nodes at the early stage of the blowdown are shown in Figs. 17, 18, 19 and 20, respectively. As shown in Fig. 19, the absolute values of the mass fluxes decreased from 0.5 sec. and the flows became stagnant at about 2 sec. Accompanied by the decreases of the flows, the coolant qualities increased as shown in Fig. 20. At node 27, the first DNB was calculated at about 1 sec., when the CHF value was predicted by the modified Zuber pool CHF correlation^{(20), (21)}. Just after the DNB was calculated, heat transfer modes changed from mode 4-3 (pool transition boiling) to mode 4-4 (pool film boiling) as shown in Fig. 18. After about 2 sec., the mass flux started to increase and the coolant quality decreased since relatively low enthalpy coolant flowed into the core through the downcomer and lower plenum. At about 3.4 sec., the mass flux exceeded G_{min} ($= 300 \text{ kg/m}^2 \text{ sec}$) and the heat transfer mode changed from mode 4-4 to mode 4-1 (forced-convection transition boiling). Once mode 4-1 was assumed, the cladding surface temperature rapidly decreased to almost the coolant saturation temperature and finally the heat transfer mode changed to mode 3 (nucleate boiling), when the CHF value was calculated by the Biasi correlation.

Cladding surface temperature behavior such as the occurrence of the peak is closely related to hydraulics. In this sense, the reason why the quenching was calculated to occur earlier than the experiment might be attributed to hydraulics. For example, the calculated mass fluxes at the core nodes might be overestimated from 4 to 6 sec.

As shown in Fig. 15, the calculated mass flux at core node 28 became less than G_{min} at about 10 sec. and coolant became almost stagnant at about 16 sec. In accordance with the decrease of the flow, the calculated coolant quality again increased and the second DNB was calculated at 16 sec. under the pool flow condition.

(2) Refill-Reflood Phase

The calculated cladding temperatures at nodes 27 and 28, which are shown in Figs. 13(a) and (b), respectively, started to increase again at about 30 sec. That was because that coolant became superheated and the calculated heat transfer coefficients suddenly decreased as shown in Figs. 14(a) and (b). After about 40 sec., ECC water began to flow into the core nodes and coolant returned to be saturated. At about 50 sec., the coolant quality became below 5% and therefore the heat transfer mode changed to mode 4-5 (pool transition boiling). Then the cladding surface temperature suddenly decreased and finally the mode returned to mode 3 (nucleate boiling). The result showed about 10 sec. delay for the final quenching as compared with the experimental data. The delay parameters assigned to the nodes along the path of ECC water have large effects on the time during which condensation processes proceeded, so that the final quenching time is hoped to be improved by introducing a realistic model to estimate the delay parameters. It should be noted about the observed cladding surface temperature that the thermocouples are attached on the outside surface of the cladding so that they tend to indicate much faster quenching time, i.e. more than 10 sec⁽¹⁵⁾.

6.2 ECC Water penetration through Core

The calculated mass fluxes and coolant enthalpies at the inlet and outlet points of nodes 27 and 28 in the refill-reflood phase are shown in Figs. 21 and 22, respectively. It is clearly shown in these figures that the rapid condensation processes were successively calculated at nodes 27 and 28. The rapid condensation process first started at node 27 at about 50 sec. and mass flow into the node suddenly increased until $|G_{27}^A - G_{27}^E| \approx 180 \text{ kgm/m}^2\text{sec}$. If the non-equilibrium model were not to be used it might become much more larger and the calculation might surely fail. After the maximum value was reached, it was gradually decreased to zero. In this period, the equilibrium void fraction α_{27} was already zero, but the non-equilibrium void fraction α_{27}^* was still not zero and was decreasing obeying Eq. (24). Next the rapid condensation started at node 28 at about 53 sec.

The maximum value of $|G^A - G^E|$ and the time during which the condensation proceeds are strongly dependent on the delay parameter. For example,

if the delay parameters were assumed to be infinitely large, ECC water might go through the downcomer, lower plenum and core rapidly. It is because no mass accumulation is calculated, i.e. $d\dot{\rho}/dt = 0$. Therefore, it is an important problem to develop a model to evaluate the delay parameters. The experimental results such as those in the LOFT program are hoped to give some important information to improve or upgrade the THYDE-P code concerning the non-equilibrium model.

6.3 Broken Loop Hot Leg

The calculated mass flow rate and coolant density at the broken loop hot leg are shown in Figs. 23 and 24, respectively. The calculated mass flow rate, which is identical with the break flow, was overestimated from 4 to 12 sec. in comparison with the experimental data. In this period, the flow was calculated by the Moody correlation⁽⁶⁾ with the discharge coefficient $c_d = 0.8$. It could be said that the overestimation of the flow might be brought about by relatively low enthalpy coolant from the core region. In fact the calculated coolant density in this period was larger than the experimental density as shown in Fig. 24. In the calculation, the core flow from 4 to 8 sec. was very large and the coolant quality became low as mentioned in Subsec. 6.1.

After about 40 sec. in the experiment, ECC water was considered to be entrained in the steam flow and to increase the mass flow and coolant density at the broken loop hot leg as shown in the figures. On the other hand in the analysis, such phenomena were not calculated.

6.4 Broken Loop Cold Leg

The calculated mass flow rate and coolant density at the broken loop cold leg are compared with the experimental data in Figs. 25 and 26, respectively. A critical flow was calculated at the break point until 3.9 sec. by the modified Zaloudek correlation⁽⁵⁾ and from 3.9 to 18 sec. by the Moody correlation⁽⁶⁾. After 18 sec., an inertial flow calculation⁽²⁾ was made.

There are two prominent differences between the calculated and experimental results as follows:

- (1) The calculated mass flow rate was underestimated at the early stage of the blowdown,
- (2) After about 30 sec., in the analysis, the coolant in the leg became subcooled, but in the experiment it still remained saturated.

One of the reason for (1) is thought to come from the discharge coefficients. The method to connect the critical flows calculated by these two correlations at the transition quality 0.02⁽²⁾ should be modified since the discharge coefficient for the modified Zaloudek correlation⁽⁵⁾ seems larger than the present values when the calculated results are compared with the experimental data. This underestimation of the mass flow rate in the broken loop cold leg and the overestimation of the mass flow rate in the intact loop cold leg, which will be discussed later, may have brought about the over-estimated core flow in the blowdown phase.

As to the difference mentioned in (2), the nodalization of the downcomer region might be relevant. In the present nodalization, where the downcomer was simulated by a single node, bypassing water to the broken loop cold leg had to become subcooled soon after ECC water reached the downcomer top. The fact implies that two-dimensional effects in the downcomer flow have to be taken into consideration in some way. If the downcomer is nodalized into more than two nodes azimuthally, a reverse flow from the core, which has high enthalpy and warms bypassing water, is able to be simulated even in the downcomer penetration period whereas the bypassing flow might become saturated. Such a situation was calculated in an analysis made not for Test L2-2 but for a large scale PWR LOCA with split downcomer nodalization as shown in Fig. 27.

Concerning the difference (2), heat transfer between coolant and structures might also be relevant. After 30 sec. in both the experiment and analysis, the coolant in the broken loop cold leg tended to be almost stagnant. Therefore the heat addition to the coolant from ducts might not be negligibly small. Another reason for (2) also existed in the present break flow calculation when a reverse flow was calculated. After 40 sec., reverse flow was calculated for a considerably long time, during which subcooled water flowed into the system according to the present break flow model. In the experiment, however, steam or air-steam mixture might flow into the duct from the

suppression tank header when reverse flow occurred. In the present analysis, the effects of subcooled water flowed into the system was made small in comparison with those of ECC water by a large loss coefficient at the break node for a reverse flow. It is desired, therefore, to implement a discharge tank model.

6.5 Intact Loop Hot Leg and Pressurizer

The calculated mass flow rate and coolant density at intact loop hot leg (node 11) are shown in Figs. 28 and 29, respectively, along with the experimental data. The calculated mass flow rate did not agree well with the experimental data at the blowdown phase. The reason is not clear because of lack of the experimental data. In spite of the fact that the hydraulic behavior in the intact loop hot leg is highly dependent on the pressurizer, no qualified engineering units data (QEUD) is available for the pressurizer and its surge line. The overestimation of the mass flow rate in the intact loop hot leg until 4 sec. seems to be due to large outsurge flow from the pressurizer. Therefore, one of the reasons for the overestimation may exist in the loss coefficients in the surge line, whose values are shown in Fig. 12. The calculated results of pressure and water level at the pressurizer are shown in Fig. 30. It should be noted that the definition of the water level⁽²⁾ in THYDE-P is different from so called "mixture or collapsed level".

6.6 Intact Loop Cold Leg and Primary Coolant Pumps

The calculated mass flow rate and coolant density in the intact loop cold leg at node 20, which is located between the ECC injection point and primary coolant pumps, are shown in Figs. 31 and 32, respectively, along with the experimental data. Both the mass flow rate and coolant density are overestimated at the blowdown phase. The reasons are not understood but the pump performance might be relevant. As shown in Fig. 31, the calculated flow was almost stagnant in the refill-reflood phase, while in the experiment, many sharp peaks for flow and density were observed as shown in Figs. 31 and 32. It implies existence of drops or slugs of subcooled water in this region in the experiment.

In the refill-reflood phase, the coolant behavior in the intact loop

cold leg played an important role. The calculated mass fluxes and coolant enthalpies at the inlet and outlet points of node 20 in the refill-reflood phase are shown in Figs. 33 and 34, respectively. There are two prominent negative and positive peakes in the calculated mass flux at the outlet point of node 20 as shown in Fig. 33. These two peakes were calculated according to the following sequence.

- (1) At about 33 sec. at the outlet point of node 20, flow reversal was calculated to occur and subcooled ECC water started to flow into the node, which was filled with superheated steam at the time.
- (2) Once the flow reversal was calculated, a large amount of ECC water flowed into the node until the node was completely filled with subcooled water. In conjunction with this condensation process, an unrealistically large pressure drop might surely be calculated without the non-equilibrium model.
- (3) At about 41 sec. also in node 20, boiling was calculated to start due to high enthalpy steam from the steam generator through the pump nodes until about 44 sec., when the coolant at the outlet point of node 20 became again superheated.

During the period when ECC water flowed into node 20, the mass flow to the core nodes considerably decreased. The phenomena had an effect to delay the core reflooding time. On the other hand, the boiling calculated at node 20 supplied much water into the core region so that it had the opposite effect. These processes described in (1), (2) and (3) are clearly shown in the density change in Fig. 32, which shows coolant from about 33 to 41 sec. were subcooled. In the experiment, however, such distinct over-all condensation and boiling were not observed but existence of drops or slugs were implied. These facts imply that non-homogeneous and non-equilibrium effects might play an important role in this period in the experiment.

The calculated normalized pump speed is shown in Fig. 35 along with the experimental data. In the present analysis, the pump speed is assumed to be constant throughout the analysis. The calculated pump head is shown in Fig. 36. The calculated normalized pump volumetric flow rate and coolant quality

at pump node 18 are shown in Fig. 37. Since the pump speed was assumed to be constant, the pump head was calculated as a function of the pump flow and void fraction only according to the homologous head curves. From about 40 to 44 sec., the coolant at the pump node became superheated, so that the two-phase head multiplier m_h was calculated to be zero as shown in Fig. 6. In this period, the normalized pump flow is, as shown in Fig. 37, as follows:

$$w \approx 20 \quad .$$

Then

$$\begin{aligned} a/w &\approx 0.36/2.0 \\ &= 0.18 \quad . \end{aligned}$$

The homologous head curve indicated by HWN in Fig. 4 shows that

$$h_{\text{head}}/w^2 \approx -0.6$$

which gives

$$h_{\text{head}} \approx -2.4 \quad (-260 \text{ m})$$

This is the reason why the calculated pump head was negative and very large in this period.

6.7 ECC Water Penetration through Downcomer

The calculated mass fluxes and coolant enthalpies at the inlet and outlet points of downcomer node 22 are shown in Fig. 38 and 39, respectively. The calculated mass fluxes indicate that the first flashing started at about 4.5 sec. at the early stage of the blowdown and the increase of the void fraction continued until about 20 sec. Then effects of ECC water appeared in the following way. Low enthalpy ECC water prematurely penetrated into the downcomer node but was again pushed out due to a boiling process caused by a high enthalpy flow from the core nodes. As shown in Fig. 39, such processes repeated from 20 to 36 sec. Finally, at about 36 sec., a constantly forward flow was established at the inlet and the final condensation process was calculated to start. Therefore, we can define that the initiation of refill

was about 36 sec., in the present analysis.

6.8 Steam Generator

The calculated coolant temperatures at the inlet plenum and outlet plenum of the steam generator are shown in Fig. 40. The qualified engineering units data for these properties are not available. The calculated results concerning the steam generator primary system were as follows:

- (1) Flashing started at the inlet plenum just after the break,
- (2) In the outlet plenum, the flashing started at about 3.7 sec., after which the coolant temperatures at both inlet and outlet plenums became nearly equal,
- (3) At about 30 sec., the outlet plenum became filled with superheated steam due to the heat addition from the secondary system, so that the coolant temperature departed from the coolant saturation temperature.

The calculated pressure at the SG secondary and primary systems are shown in Fig. 41. The secondary system behaved like a heat reservoir since feed and outsurge flow were shut off just after the break. In the present analysis, the calculated pressure at the secondary system first increased due to the heat addition from the primary system, and then gradually decreased from about 4 sec. due to the heat removal to the primary system. After the SG secondary system changed from heat sink to heat source, the DNB was calculated at the primary side wall. Therefore, the pressure difference between the secondary and primary systems was calculated to be large in the refill-reflood phase as shown in Fig. 41.

6.9 Accumulator

The calculated mass flow rate and pressure at the accumulator are shown in Figs. 42 and 43, respectively, along with the experimental data. Negative values of the mass flow rate data indicate injection. The experimental mass flow rate were calculated from the experimental volumetric flow rate data

assuming the coolant density constant.

The time when the injection was calculated to start was a little earlier than the experimental data. The fact implies that the pressure at the injection point, i.e. mixing junction 26, was well simulated but a little underestimated in comparison with the experiment. The calculated enthalpies at the accumulator, the inlet and outlet points of node 40 are shown in Fig 44. It took about 10 sec. for the enthalpy of node 40 (ACC side) to become equal to the accumulator enthalpy (40 kcal/kgm).

6.10 Temporal Behavior of Pressure

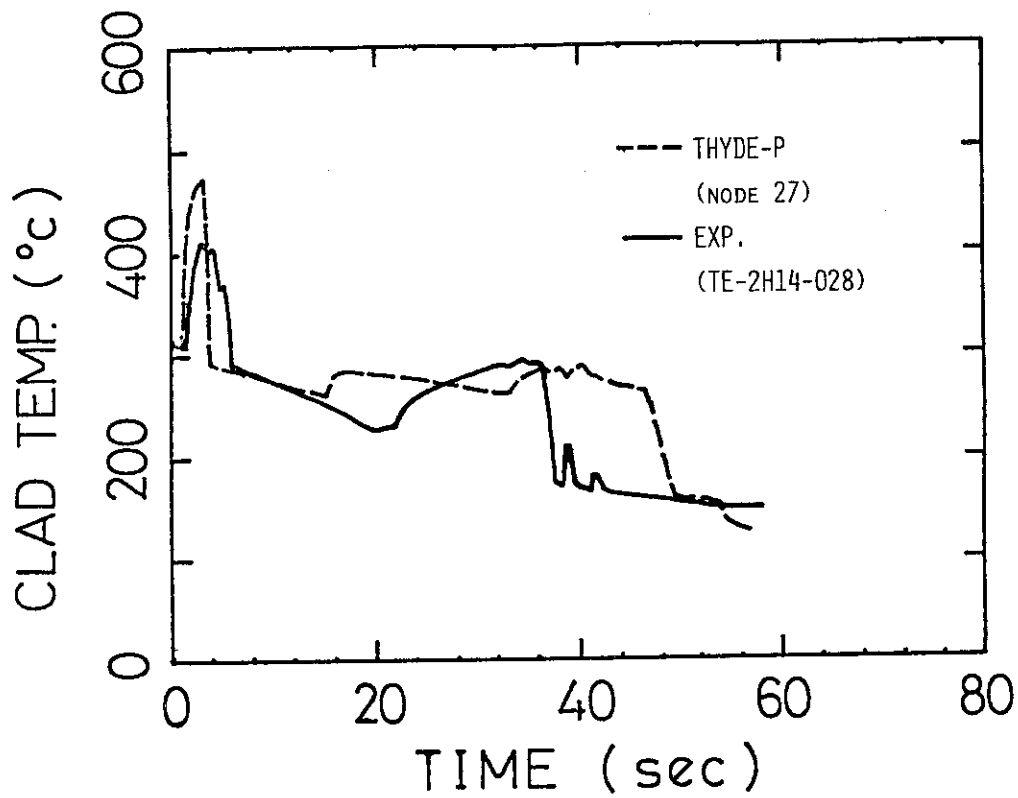
Generally speaking, the calculated pressures at nodes in the hydraulic network were in good agreement with the experimental data. The calculated pressure at just above the active core, i.e. node 31, is shown in Fig. 45 along with the experimental data. A good agreement was obtained.

6.11 Time Step Width and CPU Time

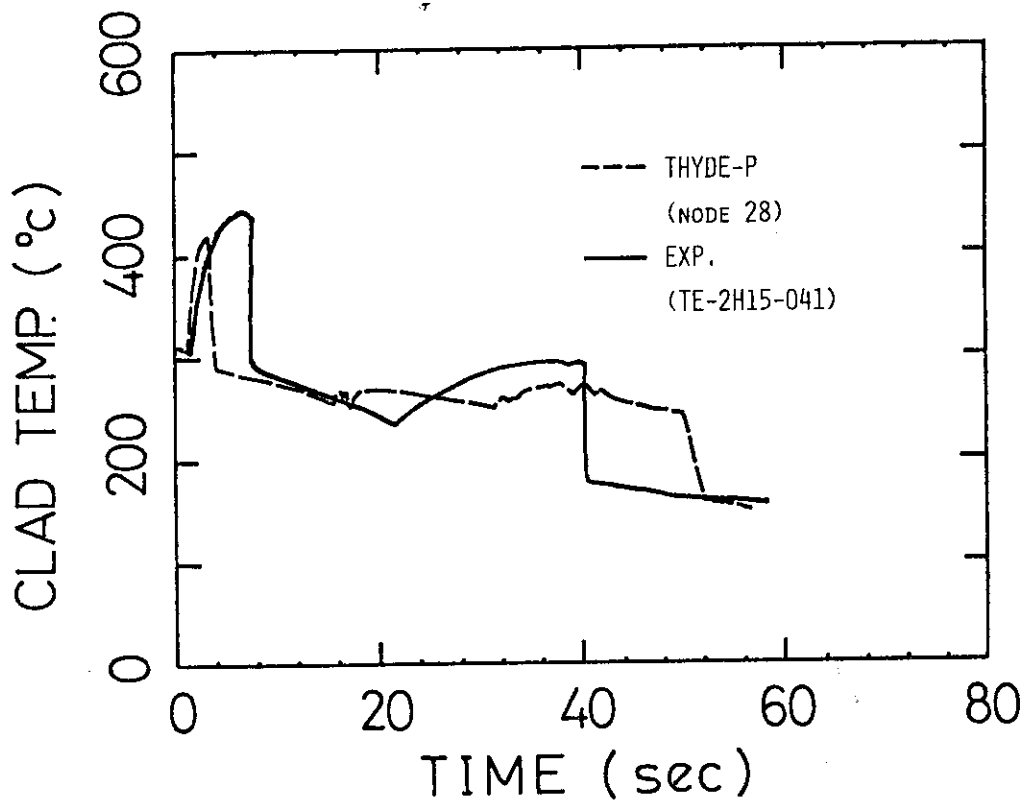
The CPU time required for the present calculation by a FACOM M200 computer was about 2 hours. The maximum time step width allowed in the present calculation was given as inputs as follows:

$$\Delta t = \begin{cases} 0.001 \text{ sec.} & \text{for } 0.0 < t < 0.3 \text{ sec.} \\ 0.004 \text{ sec.} & \text{for } 0.3 < t \end{cases}$$

The whole calculation proceeded by the maximum time step width except when rapid transients were calculated.

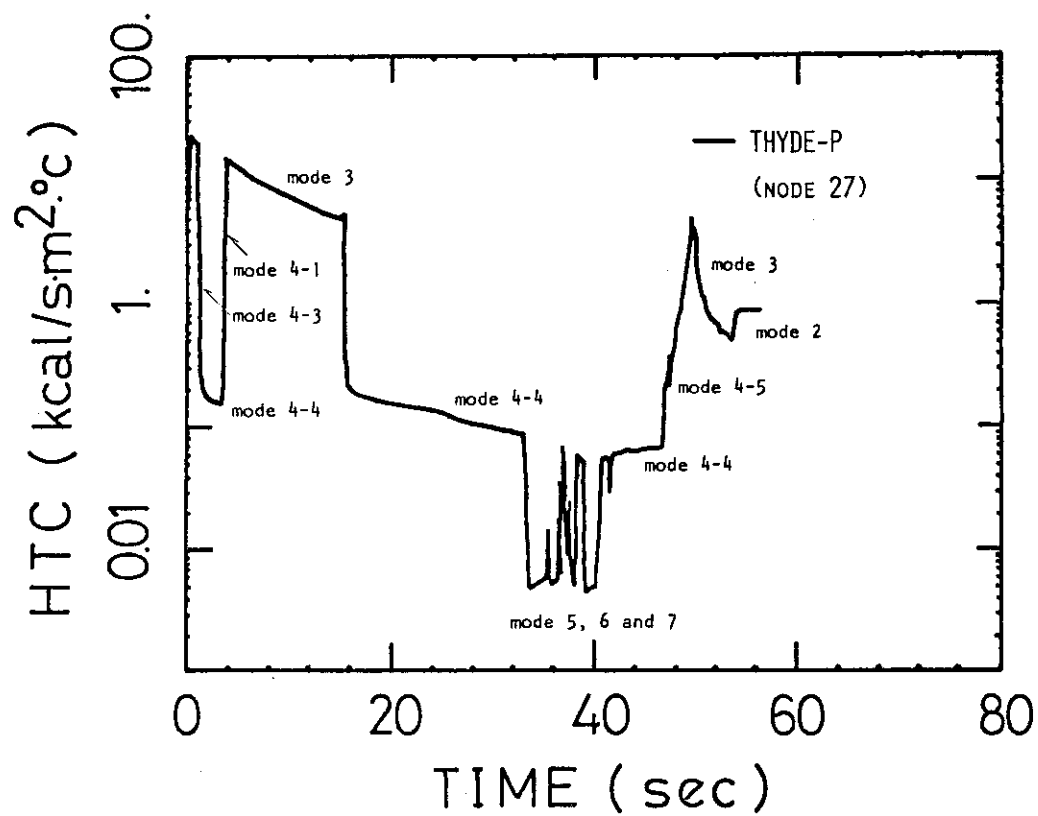


(a) Comparison of calculated cladding surface temperature at node 27 with experimental data

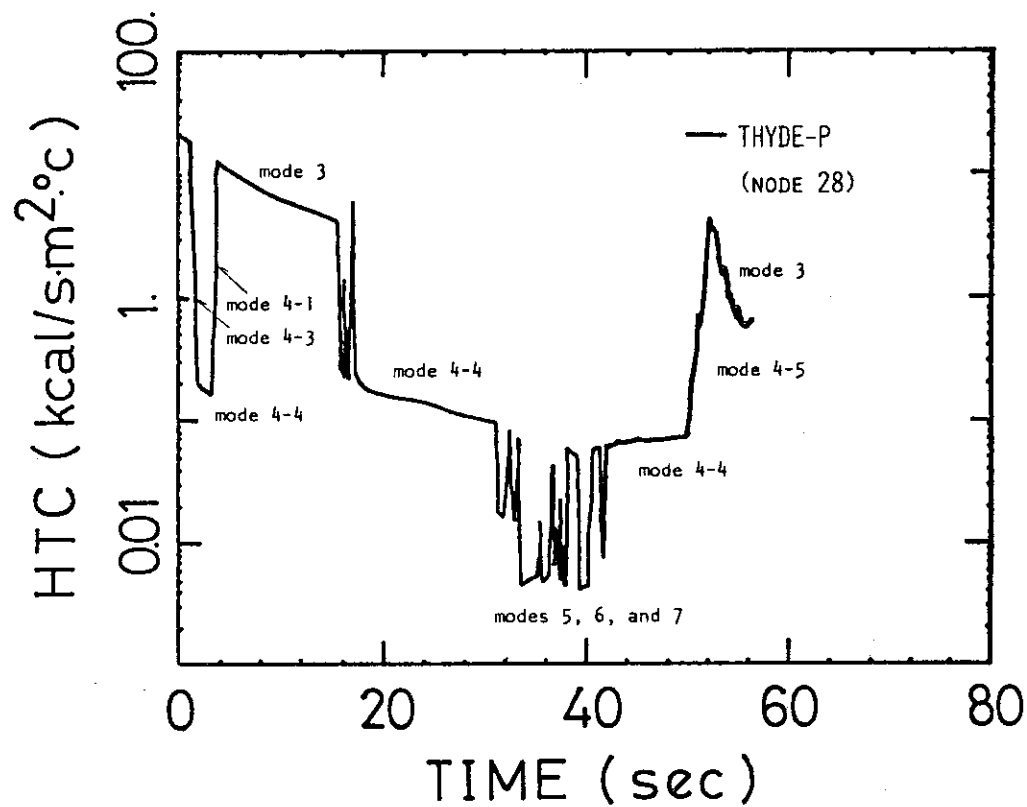


(b) Comparison of calculated cladding surface temperature at node 28 with experimental data

Fig. 13 Cladding surface temperatures



(a) Core node 27



(b) Core node 28

Fig. 14 Calculated heat transfer coefficient

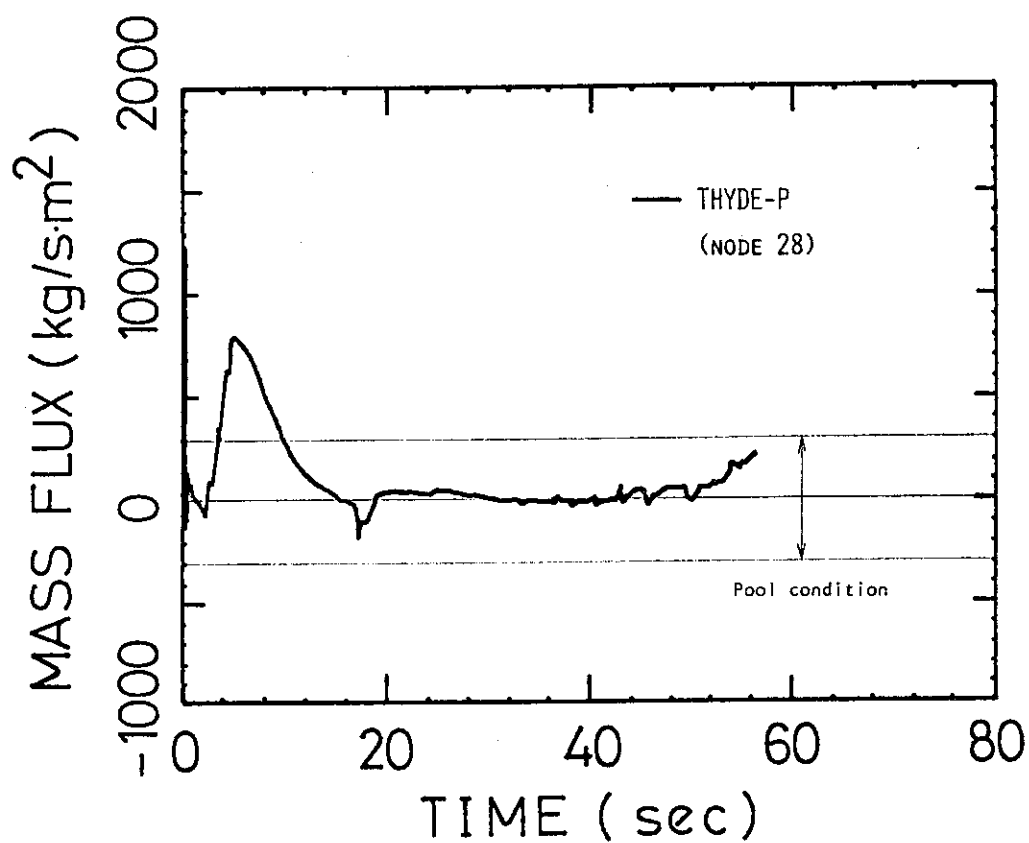


Fig. 15 Calculated mass flux at core node 28

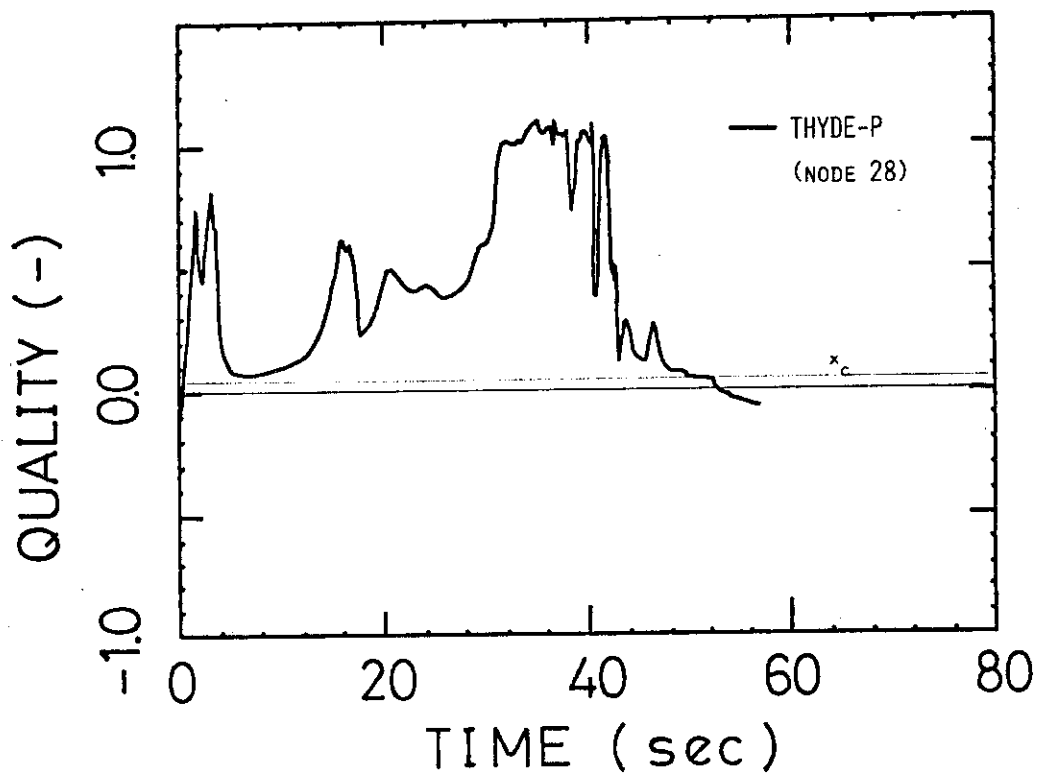


Fig. 16 Calculated coolant quality at core node 28

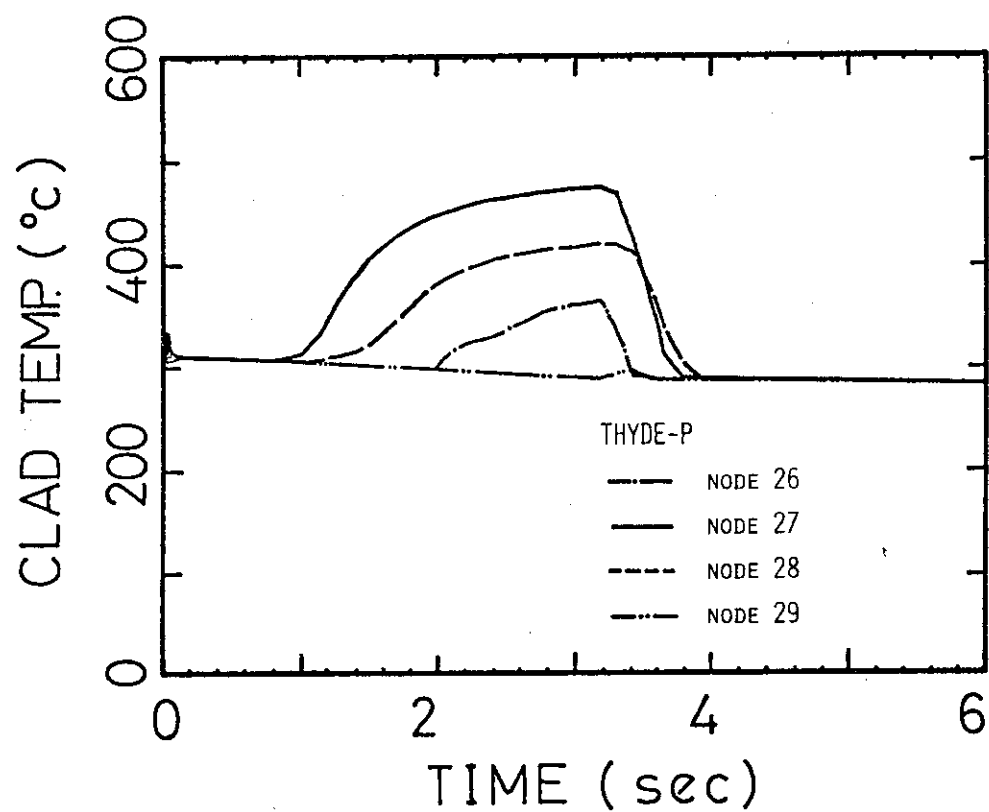


Fig. 17 Calculated cladding surface temperatures at core nodes at early stage of blowdown

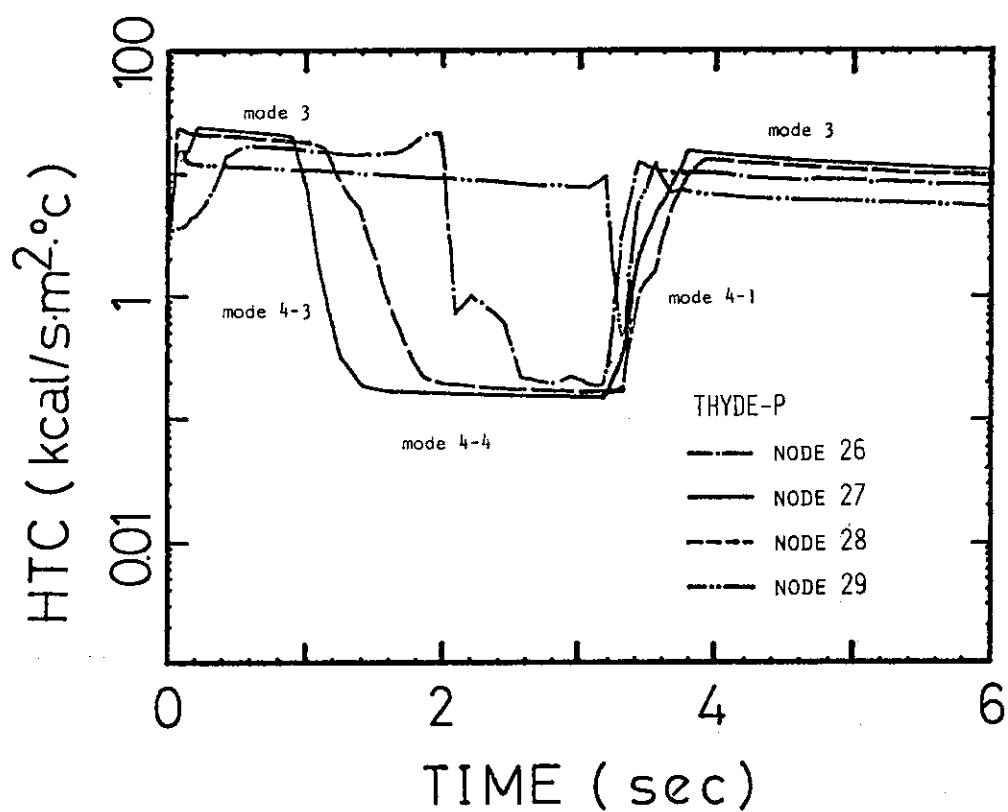


Fig. 18 Calculated heat transfer coefficients at core nodes at early stage of blowdown

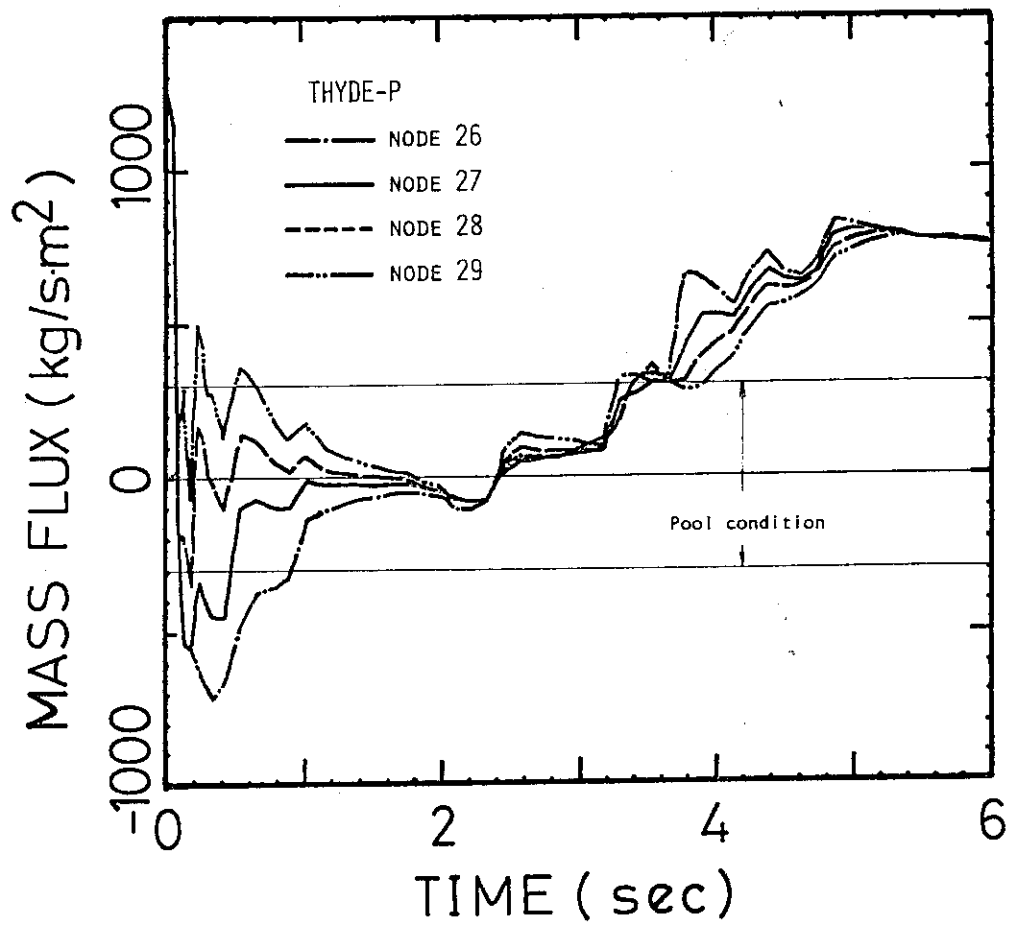


Fig. 19 Calculated mass fluxes at core nodes at early stage of blowdown

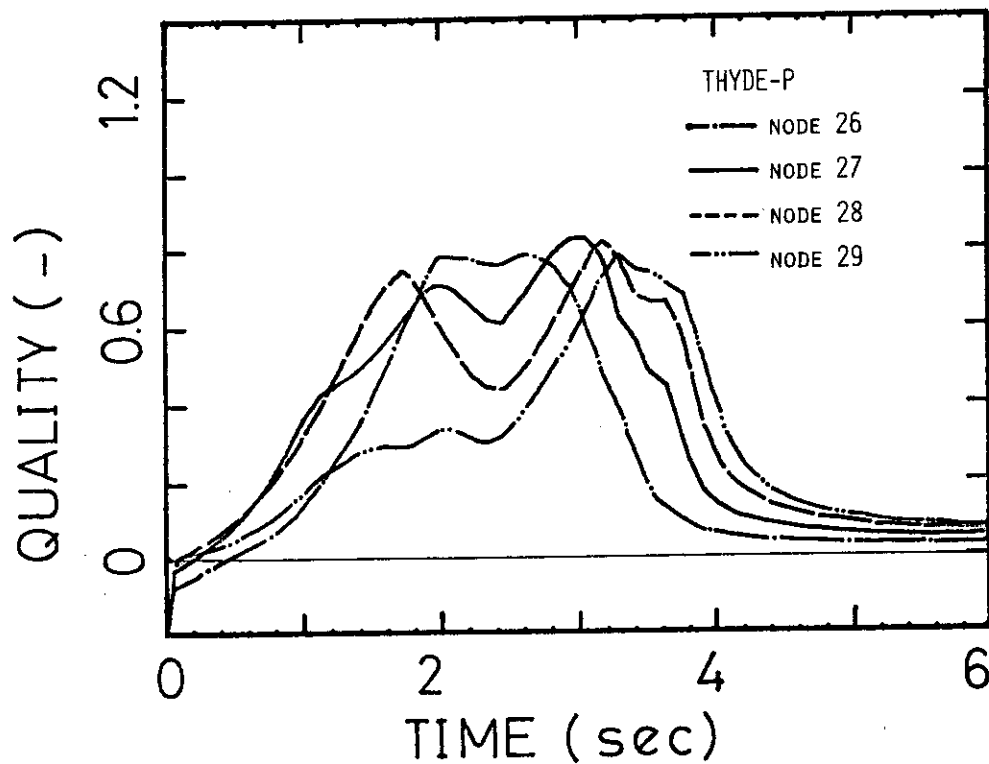


Fig. 20 Calculated coolant qualities at core nodes at early stage of blowdown

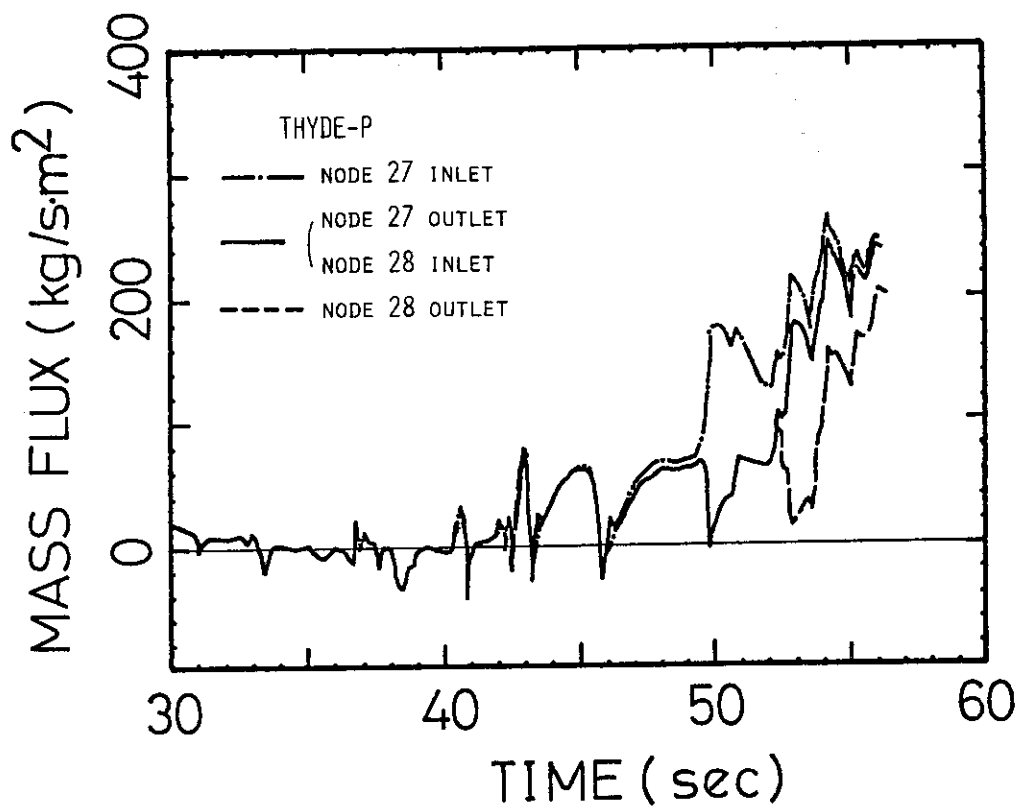


Fig. 21 Calculated mass fluxes at inlet and outlet points of core nodes 27 and 28 in refill-reflood phase

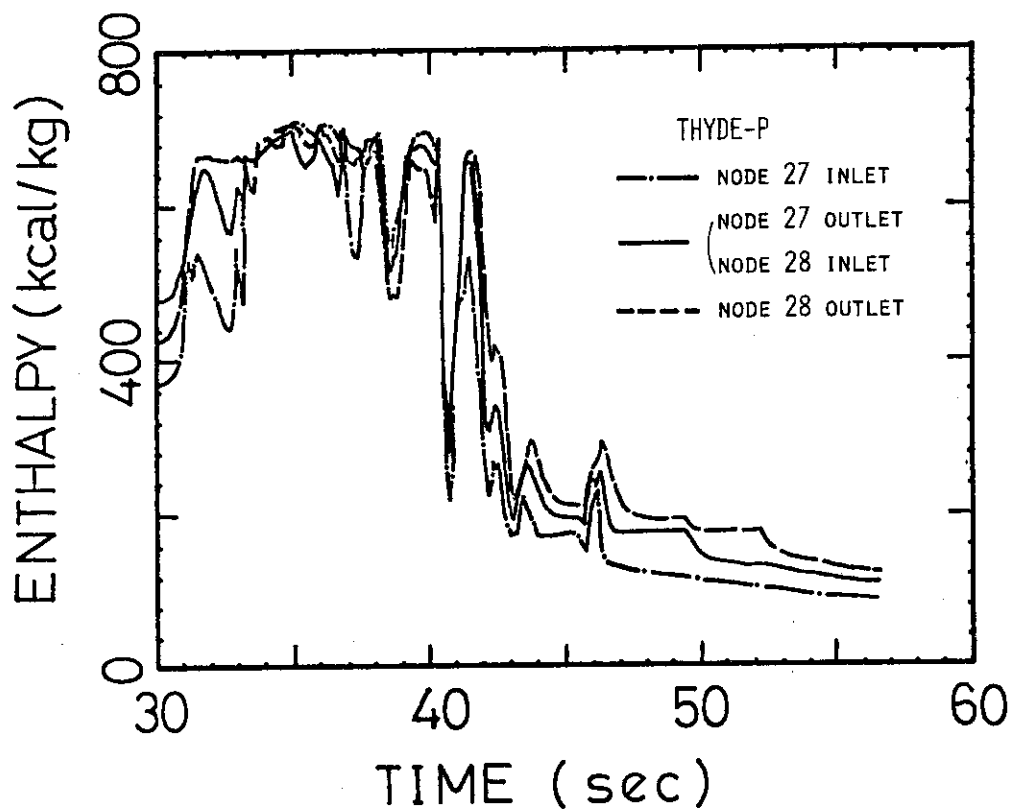


Fig. 22 Calculated enthalpies at inlet and outlet points of core nodes 27 and 28 in refill-reflood phase

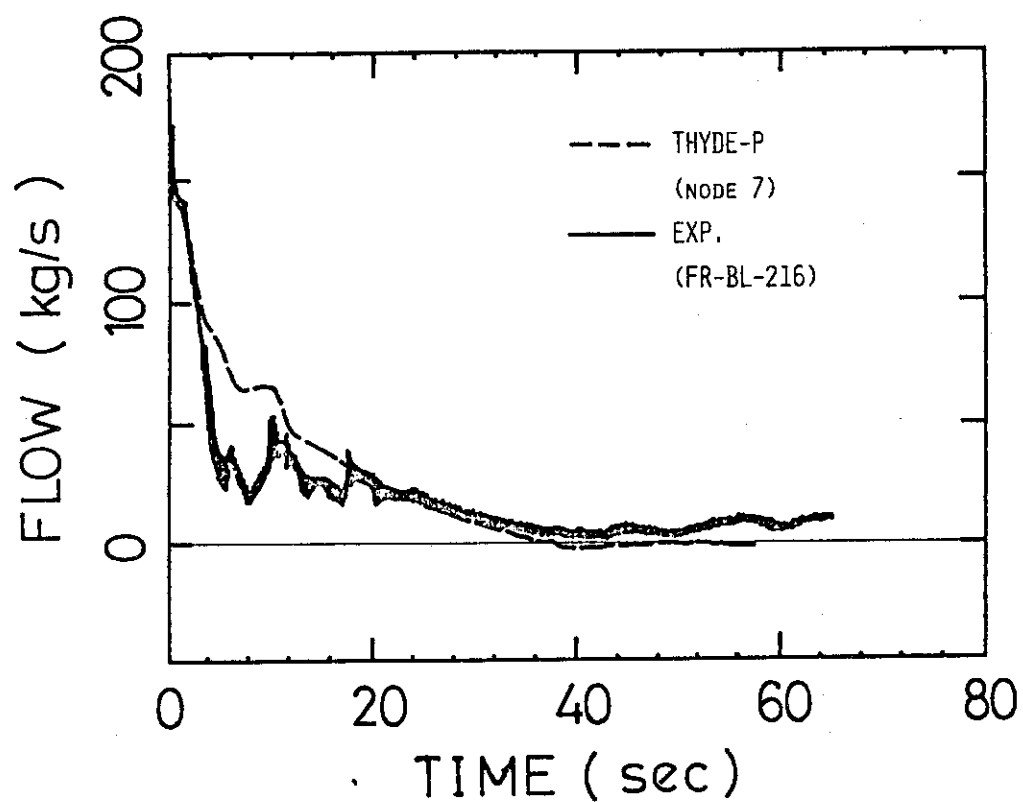


Fig. 23 Mass flow rate at broken loop hot leg

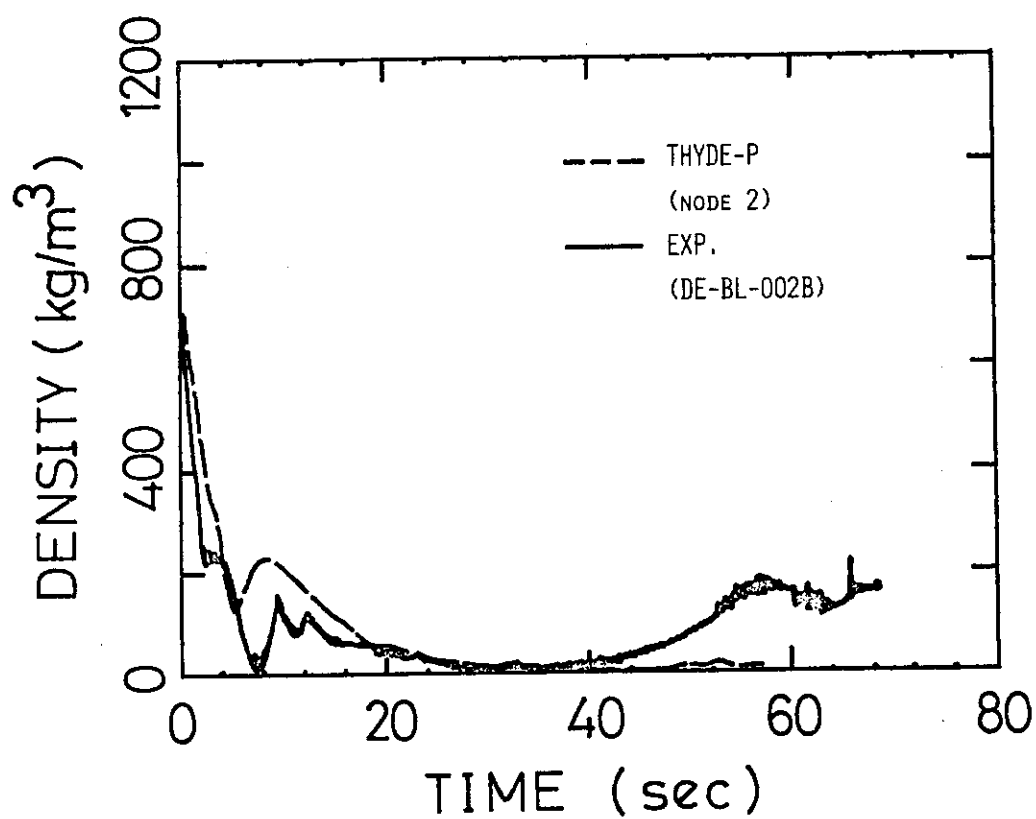


Fig. 24 Coolant density at broken loop hot leg

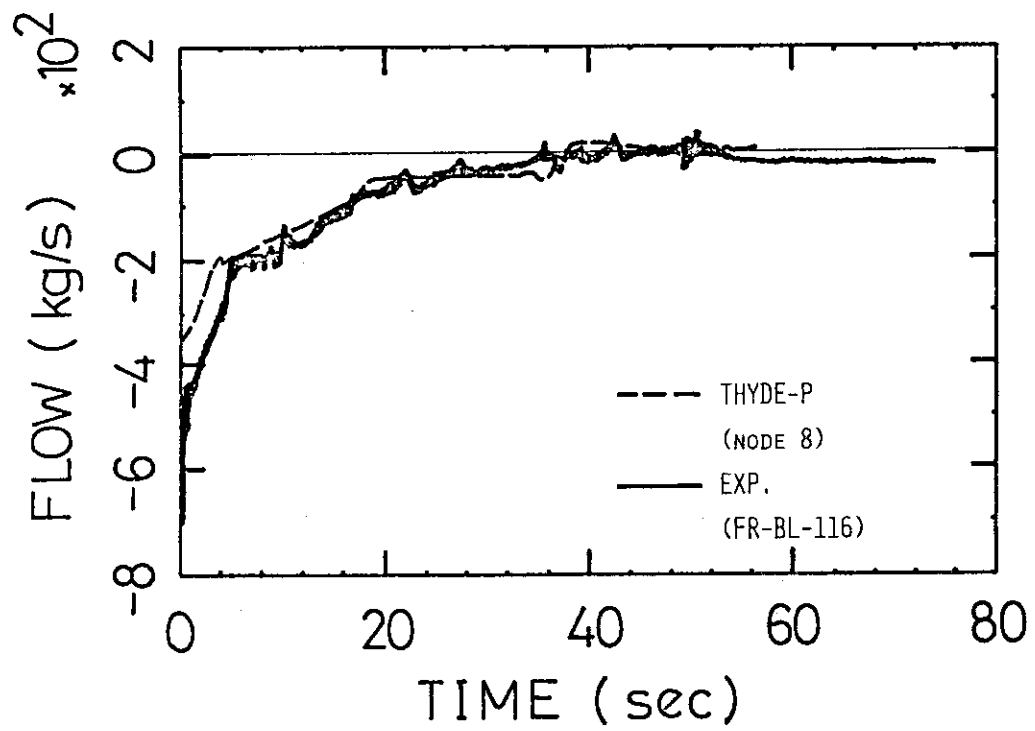


Fig. 25 Mass flow rate at broken loop cold leg

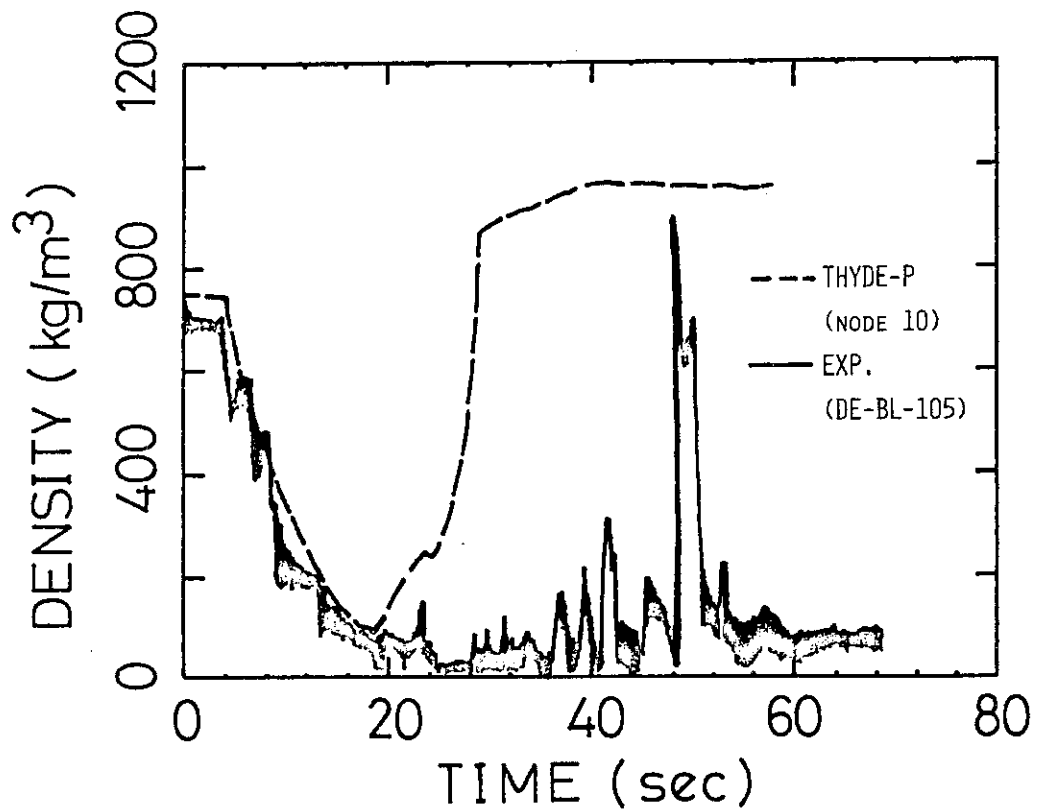
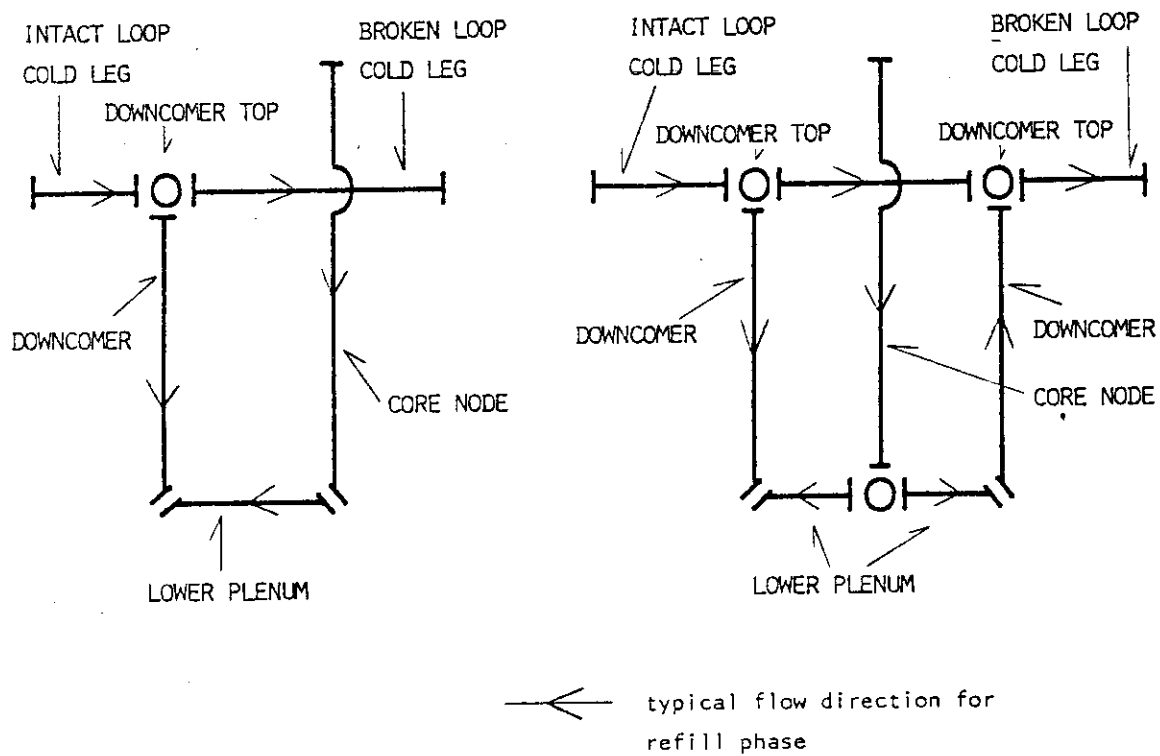


Fig. 26 Coolant density at broken loop cold leg



(a) Present analysis

(b) Example for split downcomer

Fig. 27 Nodalization for downcomer region

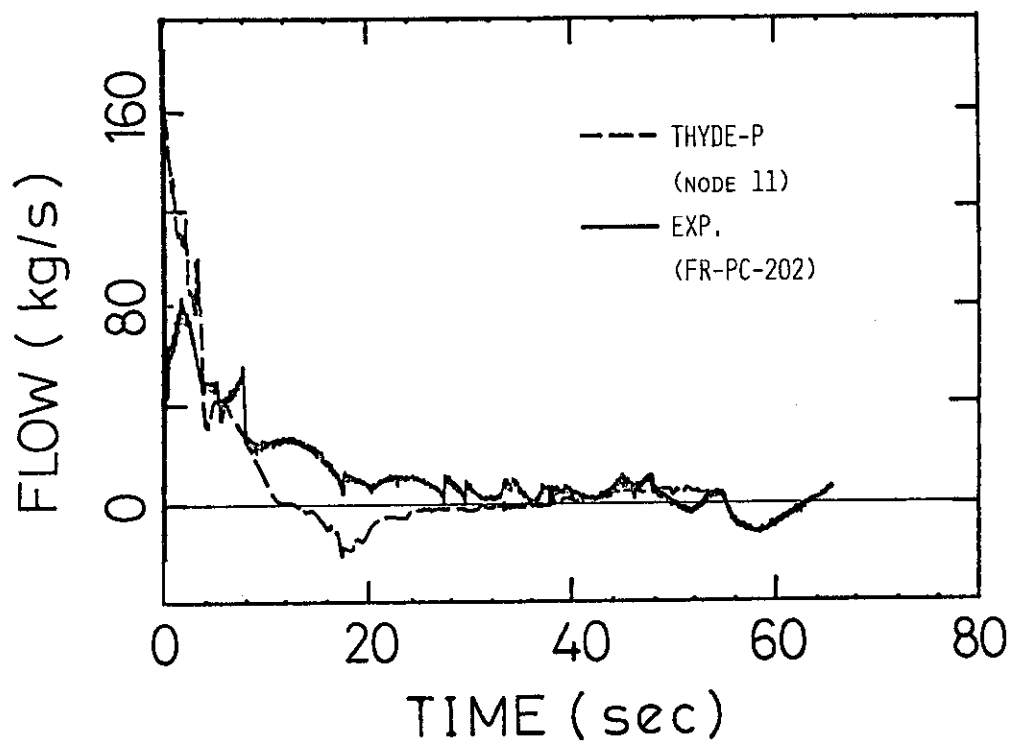


Fig. 28 Mass flow rate at intact loop hot leg

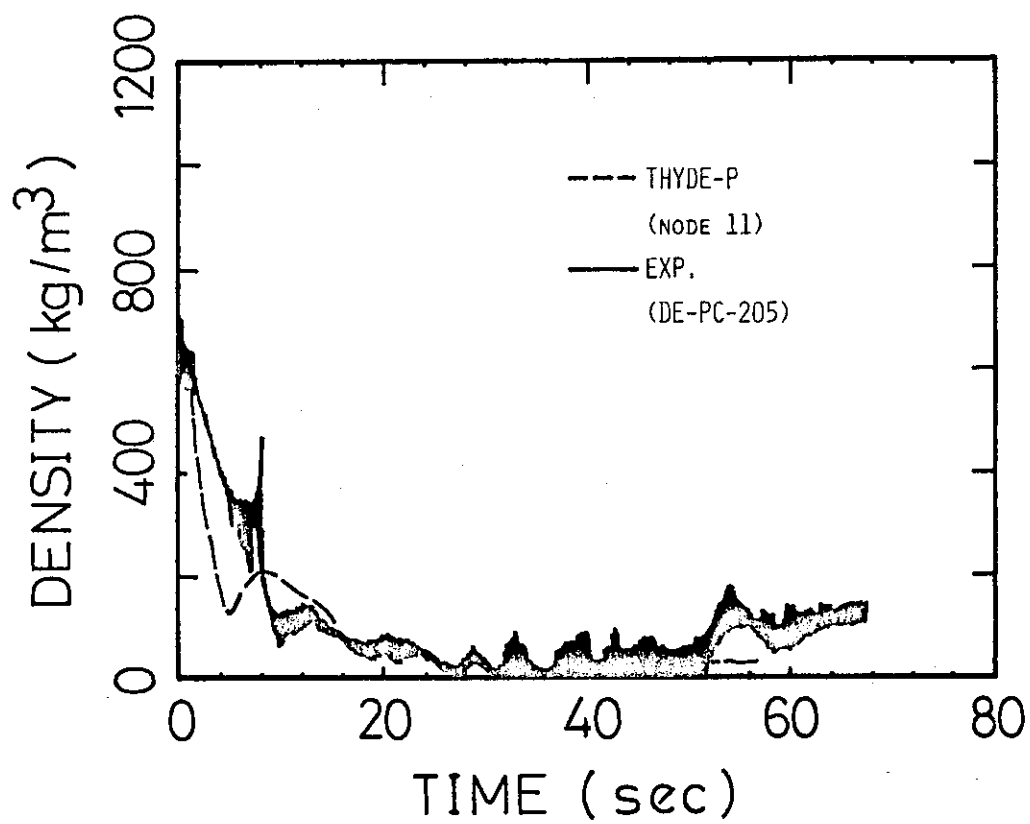


Fig. 29 Coolant density at intact loop hot leg

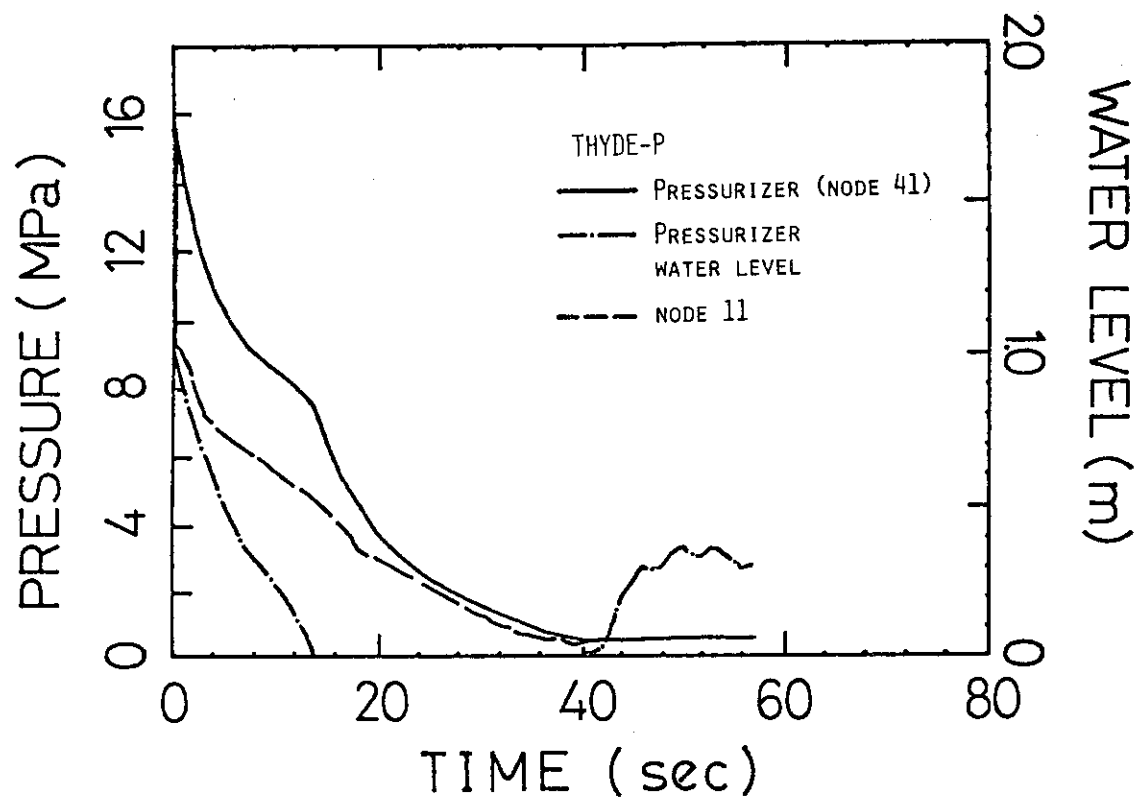


Fig. 30 Calculated pressure and water level at pressurizer

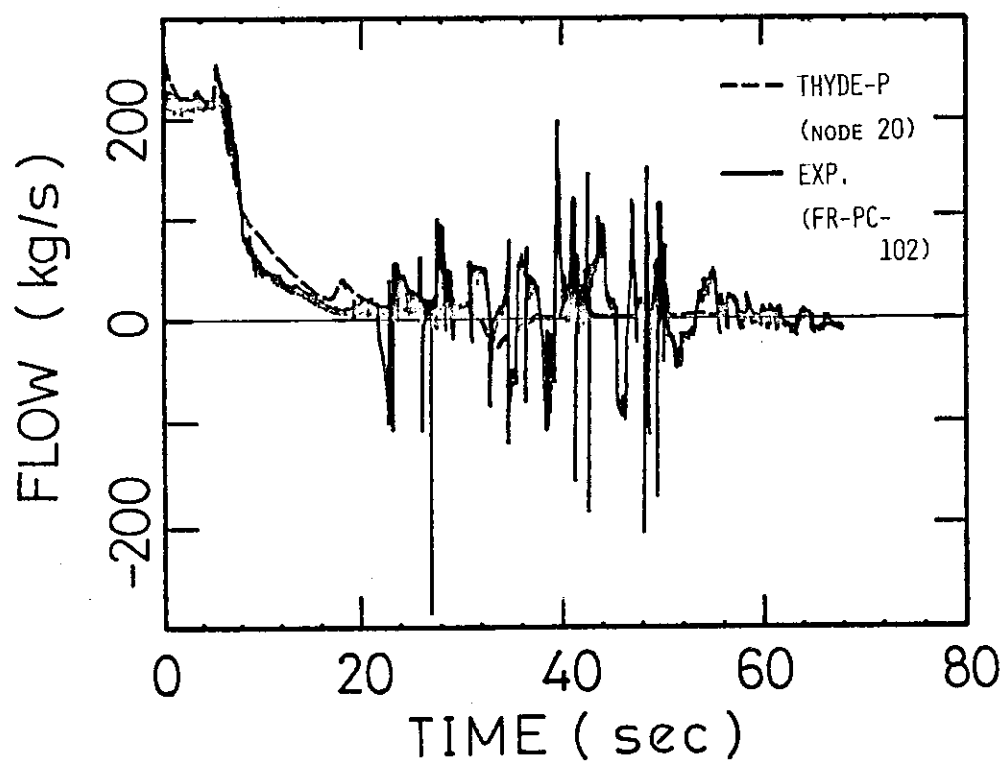


Fig. 31 Mass flow rate at intact loop cold leg

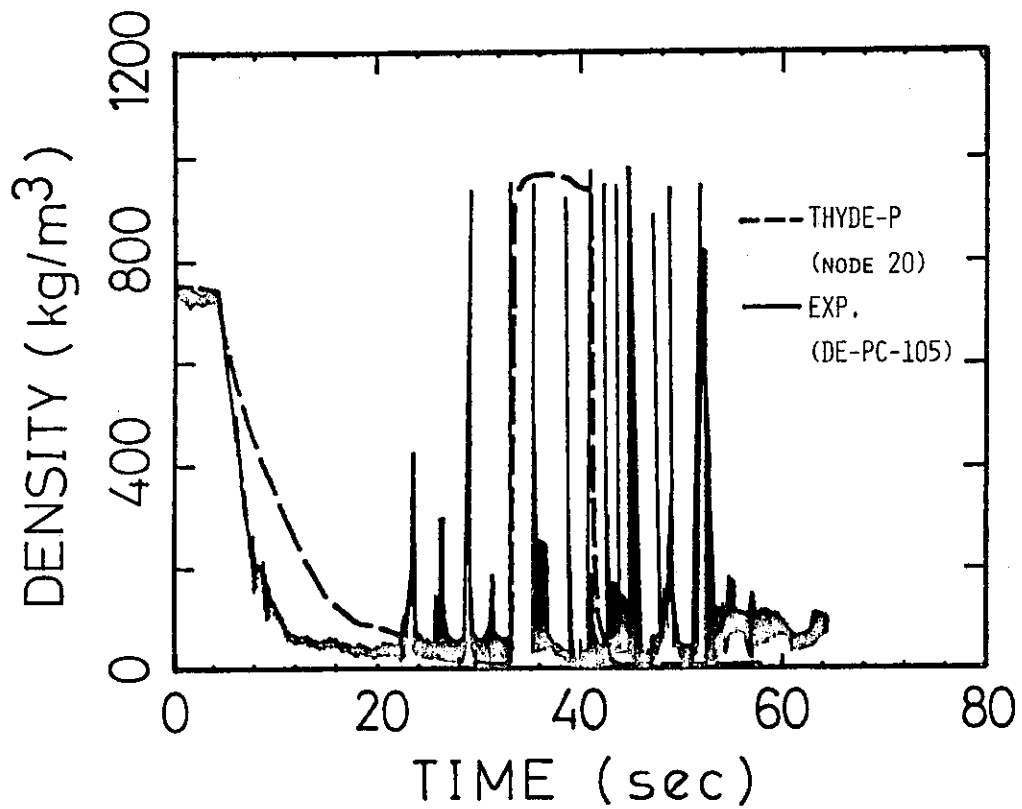


Fig. 32 Coolant density at intact loop cold leg

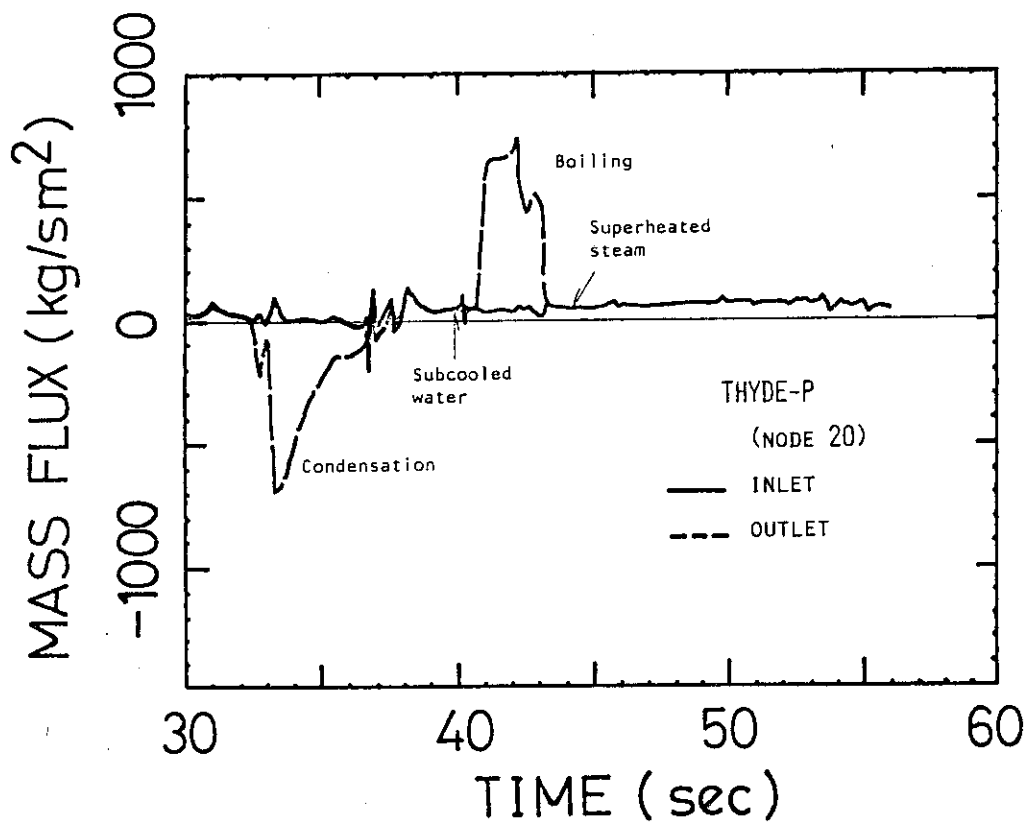


Fig. 33 Calculated mass fluxes at intact loop cold leg (node 20) in refill-reflood phase

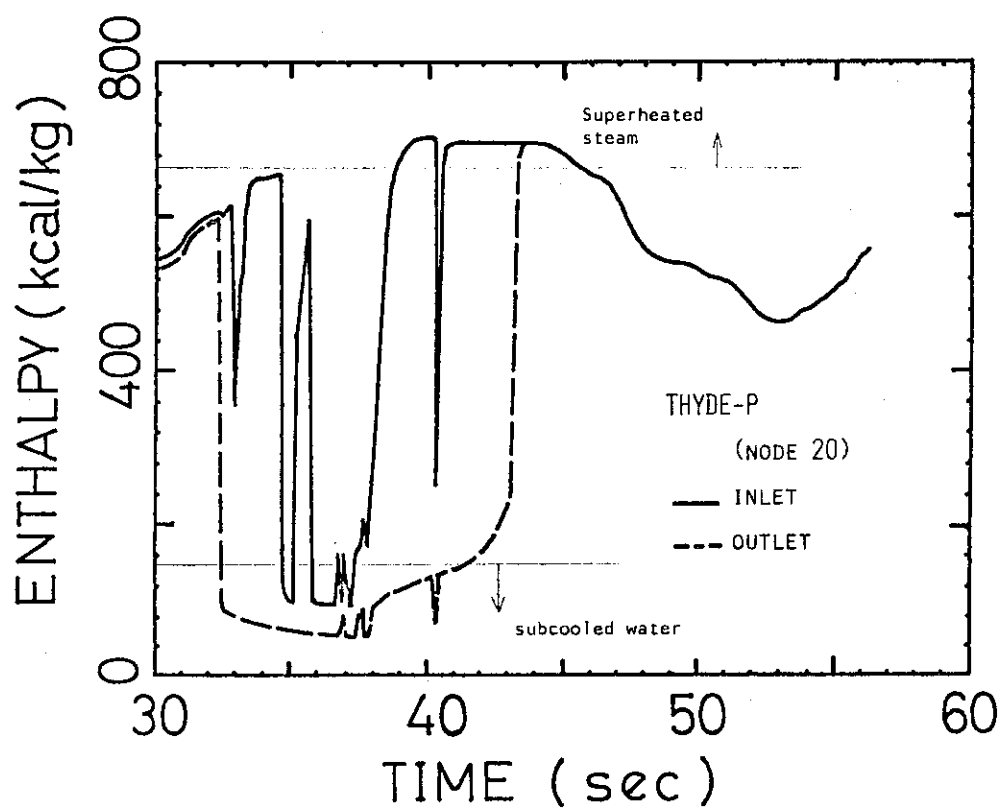


Fig. 34 Calculated enthalpies at intact loop cold leg (node 20) in refill-reflood phase

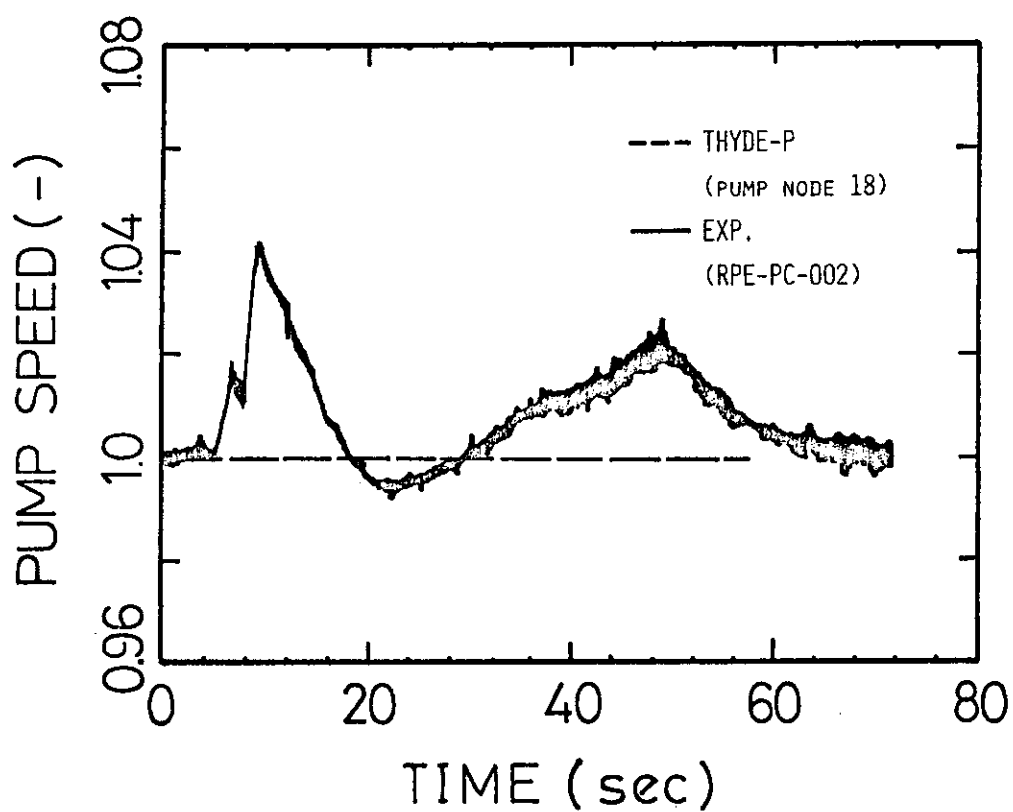


Fig. 35 Normalized pump speed

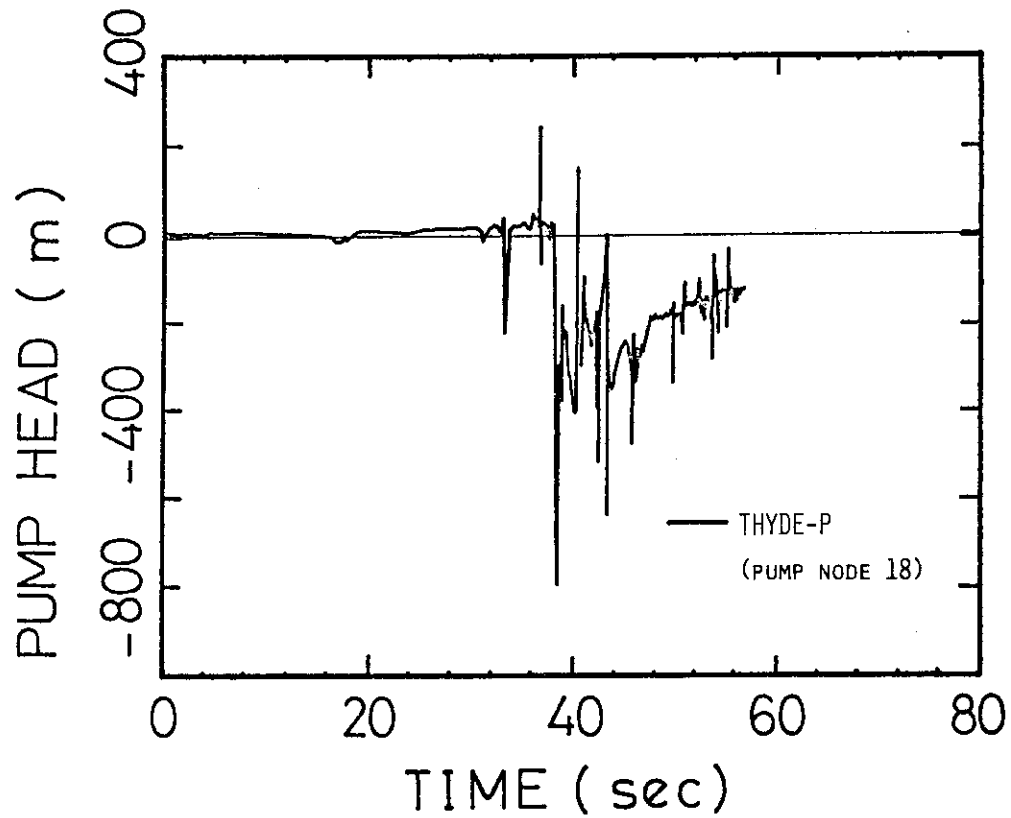


Fig. 36 Calculated pump head at pump node 18

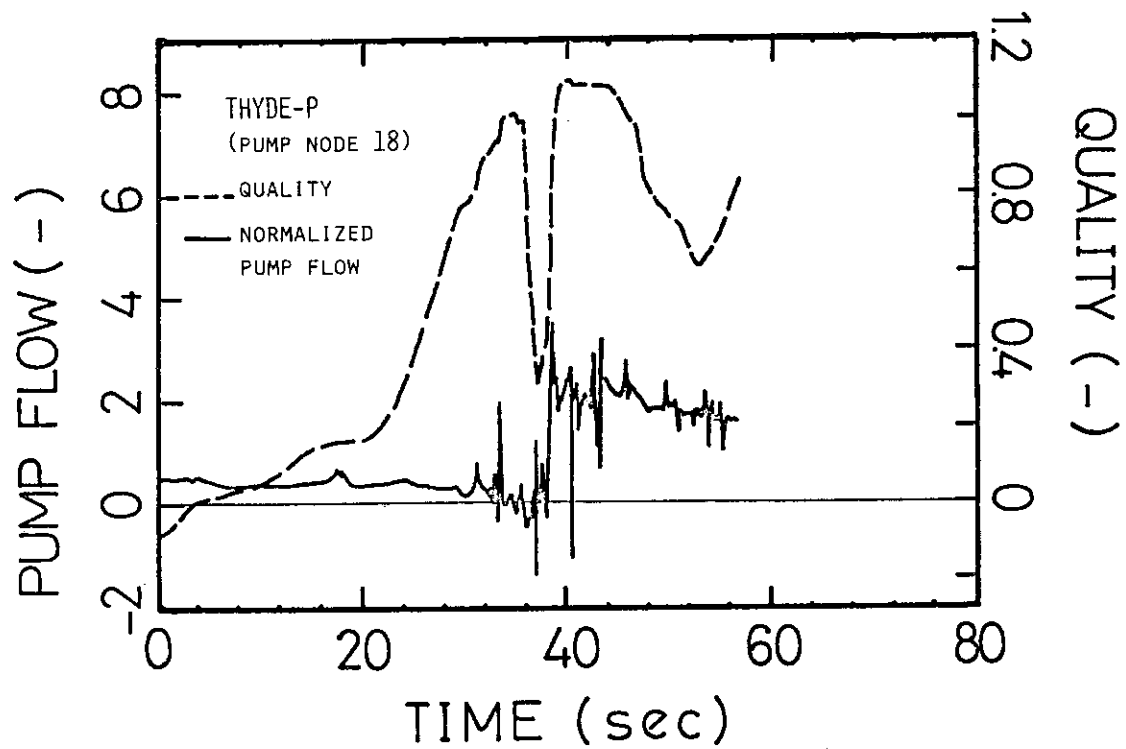


Fig. 37 Calculated normalized pump volumetric flow rate and coolant quality at pump node 18

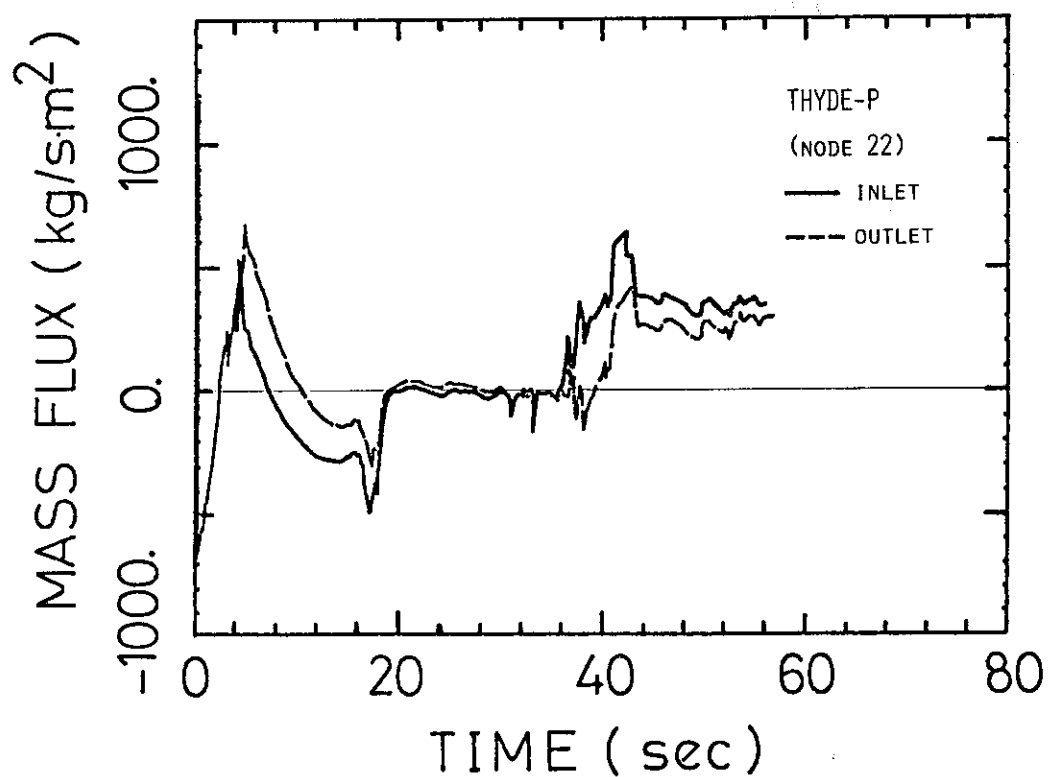


Fig. 38 Calculated mass fluxes at downcomer node 22

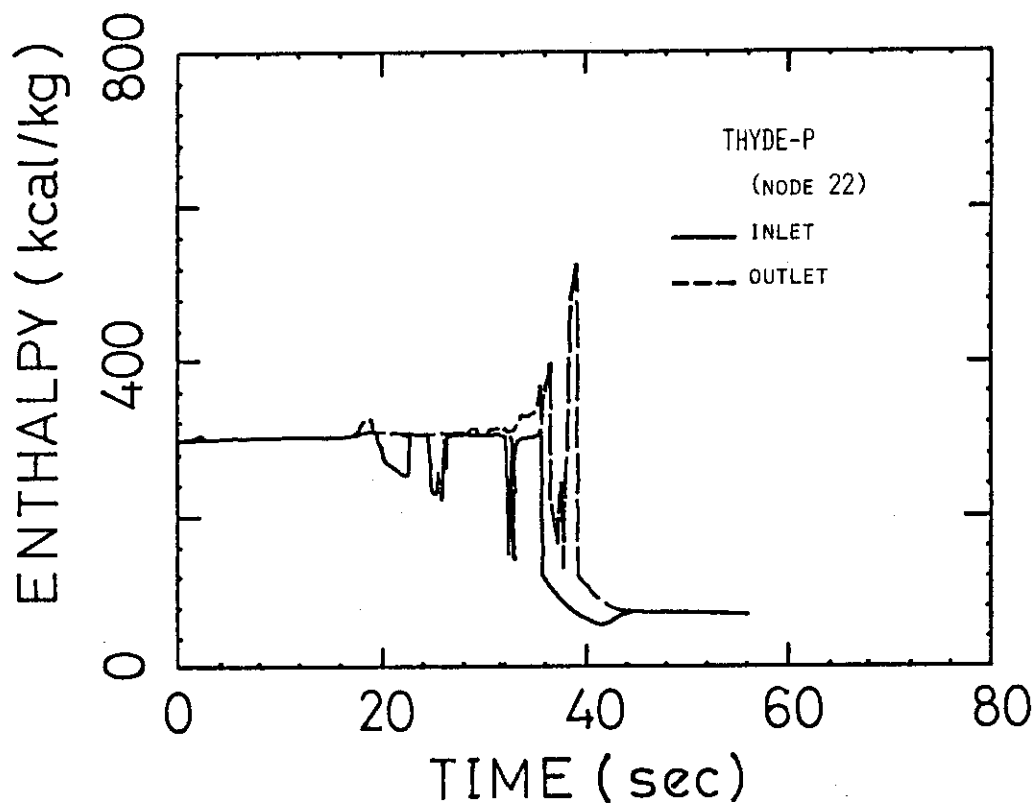


Fig. 39 Calculated enthalpies at downcomer node 22

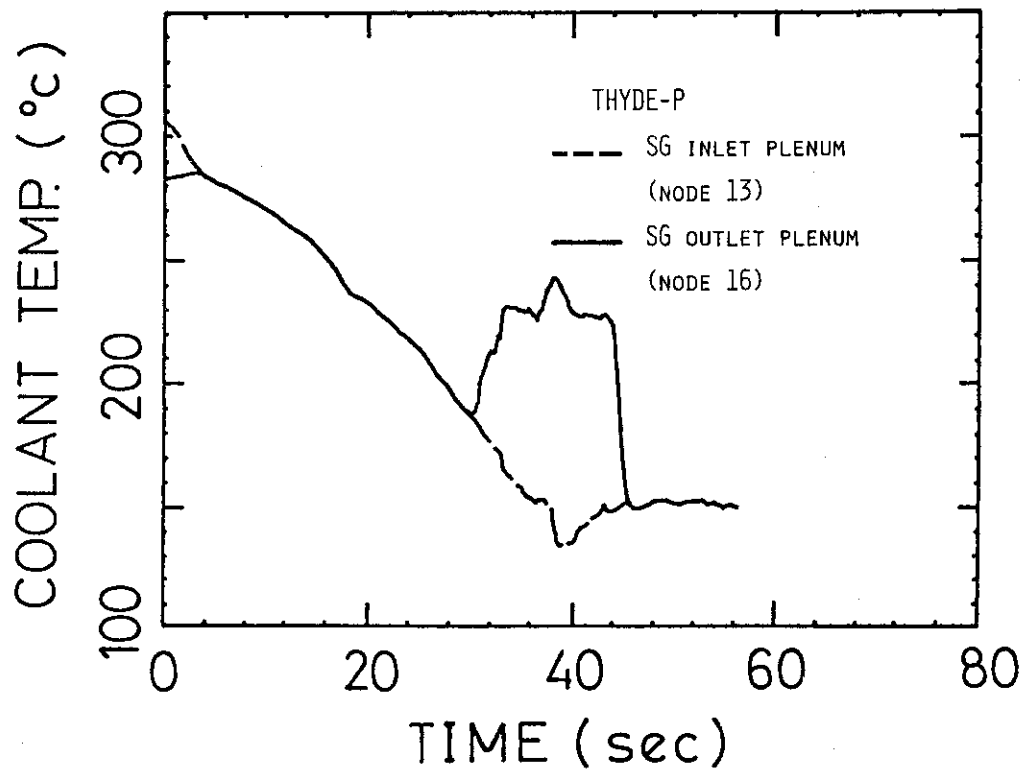


Fig. 40 Calculated coolant temperatures at inlet and outlet plenums of SG (nodes 13 and 16)

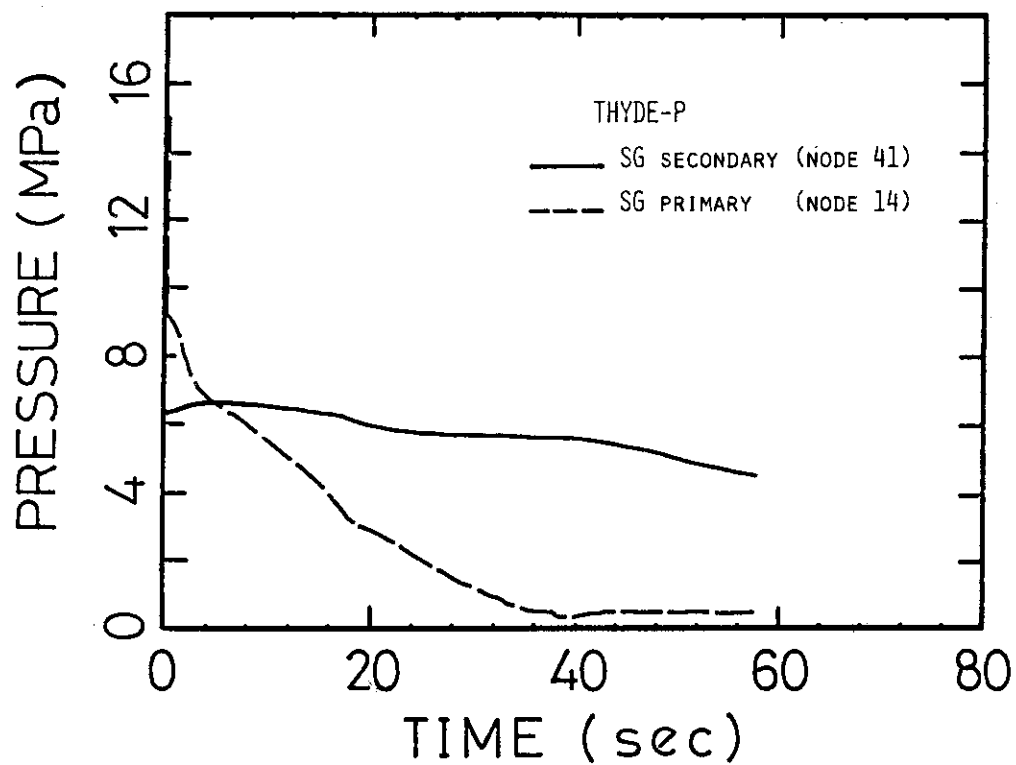


Fig. 41 Calculated pressures at SG secondary and primary systems

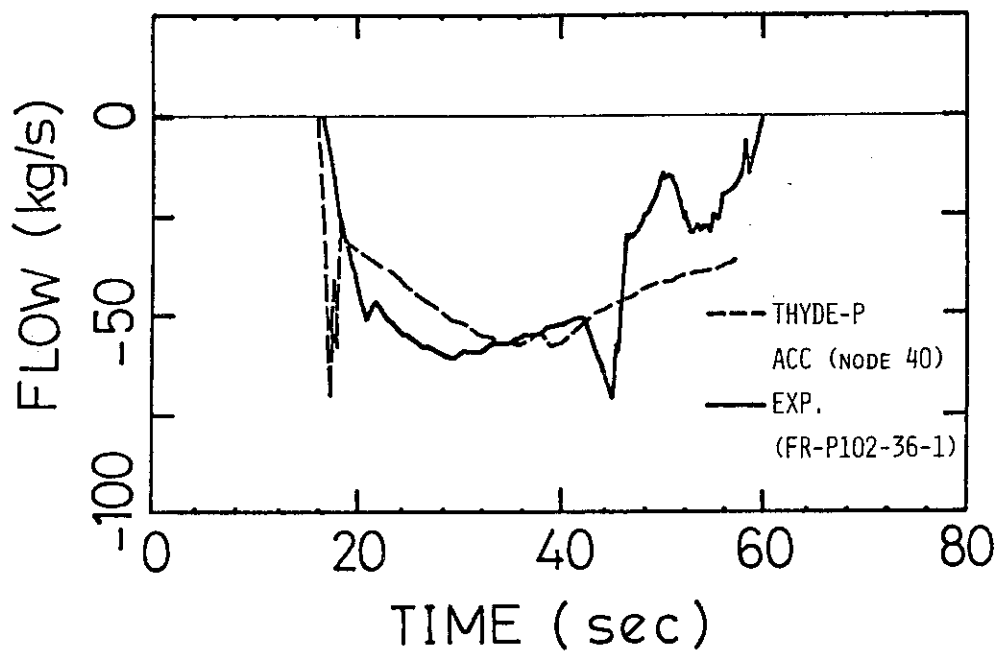


Fig. 42 Mass flow rate at accumulator

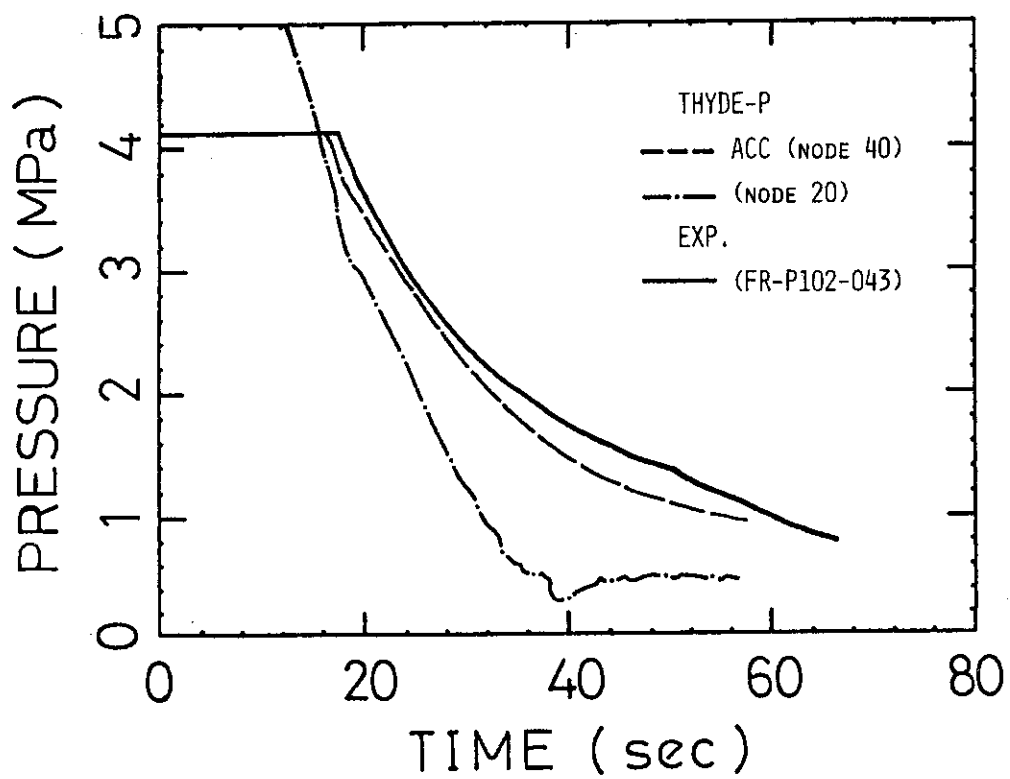


Fig. 43 Accumulator pressure

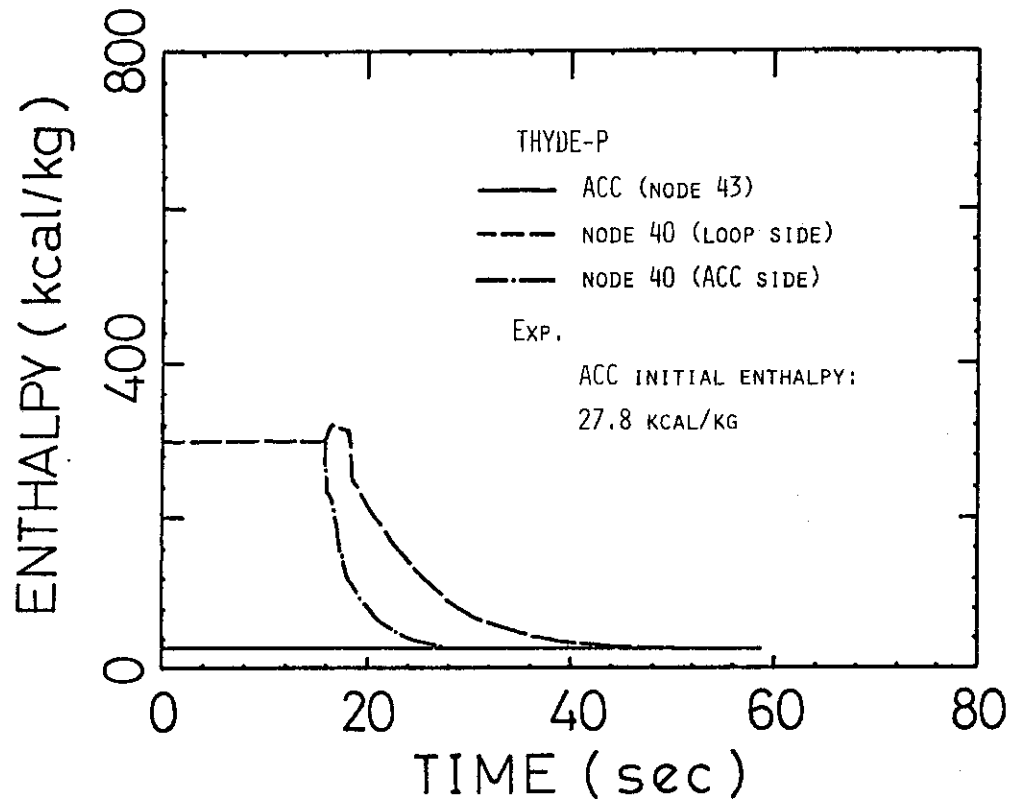


Fig. 44 Enthalpy at accumulator

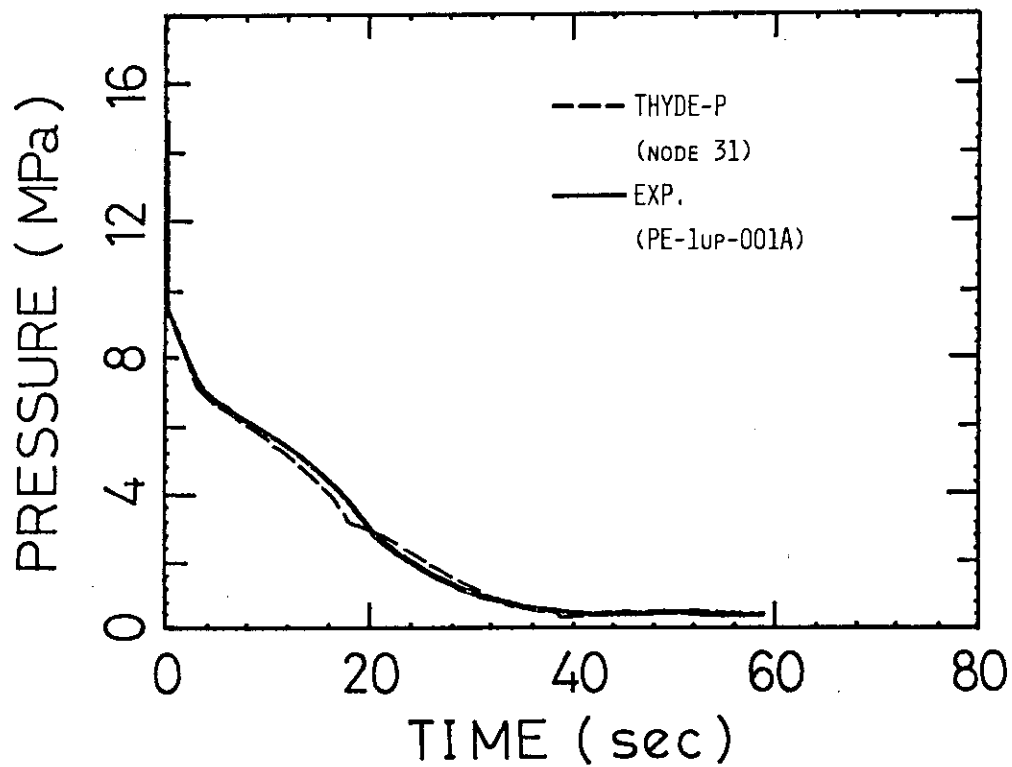


Fig. 45 Pressure above active core

7. Conclusion

Major problems pointed out in the preceeding sections are summarized as follows:

- (1) The calculated break flows were not in good agreement with the experimental data especially at the early stage of the blowdown,
- (2) The calculated core flow was overestimated due to the underestimated break flow at the broken loop cold leg in the blowdown phase,
- (3) The calculated results in the refill-reflood phase might be strongly dependent on the nodalization along the path of ECC water,
- (4) Coolant bypassing to the broken loop cold leg was subcooled in the analysis, but was saturated in the experiment,
- (5) Most of fuel rods have quenched at about 40 sec. in the experiment, but about 50 sec. in the analysis,
- (6) The present non-equilibrium model was very simple. Since the delay parameter had strong effects on the core reflood time, the physical models to estimate the delay parameter are yet to be developed.

In spite of these facts, the major purposes of the present analysis were thought to be successfully obtained. Much efforts, however, are needed to be made in conjunction with the non-equilibrium model.

Acknowledgment

The authors would like to express their sincere thanks to Mr. K. Sato, Chief of Reactor Safety Code Development Laboratory, for his valuable suggestions to this work. The authors are also grateful to the members of the laboratory for their useful discussions.

The authors' thanks are due to the members of Systems Section, Nuclear Energy Systems Development Department, FUJITSU LIMITED, who gave us a number of proper suggestions in performing the computer calculation.

7. Conclusion

Major problems pointed out in the preceeding sections are summarized as follows:

- (1) The calculated break flows were not in good agreement with the experimental data especially at the early stage of the blowdown,
- (2) The calculated core flow was overestimated due to the underestimated break flow at the broken loop cold leg in the blowdown phase,
- (3) The calculated results in the refill-reflood phase might be strongly dependent on the nodalization along the path of ECC water,
- (4) Coolant bypassing to the broken loop cold leg was subcooled in the analysis, but was saturated in the experiment,
- (5) Most of fuel rods have quenched at about 40 sec. in the experiment, but about 50 sec. in the analysis,
- (6) The present non-equilibrium model was very simple. Since the delay parameter had strong effects on the core reflood time, the physical models to estimate the delay parameter are yet to be developed.

In spite of these facts, the major purposes of the present analysis were thought to be successfully obtained. Much efforts, however, are needed to be made in conjunction with the non-equilibrium model.

Acknowledgment

The authors would like to express their sincere thanks to Mr. K. Sato, Chief of Reactor Safety Code Development Laboratory, for his valuable suggestions to this work. The authors are also grateful to the members of the laboratory for their useful discussions.

The authors' thanks are due to the members of Systems Section, Nuclear Energy Systems Development Department, FUJITSU LIMITED, who gave us a number of proper suggestions in performing the computer calculation.

References

- (1) McCormic-Barger, M., "Experimental Data Report for LOFT Power Ascension Test L2-2", NUREG/CR-0492 TREE-1322R, February 1979.
- (2) Asahi, Y., "Description of THYDE-P Code (Preliminary Report of Methods and Models)", JAERI-M7751, 1978.
- (3) Asahi, Y. and Hirano, M., "Verification Study of LOCA Analysis Code THYDE-P (Sample Calculation Run 10)", JAERI-M8560, 1979.
- (4) Tolman, E. L., "Cladding Rewets Observed in The LOFT Large Break Loss-of-Coolant Accident Tests", Presented at The Seventh Water Reactor Safety Information Meeting, November, 5-9, Gaithersburg, Maryland.
- (5) Zaloudek, F. R., "Steam-Water Critical Flow from High Pressure Systems", HW-68936, Hanford Works, 1963.
- (6) Moody, F. J., "Maximum Flow Rate of Single Component, Two-Phase Mixture", Heat Trans.-Trans. ASME, 87 n1, pp 134-142, 1965.
- (7) Slifer, B. C. and Hensch, J. E., "Loss-of-Coolant Accident and Emergency Core Cooling Models for General Electric Boiling Water Reactors", NEDO-10329, General Electric Company, April 1971.
- (8) "WREM : Water Reactor Evaluation Model (revision 1)", NUREG-75/056, USNRC, May 1975.
- (9) Kramers, H., Physische Transportverschijnselen, Technische Hogeschool, Delft, Holland, pp 53-54, 1958.
- (10) Dittus, F. W. and Boelter, L. M. K., "Heat Transfer in Automobile Radiators of The Tubular Tube", 2, No. 13, pp 443-461, 1930.
- (11) Jens, W. H. and Lottes, P. A., "Analysis of Heat Transfer, Burnout, Pressure Drop and Density Data for High-Pressure Water", ANL-4627, 1951.
- (12) Groenevelt, D. C., "An investigation of Heat Transfer in The Liquid Deficient Regime", Report AECL-3281, Chalk River, Ontario, December 1968.
- (13) McEligot, D. M., Ormand, L. W. and Perkins, H. C., J. Trans. Amer. Soc. Mech. Engrs., 88, Series C, pp 239-245, May 1966.
- (14) Biasi, L., et. al, "Studies on Burnout : Part 3", Energia Nucleare, 550-536, 1967.

- (15) "PBF-LOCA Test Series, Test LOC-11c, Quick Look Report", TFPB-TR-261, 1980, or S. C. Wilkins, "Embedded Cladding Surface Thermocouples on Zircaloy-Sheathed Heater Rods", TREE-NUREG-1072, 1977
- (16) McAdams, W. H., "Heat Transmission", 3rd Ed., pp. 337, McGraw-Hill, 1954
- (17) Reeder, D. L., "LOFT SYSTEM AND TEST DESCRIPTION (5.5FT CORE1 LOCES)", NUREG/CR-0247, July 1978.
- (18) McDonough, J. B., Milich, W. and King, E. C., "Partial Film Boiling with Water at 2000 psig in a Round Vertical Tube", MSA Research Corp., Technical Report 62(NP-6976), 1958.
- (19) Moore, K. U. and Retting, W. H., "RELAP-4 Computer Program for Transient Thermal-Hydraulic Analysis", ANCR-1127, December 1973.
- (20) Zuber, N., Tribus, M. and Westwater, J. W., "The Hydrodynamic Crisis in Pool Boiling of Saturated and Subcooled Liquids", International Developments in Heat Transfer, Part II, pp 230-236, 1961.
- (21) Griffith, P., Auedisian, C. T. and Walkush, J. F., "Countercurrent Flow Critical Heat Flux", presented at National Heat Transfer Conference, San Francisco, August 1975.
- (22) Thom, J. R. S., et al, "Boiling in Subcooled Water During Flow Up Heated Tubes or Annuli", Proc. Instn. Mech. Engrs., Vol. 180, Part 3C, pp 226-246, 1966
- (23) Berenson, P. J., "Film-Boiling Heat Transfer from a Horizontal Surface", J. of Heat Transfer, Vol. 83, pp 351-358, August 1961.

Appendix A Input Data List

```

-- LOFT L2-2 ANALISYS BY THYDE-P CODE -- L22P04      80.07.24      00000100
/                                                     00000200
/  **** DIMENSION DATA ****                        00000300
BB01                                                  00000400
  0  0  9  3  17  43  37  9  2  2  1  1  2  6  5  3      00000500
/                                                     00000600
/  **** MINOR EDIT DATA ****                      00000700
BB02                                                  00000800
PRE-30  PRA-08  PRA-07  GLA-21  GLE-07  GLA-08  GLE-35  GLA-23  GLA-23  00000900
/                                                     00001000
/  **** TIME STEP CONTROL DATA ****                00001100
BB03                                                  00001200
SB0301                                              00001300
  0.2  0.2  100.                                       00001400
SB0304                                              00001500
  30  3  50  0  1.0E-3  1.0E-6  0.3  0.1             00001600
SB0305                                              00001700
  30  3  50  0  4.0E-3  1.0E-6  90.0  0.1            00001800
SB0308                                              00001900
  40  1  1  0  4.0E-3  1.0E-6  2000.0  0.1           00002000
/                                                     00002100
/  **** TRIP CONTROLL DATA ****                    00002200
BB04                                                  00002300
SB0480                                              00002400
  1  0  1  0  1000.0  0.0                             00002500
SB0481                                              00002600
  5  42  1  0  0.002  0.0                             00002700
SB0482                                              00002800
  2  18  1  0  1000.0  0.0                             00002900
SB0483                                              00003000
  2  19  1  0  1000.0  0.0                             00003100
SB0484                                              00003200
  3  0  1  0  0.085  0.0                               00003300
SB0485                                              00003400
  4  1  1  0  12.0  0.0                                00003500
SB0486                                              00003600
  4  2  1  0  29.0  0.0                                00003700
SB0487                                              00003800
 -4  1  1  0  1000.0  0.0                              00003900
SB0488                                              00004000
 -4  2  1  0  1000.0  0.0                              00004100
SB0489                                              00004200
  6  1  -3  1  240.0  0.005                            00004300
SB0490                                              00004400
  6  2  -3  1  250.0  0.0                              00004500
SB0491                                              00004600
  6  3  -3  1  360.0  0.0                              00004700
SB0492                                              00004800
 -6  1  3  1  350.0  0.0                              00004900
SB0493                                              00005000

```

	1	2	3	4	5	6	7-R	8
-6 2 3 1 305.0 0.0								00005100
SB0494								00005200
-6 3 3 1 380.0 0.0								00005300
SB0495								00005400
6 2 -2 1 160.0 0.0								00005500
SB0496								00005600
-6 2 2 1 190.0 0.0								00005700
/								00005800
/ **** FLOW AJUST DATA ****								00005900
BB05								00006000
1 3.0644 329.2								00006100
/								00006200
/ **** NODE DATA ****								00006300
BB06								00006400
SB0601								00006500
1 1 22 29 0 154.526047915	0.2842	0.0	1.332	0.0				00006600
	0.4	0.8	0.0	0.0				00006700
SB0602								00006800
2 1 29 1 0 154.380793779	0.2842	0.0	0.6965	0.0				00006900
	0.0	0.0	-1.0	-1.0				00007000
SB0603								00007100
3 1 1 2 0 154.380788629	0.1032	0.0	1.517	-0.7174				00007200
	-1.0	-1.0	1.52	1.09				00007300
SB0604								00007400
4 1 2 3 0 154.331420869	0.3485	0.0	3.228	2.705				00007500
	0.0	0.0	189.0	189.0				00007600
SB0605								00007700
5 1 3 4 0 154.145289496	0.3485	0.0	3.228	-2.705				00007800
	0.0	0.0	142.0	198.0				00007900
SB0606								00008000
6 1 4 5 0 154.331409722	0.1272	0.0	2.423	-2.0394				00008100
	0.0	0.0	20.0	20.0				00008200
SB0607								00008300
7 1 5 6 0 154.471707114	0.1032	0.0	1.883	1.322				00008400
	0.0	0.0	-118624.588	0.0				00008500
SB0608								00008600
8 1 6 7 0 154.825070056	0.1032	0.0	0.4877	0.0				00008700
	0.0	0.0	0.0	0.0				00008800
SB0609								00008900
9 1 7 30 0 154.825070402	0.2842	0.0	0.6965	0.0				00009000
	-1.0	-1.0	0.0	0.0				00009100
SB0610								00009200
10 1 30 27 0 154.825070395	0.2842	0.0	0.9510	0.0				00009300
	0.0	0.0	3.58	10.0				00009400
SB0611								00009500
11 1 22 23 0 154.14454	0.2842	0.0	2.616	0.0				00009600
	0.4	0.8	0.0	0.0				00009700
SB0612								00009800
12 1 23 8 0 154.28418	0.2832	0.0	2.643	0.2432				00009900
	0.0	0.0	-1.0	-1.0				00010000
SB0613								00010100
13 1 8 9 0 154.27422	0.9084	0.0	0.5175	0.5175				00010200
	-1.0	-1.0	-1.0	-1.0				00010300
SB0614								00010400
14 7 9 10 1 154.22380	0.01021	0.0	2.568	2.483				00010500
	-1.0	-1.0	-1.0	-1.0				00010600
SB0615								00010700
15 7 10 11 1 153.99431	0.01021	0.0	2.568	-2.483				00010800
	-1.0	-1.0	-1.0	-1.0				00010900

-----1-----2-----3-----4-----5-----6-----7-R-----8												
SB0616												00011000
16	1	11	12	0	154.13590	0.9084	0.0	0.5175	-0.5175			00011100
						-1.0	-1.0	-1.0	-1.0			00011200
SB0617												00011300
17	1	12	24	0	154.09992	0.2941	0.0	2.426	-1.523			00011400
						-1.0	-1.0	0.0	0.0			00011500
SB0618												00011600
18	8	24	25	0	154.25687	0.3468	0.0	1.867	1.2807			00011700
						0.0	0.0	0.0	0.0			00011800
SB0619												00011900
19	8	24	25	0	154.24707	0.3043	0.0	3.111	1.2807			00012000
						0.0	0.0	0.0	0.0			00012100
SB0620												00012200
20	1	25	26	0	154.97917	0.2757	0.0	1.399	0.0			00012300
						0.0	0.0	0.0	0.0			00012400
SB0621												00012500
21	1	26	27	0	154.98417	0.2842	0.0	0.5313	0.0			00012600
						0.0	0.0	3.58	10.0			00012700
SB0622												00012800
22	4	27	13	0	154.80960	0.45190	0.0426	4.256	-4.256			00012900
						0.62	0.62	3.5	3.5			00013000
SB0623												00013100
23	5	13	28	0	155.0864	1.004	0.0	0.7318	0.0			00013200
						0.0	0.0	0.0	0.0			00013300
SB0624												00013400
24	1	28	14	0	155.0770	0.4417	0.0	0.4285	0.4285			00013500
						0.0	0.0	-1.0	-1.0			00013600
SB0625												00013700
25	2	14	15	0	154.9449	1.0	0.0	0.09423	0.09423			00013800
						-1.0	-1.0	0.0	0.0			00013900
SB0626												00014000
26	2	15	16	1	154.9022	1.0	0.0	0.4191	0.4191			00014100
						0.0	0.0	0.0	0.0			00014200
SB0627												00014300
27	2	16	17	1	154.8312	1.0	0.0	0.4191	0.4191			00014400
						0.0	0.0	0.0	0.0			00014500
SB0628												00014600
28	2	17	18	1	154.7579	1.0	0.0	0.4191	0.4191			00014700
						0.0	0.0	0.0	0.0			00014800
SB0629												00014900
29	2	18	19	1	154.6882	1.0	0.0	0.4191	0.4191			00015000
						0.0	0.0	0.0	0.0			00015100
SB0630												00015200
30	2	19	20	0	154.6167	1.0	0.0	0.01753	0.01753			00015300
						0.0	0.0	-1.0	-1.0			00015400
SB0631												00015500
31	1	20	22	0	154.5833	0.5513	0.05486	1.668	1.668			00015600
						-1.0	-1.0	0.0	0.0			00015700
SB0632												00015800
32	1	28	22	0	155.0770	0.0779	0.0	4.164	4.164			00015900
						0.0	0.0	0.0	0.0			00016000
SB0633												00016100
33	13	22	37	0	0.1	0.5419	0.0	0.9144	0.9144	0.0	0.0	0.0
SB0634												00016200
34	13	29	35	0	0.1	0.222	0.0	4.048	0.8620	0.4	0.8	0.0
SB0635												00016300
35	13	30	36	0	0.1	0.222	0.0	4.840	0.6075	0.4	0.8	0.0
SB0636												00016400
36	13	23	21	0	10.0	0.043	0.0	4.592	0.4255	0.4	0.8	9.0
												00016500
												00016600
												00016700
												00016800

```

-----*-----1-----*-----2-----*-----3-----*-----4-----*-----5-----*-----6-----*-----7-R-----*-----8
SB0637 37 13 21 34 0 10.0 0.043 0.0 4.767 0.7678 0.0 0.0 0.0 0.0 00016900
SB0638 38 13 26 31 0 10.0 0.089 0.0 5.5 0.0 0.4 0.8 0.0 0.0 00017000
SB0639 39 13 26 32 0 10.0 0.089 0.0 5.5 0.0 0.4 0.8 0.0 0.0 00017100
SB0640 40 13 26 33 0 20.0 0.089 0.0 58.0 0.0 0.4 0.8 0.0 0.0 00017200
/ 00017300
/ 00017400
/ 00017500
/ 00017600
/ 00017700
/ 00017800
/ **** JUNCTION DATA **** 00017900
BB07 00018000
1 1 0.0 00018100
2 1 0.0 00018200
3 1 0.0 00018300
4 1 0.0 00018400
5 1 0.0 00018500
6 1 0.0 00018600
7 1 0.0 00018700
8 1 0.0 00018800
9 1 0.0 00018900
10 1 0.0 00019000
11 1 0.0 00019100
12 1 0.0 00019200
13 1 0.0 00019300
14 1 0.0 00019400
15 1 0.0 00019500
16 1 0.0 00019600
17 1 0.0 00019700
18 1 0.0 00019800
19 1 0.0 00019900
20 1 0.0 00020000
21 1 0.0 00020100
22 4 0.1937 00020200
23 4 0.04149 00020300
24 4 0.05040 00020400
25 4 0.04644 00020500
26 4 0.08948 00020600
27 4 0.18 00020700
28 4 0.064 00020800
29 4 0.04474 00020900
30 4 0.04474 00021000
31 7 0.0 00021100
32 7 0.0 00021200
33 5 0.0 00021300
34 6 0.0 00021400
35 8 0.0 00021500
36 8 0.0 00021600
37 8 0.0 00021700
/ 00021800
/ **** MIXING JUNCTION DATA **** 00021900
BB08 00022000
SB0801 00022100
22 3 1 11 33 0 0.001 0.999 0. 0. 00022200
SB0802 00022300
23 2 12 36 0 0 1.0 0.0 0. 0. 00022400
SB0803 00022500
24 2 18 19 0 0 0.5 0.5 0. 0. 00022600
SB0804 00022700
25 1 20 0 0 0 1.0 0.0 0. 0.

```

JAERI-M 9535

```

-----*-----1-----*-----2-----*-----3-----*-----4-----*-----5-----*-----6-----*-----7-R-----*-----8
SB0805      26  4  21 38 39 40  1.0  0.0  0.  0. 00022800
SB0806      27  1  22  0  0  0  1.0  0.0  0.  0. 00022900
SB0807      28  2  24 32  0  0  0.97 0.03  0.  0. 00023000
SB0808      29  2   2 34  0  0  1.0  0.0  0.  0. 00023100
SB0809      30  2  10 35  0  0  1.0  0.0  0.  0. 00023200
/           00023300
/  **** PUMPED INJECTION DATA **** 00023400
BB09 00023500
SB0901 00023600
      1  31  24.0 00023700
      10 00023800
          0.0 0.00  2.0 1.80  4.0 1.47  8.0 1.50 00023900
          28.0 1.60 64.0 1.70 72.0 1.00 120.0 1.00 00024000
          140.0 1.50 200.0 1.50 00024100
SB0902 00024200
      2  32  24.0 00024300
      10 00024400
          0.0 0.00  3.0 3.50  7.0 4.80 11.0 5.30 00024500
          14.0 5.60 20.0 3.60 27.0 5.20 43.0 6.50 00024600
          59.0 7.00 200.0 7.40 00024700
/ 00024800
/  **** PUMP DATA **** 00024900
BB10 00025000
SB1001 00025100
      18 1 1 3530. .3155 500.24 108.1 613.73 1269.7 1.4328 .0 .0 1. 00025200
SB1002 00025300
      19 1 1 3530. .3155 500.24 108.1 613.73 1269.7 1.4328 .0 .0 1. 00025400
/ 00025500
/  **** PUMP DATA TABLE **** 00025600
BB11 00025700
SB1101 00025800
      1 00025900
      12 00026000
      -1.0 2.4722 -0.80574 2.0474 00026100
      -0.6096 1.831 -0.40683 1.624 00026200
      -0.200171 1.4705 0.0 1.4036 00026300
      0.19061 1.3636 0.38963 1.3186 00026400
      0.4118 1.3 0.59396 1.2328 00026500
      0.7902 1.1336 1.0 1.0078 00026600
      12 00026700
      -1.0 -1.0 -0.80574 -0.6 00026800
      -0.6096 -0.3 -0.40683 -0.05 00026900
      -0.200171 0.13 0.0 0.25 00027000
      0.19061 0.28 0.38963 0.34 00027100
      0.4118 0.2768 0.59396 0.46 00027200
      0.7902 0.70 1.0 0.9465 00027300
      17 00027400
      -1.0 -1.0 -0.82297 -0.98 00027500
      -0.63332 -0.95 -0.45534 -0.90 00027600
      -0.27109 -0.82 -0.17716 -0.78 00027700
      -0.09073 -0.72 0.0 -0.67 00027800
      0.091099 -0.60 0.186509 -0.52 00027900
      0.271762 -0.42 0.45582 -0.21 00028000
      0.574406 -0.02 0.740576 0.26 00028100
      00028200
      00028300
      00028400
      00028500
      00028600

```

1	2	3	4	5	6	7-R	8
0.766619	0.36		0.871471	0.63			00028700
1.0	1.0078						00028800
17							00028900
-1.0	2.4722	-0.82297		1.9968			00029000
-0.63332	1.5897	-0.45534		1.3279			00029100
-0.27109	1.1949	-0.17716		1.0605			00029200
-0.09073	1.0156	0.0		0.934279			00029300
0.091099	0.9229	0.186509		0.8963			00029400
0.271762	0.875	0.45582		0.8433			00029500
0.574406	0.8355	0.740576		0.8466			00029600
0.766619	0.8469	0.871471		0.8838			00029700
1.0	0.9465						00029800
14							00029900
-1.0	1.9843	-0.80096	1.394				00030000
-0.60638	1.0975	-0.40686	0.822				00030100
-0.30	0.71	-0.19928	0.6648				00030200
-0.10	0.61	0.0	0.6032				00030300
0.1930	0.6325	0.393	0.7369				00030400
0.50	0.79	0.59552	0.8381				00030500
0.79782	0.9229	1.0	0.9672				00030600
14							00030700
-1.0	-1.0	-0.80096	-0.98				00030800
-0.60638	-0.94	-0.40686	-0.91				00030900
-0.30	-0.90	-0.19928	-0.70				00031000
-0.10	-0.51	0.0	-0.45				00031100
0.1930	-0.37	0.393	-0.26				00031200
0.50	-0.01	0.59552	0.06				00031300
0.79782	0.21	1.0	0.3569				00031400
17							00031500
-1.0	-1.0	-0.82234	-0.98				00031600
-0.63371	-0.94	-0.45853	-0.92				00031700
-0.267023	-0.91	-0.176107	-0.85				00031800
-0.089310	-0.80	0.0	-0.67				00031900
0.090643	-0.59	0.188569	-0.50				00032000
0.27347	-0.40	0.455869	-0.05				00032100
0.57448	0.28	0.73816	0.52				00032200
0.76852	0.61	0.870057	0.74				00032300
1.0	0.9672						00032400
17							00032500
-1.0	1.9843	-0.82234	1.8308				00032600
-0.63371	1.6824	-0.45853	1.557				00032700
-0.267023	1.4362	-0.176107	1.3879				00032800
-0.089310	1.3481	0.0	0.23361				00032900
0.090643	1.1965	0.188569	1.1096				00033000
0.27347	1.0416	0.455869	0.8958				00033100
0.57448	0.7807	0.73816	0.6137				00033200
0.76852	0.5849	0.870057	0.4877				00033300
1.0	0.3569						00033400
12							00033500
-1.0	-1.15	-0.9	-1.24	-0.6	-2.8	-0.5	-2.9
-0.4	-2.7	0.0	0.0	0.12	0.85	0.2	1.1
0.5	1.02	0.7	1.0	0.9	0.95	1.0	1.0
4							00033900
-1.0	0.0	0.0	0.0	0.5	-0.8	1.0	-1.46
7							00034000
-1.0	0.0	0.0	0.0	0.1	-0.02	0.2	0.0
0.3	0.1	0.9	0.78	1.0	1.0		
12							00034200
-1.0	-1.15	-0.8	-0.5	-0.6	-0.2	-0.4	0.03
							00034300
							00034400
							00034500

```

-----1-----2-----3-----4-----5-----6-----7-R-----8
-0.2    0.04      0.0    0.1      0.2    0.15      0.4    0.12      00034600
0.6    0.05      0.8   -0.5      0.9   -0.9      1.0   -1.46      00034700
0                                              00034800
0                                              00034900
0                                              00035000
0                                              00035100
13                                              00035200
0.0    0.0    0.05  0.0      0.1    0.025      0.15  0.075      0.2    0.18      00035300
0.3    0.475      0.4    0.625      0.5    0.74      0.6    0.82      00035400
0.7    0.87      0.8    0.84      0.9    0.72      1.0    0.08      00035500
11                                              00035600
0.0    0.0      0.1    0.0      0.20   0.13      0.3    0.24      00035700
0.4    0.31      0.5    0.33      0.6    0.3      0.7    0.23      00035800
0.8    0.16      0.9    0.08      1.0    0.0      00035900
6 6                                              00036000
0.0    0.2    0.4    0.6    0.8    1.0      00036100
0.0    0.0    0.0    0.0    0.0    0.0    0.0      00036200
0.2    0.0    3.0650E-5  7.7239E-5  1.3263E-4  1.9460E-4  2.6207E-4      00036300
0.4    0.0    4.8660E-5  1.2261E-4  2.1053E-4  3.0996E-4  4.1602E-4      00036400
0.6    0.0    6.3760E-5  1.6066E-4  2.7587E-4  4.0485E-4  5.4514E-4      00036500
0.8    0.0    7.7239E-5  1.9463E-4  3.3419E-4  4.9044E-4  6.6037E-4      00036600
1.0    0.0    8.9628E-5  2.2585E-4  3.8780E-4  5.6910E-4  7.6631E-4      00036700
/                                              00036800
/ ***** ACCUMLATOR DATA *****      00036900
BB12                                              00037000
SB1201                                              00037100
43 33 2.63 1.05 28.7 40.562 0.9 0.1      00037200
/                                              00037300
/ ***** BREAK POINT DATA *****      00037400
BB13                                              00037500
6 2.0E-3 0.1 0.8 0.8 0.6 0.8 0.8 0.6      00037600
2                                              00037700
0.0 5.0 100.0 5.0      00037800
/                                              00037900
/ ***** PRESSURIZER DATA *****      00038000
BB14                                              00038100
41 34 1 0.557 1.7235 1.00 0.88 0.01      00038200
1.0 1.0 1.0 1.0 1.0 0.0737 0.0737 0.0737      00038300
0.313 0.313 0.313 1.0 1.0 1.0      00038400
2                                              00038500
0. 1.0 1.0 1.0 1000. 1.0 1.0 1.0      00038600
/                                              00038700
/ ***** STEAM GENERATOR DATA *****      00038800
BB15                                              00038900
SB1501                                              00039000
42 1845 14 15 2 1      00039100
1.589 4.188 1.0 1.0 0.01905 0.005105 4.469 0.6 196.0 12.67      00039200
0.000 0.99 62.67      00039300
-60.0 -20.0      00039400
0.001 80. 0.5 0.5 0.5      00039500
3                                              00039600
0.0 1.0 1.0 1.0 1.0 1.0 1.0 1.0 1000.0 1.0 1.0 0.0      00039700
/                                              00039800
/ ***** CORE DATA *****      00039900
BB16                                              00040000
1300 25 30 0 9000.      00040100
5.359E-3 6.172E-4 4.647E-3 1.43E-2 0.6 19.52E-6      00040200
0.0124 2.395E-4 0.0305 1.5897E-3 0.111 1.423E-3      00040300
0.301 2.869E-3 1.14 8.347E-4 3.01 3.048E-3      00040400

```



```

-----*-----1-----*-----2-----*-----3-----*-----4-----*-----5-----*-----6-----*-----7-R-----8
      5.0      0.6      4.91E-04  3.41E-06  1.2      1.54E03      00040500
      0.0      73.645    124.217    94.702    31.394    0.0      00040600
1.0000E-07  1.00E-07  1.00E-07  1.00E-07  1.00E-07  1.0E-7    00040700
1.0000E-07  1.00E-07  1.00E-07  1.00E-07  1.00E-07  1.0E-7    00040800
1.0000E-07  1.00E-07  1.00E-07  1.00E-07  1.00E-07  1.0E-7    00040900
1.0000E-07  1.00E-07  1.00E-07  1.00E-07  1.00E-07  1.0E-7    00041000
/
/  **** SG RELIEF VALVE DATA ****
BB17      00041100
      6      00041200
      0.  0.  0.1 -14.  0.18 -32.  0.34 -62.  0.5 -94.  0.58 -179.  00041300
      4      00041400
      50. -0.00030  380. -0.00022  1200. -0.00015  2280. -0.00008  00041500
      9      00041600
      0.0  0.0  0.2 -0.2  0.4 -0.4  0.6 -1.4  0.8 -2.6  00041700
      1.0 -5.6  1.2 -12.6  1.4 -15.4  200.0 -15.6  00041800
/      00041900
/      00042000
/      00042100
/  ****      ****      00042200
BB18      00042300
      1.54E03      0.775E-04      2.29E04      00042400
/      00042500
/  **** FUEL GAP DATA ****      00042600
BB19      00042700
      5.7E-4  0.0      5.493E-6  0.0      0.0      00042800
      0.0      0.0      0.9      0.75      0.0      00042900
      0.887      0.0355  0.0063      0.0      0.0712      00043000
      0.0      0.0      00043100
/      00043200
/  ****      ****      00043300
BB21      00043400
      2  2  5.00E7      6.96E-08  2.87E4  2.86E-03  1.15E0  1.528E0      00043500
      1.49E-07  2.0E-08  1.25E-16  1.85E-01  8.0E09  3.3E-03      00043600
/      00043700
/  **** OTHER DATA ****      00043800
BB22      00043900
      0.  1.4  1.4  0.      00044000
BEND      00044100
      5      00044200
      0      0      0      0      0      0.0      00044300
      0.  1.E-5  0.  0.  0.  0.0      00044400
END      00044500
END      00044600
LIST      00044700

HIGHEST SEVERITY CODE=00
-      END      00000170

STATISTICS: HIGHEST SEVERITY CODE=00

```

Appendix B Function Codes of Experimental Data in Figures

Fig. No	System Detector	Function Code	Location
13(a)	TE-2H14-028	TECTD215	Cladding on Fuel Assembly 2, Row H, Column 14 at 0.71m above bottom of fuel rod
13(b)	TE-2H15-041	TECTD218	Cladding on Fuel Assembly 2, Row H, Column 15 at 1.04m above bottom of fuel rod
23	FR-BL-216	FRBKD216	Broken loop hot leg
24	DE-BL-002B	DEBTG006	Broken loop hot leg
25	FR-BL-116	FRBKD116	Broken loop cold leg
26	DE-BL-105	DEBKD105	Broken loop cold leg
28	FR-PC-202	FRPKD202	Intact loop hot leg
29	DE-PC-205	DEPKD205	Intact loop hot leg
31	FR-PC-102	FRPKD102	Intact loop cold leg
32	DE-PC-105	DEPKD105	Intact loop cold leg
35	RPE-PC-002	SRPTD498	Pump speed-primary coolant pump 1
42	FT-P102-36-1	FVFTD016	Accumulator A in 6-in. line downstream of orifice
43	PT-P102-043	PAFTD115	Accumulator A, 0.69m above water outlet
45	PE-1up-001A	PAUTD103	Above Fuel Assembly 1 upper end box, high range

Appendix C Nomenclature

C.1 Alphabetic Symbols

a	Normalized pump speed
a_0	Normalized initial pump speed
a_1, a_2	Quantities defined in Eq. (21), s^2/m^2 and $kgm^2/m^3 \text{ kcal}$
A	Flow area, m^2
b	Normalized pump hydraulic torque
c	Quantity defined in Eq. (26), s
D	Diameter, m
D_b	Diameter, cm
f_{nl}	Function defined in Eq. (20)
F	Function defined in Table 4
g	Gravitational acceleration, m/s^2
g_c	Dimensional conversion ratio, $kgm/kgf \text{ m/s}^2$
G	Mass flux, kgm/m^2s
G_b	Mass flux, gm/cm^2s
G_{min}	Minimum mass flux for forced convection condition, kgm/m^2s
h	Enthalpy, $kcal/kgm$
h_{fg}	Latent heat, $kcal/kgm$
h_{head}	Normalized pump head
h_t	Function defined in Eq. (7)
h_{tr}	Heat transfer coefficient, $kcal/m^2s \text{ } ^\circ C$
Δh	Enthalpy difference, $kcal/kgm$
H	Function defined in Eq. (4)
H_L	Node length, m
J_c	Dimensional conversion ratio, J/cal
k	Loss coefficient
k_g, k_l	Thermal conductivities of gas and liquid phases, respectively, $kcal/m \text{ s } ^\circ C$
L	Node length, m
L_b	Length, m
m_b, m_h	Two-phase pump torque and head multipliers, respectively
p	Pressure, Pa
p_b	Pressure, ata

p^*	Pressure, psia
Δp	Pressure difference, Pa
Re	Reynolds number
t	Time, s
Δt	Time step width
T	Temperature, °C
T_w	Wall temperature, °C
T_w^*	Wall temperature, °F
ΔT_s	Wall superheat, °C
ΔT_s^*	Wall superheat, °F
ΔT_{min}^*	Quantity defined in Eq. (9), °F
V	Node volume, m ³
V^*	Dimensionless node volume defined in Eq. (33)
w	Normalized pump volumetric flow rate
W	Mass flow rate, kgm/s
x	Equilibrium quality
x_0	Quantity defined in Eq. (26)
x_c	Quantity defined in Eq. (13)
x_{in}	Inlet quality
x_{out}	Outlet quality
Y	Function defined in Eq. (3)

C.2 Greek Symbols

α	Equilibrium void fraction
α^*	Non-equilibrium void fraction
β	Quantity defined in Eq. (18)
ρ	Equilibrium density, kgm/m ³
ρ^*	Non-equilibrium density, kgm/m ³
ϕ	Heat flux, kcal/m ² s
ϕ^*	Heat flux, Btu/ft ² hr
σ	Surface tension, kgf/m
τ_α	Delay parameter, s
λ_c	Quantity defined in Eq. (11)

C.3 Subscripts and Superscripts

Subscripts

coolant	Coolant
core	Core nodes
CHF	Critical heat flux
ECC	Emergency core cooling water
fs	Saturated fluid
gs	Saturated steam
g	Gas phase
l	Liquid phase
n	Node number
pZR	Pressurizer
sat	Saturated property
4-1	Evaluated in heat transfer mode 4-1
4-2	Evaluated in heat transfer mode 4-2

Superscripts

A	Inlet point of node
E	Outlet point of node
f	Forward flow
j	Junction number
n	Node number
new	Present time
old	Time which is one time step past
r	Reverse flow
1 ϕ	Single-phase
2 ϕ	Two-phase